DEVELOPMENT OF NEW LOW FRICTION THRUST BALL BEARING WITH OPTIMIZE GEOMETRY

ALIF IQMAL BIN ABDUL KHALID

B092010108

UNIVERSITI TEKNIKAL MALAYSIA MELAKA

BACHELOR OF MECHANICAL ENGINEERING TECHNOLOGY (AUTOMOTIVE) WITH HONOURS

2024

Faculty of Mechanical Technology and Engineering

DEVELOPMENT OF NEW LOW FRICTION THRUST BALL BEARING WITH OPTIMIZE GEOMETRY

Alif Iqmal Bin Abdul Khalid

Bachelor of Mechanical Engineering Technology (Automotive) with Honours

2024

DEVELOPMENT OF NEW LOW FRICTION THRUST BALL BEARING WITH OPTIMIZE GEOMETRY

ALIF IQMAL BIN ABDUL KHALID

A thesis submitted
in fulfillment of the requirements for the degree of
Bachelor of Mechanical Engineering Technology (Automotive) with Honours

اونيۏرسيتي تيكنيكل مليسيا ملاك
UNIVERSITI TEKNIKAL MALAYSIA MELAKA

Faculty of Mechanical Technology and Engineering

UNIVERSITI TEKNIKAL MALAYSIA MELAKA

2024

UNIVERSITI TEKNIKAL MALAYSIA MELAKA

BORANG PENGESAHAN STATUS LAPORAN PROJEK SARJANA MUDA

TAJUK: **DEVELOPMENT OF NEW LOW FRICTION THRUST BALL BEARING WITH OPTIMIZE GEOMETRY**

SESI PENGAJIAN: **2023-2024 Semester 1**

Saya **ALIF IQMAL BIN ABDUL KHALID**

mengaku membenarkan tesis ini disimpan di Perpustakaan Universiti Teknikal Malaysia Melaka (UTeM) dengan syarat-syarat kegunaan seperti berikut:

1. Tesis adalah hak milik Universiti Teknikal Malaysia Melaka dan penulis.
2. Perpustakaan Universiti Teknikal Malaysia Melaka dibenarkan membuat salinan untuk tujuan pengajian sahaja dengan izin penulis.
3. Perpustakaan dibenarkan membuat salinan tesis ini sebagai bahan pertukaran antara institusi pengajian tinggi.
4. **Sila tandakan (✓)

☐	TERHAD	(Mengandungi maklumat yang berdarjah keselamatan atau kepentingan Malaysia sebagaimana yang termaktub dalam AKTA RAHSIA RASMI 1972)
☐	SULIT	(Mengandungi maklumat TERHAD yang telah ditentukan oleh organisasi/badan di mana penyelidikan dijalankan)
√	TIDAK TERHAD	

UNIVERSITI TEKNIKAL MALAYSIA MELAKA

Disahkan oleh:

Alamat Tetap: Lot 2986, Jalan Kadir Adabi,
17500 Tanah Merah,
Kelantan.

Cop Rasmi:

DR. MUHAMMAD ILMAN HAKIMI CHUA BIN ABDULLAH
PENSYARAH KANAN
JABATAN TEKNOLOGI KEJURUTERAAN MEKANIKAL
FAKULTI TEKNOLOGI KEJURUTERAAN MEKANIKAL & PEMBUATAN
UNIVERSITI TEKNIKAL MALAYSIA MELAKA

Tarikh: 09.01.2024

Tarikh: 11/01/2024

** Jika tesis ini SULIT atau TERHAD, sila lampirkan surat daripada pihak berkuasa/organisasi berkenaan dengan menyatakan sekali sebab dan tempoh laporan PSM ini perlu dikelaskan sebagai SULIT atau TERHAD.

DECLARATION

I declare that this project entitled " Development of New Model Low Friction Thrust Ball Bearing With Optimize Geometry" is the result of my own research except as cited in the references. The thesis has not been accepted for any degree and is not concurrently submitted in candidature of any other degree.

Signature	:	
Name	:	Alif Iqmal Bin Abdul Khalid
Date	:	09.01.2024

اونيۆرسيتي تيكنيكل مليسيا ملاك
UNIVERSITI TEKNIKAL MALAYSIA MELAKA

APPROVAL

I hereby declare that I have checked this thesis and in my opinion, this thesis is adequate in terms of scope and quality for the award of the degree of Bachelor of Mechanical Engineering Technology (Automotive) with Honours

Signature	:	
Supervisor Name	:	Dr. Muhammad Ilman Hakimi Chua Bin Abdullah
Date	:	09.01.2024

UTeM
اونيۏرسيتي تيكنيكل مليسيا ملاك
UNIVERSITI TEKNIKAL MALAYSIA MELAKA

DEDICATION

I would want to dedicate this work to my dearly loved parents as well as to my supervisor, Dr. Muhammad Ilman Hakimi Chua Bin Abdullah, who have shown me love and support without condition and have been there for me no matter what. I cannot express how grateful I am to you for providing the motivation I needed to complete my Senior Project.

اونيۏرسيتي تيکنيکل مليسيا ملاک
UNIVERSITI TEKNIKAL MALAYSIA MELAKA

ABSTRACT

Bearings serve a variety of functions and are among the most common types of components found in mechanical and civil engineering structures. Because of its versatility and capacity to withstand axial loads while permitting rotation, thrust ball bearings find extensive use in mechanical systems. Traditional thrust ball bearings suffer from excessive energy consumption and poor efficiency due to large frictional losses. In response, a fresh strategy is developed to improve the thrust ball bearing's design. Improving the geometry of thrust ball bearings in order to decrease friction is the primary goal of this work. Using Catia V5 software for design and SLS 3D printing technology for prototype creation, the study the bearing's structural properties and detect any prospective weak places. To find and discover any potential weak places, the bearing is simulated using Simsolid software. The outcome for Simsolid was evaluated in comparison to the prior project's roller bearing results in order to guarantee improved performance. Modifying the contact angle, groove form, and ball diameter are all potential ways to lessen the frictional losses. The results demonstrate that the prior project's low measurement values indicate that roller bearings, not thrust ball bearings, provide superior simulation results. This is because, instead of using thrust ball bearings, the rollers used in the action have a broad contacting surface. Through the use of vibration analysis experiments, the prototype's efficacy and performance were assessed. Using vibration testing and a scanning electron microscope (SEM), a series of tests will be conducted to evaluate the friction, load capacity, and durability of the proposed low friction thrust ball bearing. To define their parameters, the new bearing design's prospective benefits are contrasted with those of the prior project, which included roller bearings. The majority of the enhanced prototypes outperformed the baseline versions, according to the study's overall results. A key component influencing the rotational force acting on the contact surface of the bearing was identified. Importantly, when subjected to greater stresses, prototypes created utilising selective laser sintered (SLS) technology underwent plastic deformation and merged with steel, resulting in a smoother surface. The material used in the previous project made the vibration testing go more smoothly than with the thrust ball bearing. While the roller bearings were entirely made of Nylon P12, the ball bearings in this project were steel with some Nylon PA12 added. The procedure significantly increased the lifetime and durability of the bearings employed. The result was a less noticeable amount of vibration from the machine because of the improved surface. Photos taken with a scanning electron microscope (SEM) provide credence to the study and show that squares are the best form for any kind of research. Furthermore, it was observed that thrust ball bearings outperformed the previously used roller bearings in terms of performance and longevity, despite the fact that their Nylon PA12 substance made their surfaces less smooth. The optimised design of the bearing shows its promise in many future applications.

ABSTRAK

Galas mempunyai pelbagai fungsi dan merupakan antara jenis komponen yang paling biasa ditemui dalam struktur kejuruteraan mekanikal dan awam. Oleh kerana kepelbagaian dan kapasitinya untuk menahan beban paksi sambil membenarkan putaran, galas bebola tujah banyak digunakan dalam sistem mekanikal. Galas bebola tujahan tradisional mengalami penggunaan tenaga yang berlebihan dan kecekapan yang lemah akibat kehilangan geseran yang besar. Sebagai tindak balas, strategi baru dibangunkan untuk menambah baik reka bentuk galas bebola tujahan. Memperbaik geometri galas bebola tujahan untuk mengurangkan geseran adalah matlamat utama kerja ini. Menggunakan perisian Catia V5 untuk reka bentuk dan teknologi pencetakan SLS 3D untuk penciptaan prototaip, mengkaji sifat struktur galas dan mengesan sebarang kemungkinan tempat yang lemah. Untuk mencari dan menemui mana-mana tempat lemah yang berpotensi, bearing disimulasikan menggunakan perisian Simsolid. Hasil untuk Simsolid telah dinilai berbanding dengan hasil galas silinder projek sebelumnya untuk menjamin prestasi yang lebih baik. Mengubah suai sudut sentuhan, bentuk alur dan diameter bola adalah semua cara yang berpotensi untuk mengurangkan kehilangan geseran. Keputusan menunjukkan bahawa nilai pengukuran rendah projek terdahulu menunjukkan bahawa galas penggelek, bukan galas bebola tujah, memberikan hasil simulasi yang unggul. Ini kerana, daripada menggunakan galas bebola tujahan, penggelek yang digunakan dalam tindakan mempunyai permukaan sentuhan yang luas. Melalui penggunaan eksperimen analisis getaran, keberkesanan dan prestasi prototaip telah dinilai. Menggunakan ujian getaran dan mikroskop elektron pengimbasan (SEM), satu siri ujian akan dijalankan untuk menilai geseran, kapasiti beban dan ketahanan galas bebola tujahan geseran rendah yang dicadangkan. Untuk menentukan parameter mereka, manfaat prospektif reka bentuk galas baharu adalah berbeza dengan projek sebelumnya, yang termasuk galas silinder. Majoriti prototaip yang dipertingkatkan mengatasi versi asas, menurut keputusan keseluruhan kajian. Komponen utama yang mempengaruhi daya putaran yang bertindak pada permukaan sentuhan galas telah dikenalpasti. Yang penting, apabila dikenakan tekanan yang lebih besar, prototaip yang dicipta menggunakan teknologi pensinteran laser terpilih (SLS) mengalami ubah bentuk plastik dan digabungkan dengan keluli, menghasilkan permukaan yang lebih licin. Bahan yang digunakan dalam projek sebelumnya menjadikan ujian getaran berjalan lebih lancar berbanding dengan galas bebola tujah. Walaupun galas silinder sepenuhnya diperbuat daripada Nylon P12, galas bebola dalam projek ini adalah keluli dengan beberapa Nylon PA12 ditambah. Prosedur ini meningkatkan jangka hayat dan ketahanan galas yang digunakan dengan ketara. Hasilnya ialah jumlah getaran yang kurang ketara daripada mesin kerana permukaan yang bertambah baik. Foto yang diambil dengan mikroskop elektron pengimbasan (SEM) memberikan kepercayaan kepada kajian dan menunjukkan bahawa segi empat sama adalah bentuk terbaik untuk sebarang jenis penyelidikan. Tambahan pula, diperhatikan bahawa galas bebola tujahan mengatasi galas silinder yang digunakan sebelum ini dari segi prestasi dan umur panjang, walaupun pada hakikatnya bahan Nylon PA12 mereka menjadikan permukaannya kurang licin. Reka bentuk galas yang dioptimumkan menunjukkan janjinya dalam banyak aplikasi masa hadapan.

UNIVERSITI TEKNIKAL MALAYSIA MELAKA

ACKNOWLEDGEMENTS

In the Name of Allah, the Most Gracious, the Most Merciful

To begin, I would want to express my appreciation and thanks to Allah, the everything-Mighty, who is both my Creator and my Sustainer. For everything that has been bestowed upon me from the beginning of my life, I would like to begin by expressing my gratitude and thanks to Allah. I would like to use this occasion to convey my appreciation to the University of Technical Malaysia Melaka (UTeM) for providing the facility in which the research was conducted.

My primary research supervisor, Dr. Muhammad Ilman Hakimi Chua bin Abdullah, from the Faculty of Mechanical Technology and Engineering at University Technical Malaysia Melaka (UTeM), is deserving of my utmost thanks for all the support, guidance, and inspiration he has provided me with. Together with the priceless insights he offered, his ever-present patience in directing will be remembered for all of time. In addition, I would like to extend my gratitude to Ts. Mohd Idain Fahmy bin Rosley of the University Technical Malaysia Melaka (UTeM), who has been very supportive throughout my trip and has assisted me in the SLS 3D printing of my project.

In addition, I would want to express my thanks to my wonderful family for their unfailing love, support, and sacrifices made on my behalf as they helped direct me towards a more promising future and contributed to the development of the person I am today. Finally, I would like to thank all of my other friends who have supported me, helped me along the road, and urged me to keep working towards my educational goals.

Finally, with humble as human being, I want to acknowledge my own self for believing in me, I want to thank me for doing all this hard work. I want to thank me for having no days off. I want to thank me for never quitting. I want to thank me for always being a giver and trying to give more than I receive. I want to thank me for trying to do more right than wrong. I want to thank me for being me at all times.

TABLE OF CONTENTS

UNIVERSITI TEKNIKAL MALAYSIA MELAKA

UNIVERSITI TEKNIKAL MALAYSIA MELAKA

UTeM
اونيۏرسيتي تيكنيكل مليسيا ملاك
UNIVERSITI TEKNIKAL MALAYSIA MELAKA

LIST OF TABLES

UNIVERSITI TEKNIKAL MALAYSIA MELAKA

UNIVERSITI TEKNIKAL MALAYSIA MELAKA

LIST OF FIGURES

UTeM
UNIVERSITI TEKNIKAL MALAYSIA MELAKA

UNIVERSITI TEKNIKAL MALAYSIA MELAKA

اونيۆرسيتي تيكنيكل مليسيا ملاك
UNIVERSITI TEKNIKAL MALAYSIA MELAKA

LIST OF SYMBOLS AND ABREVIATIONS

CAGR	-	Compound Annual Growth Rate
CAD	-	Computer-Aided Design
CAE	-	Certified Association Executive
SEM	-	Surface Morphological Analysis
BC	-	Before Christ
AD	-	Anno Domini
ABMA	-	American Bearing Manufacturers Association
°	-	Degree Of Angles
PTFE	-	Polytetrafluoroethylene
Mpa	-	Megapascal
J/m	-	Joules Per Meter
°C	-	Degree Of Temperature
HDT	-	Heat Deflection Temperature
HIP	-	Hot Isostatic Pressing
CNC	-	Computerized Numerical Control
SLS	-	Selective Laser Sintering
SLM	-	Selective Laser Melting
EBM	-	Electron Beam Melting
DMLS	-	Direct Metal Laser Sintering
F_f	-	Amount Of Friction
μ	-	Coefficient Of Friction
F_n	-	Normal Force
COF	-	Coefficient Of Friction
F	-	Friction Force
L	-	Force That Cause Collide
m	-	Mass
g	-	Gravitation
mm	-	Milimeter
D_w	-	Ball Diameter
D_{pw}	-	Bearing Pitch Diameter

UTeM
UNIVERSITI TEKNIKAL MALAYSIA MELAKA

Z	-	Ball Number
f_i	-	Inner Raceway Curvature Coefficient
f_o	-	Outer Raceway Curvature Coefficient
g_o	-	Clearance
CFD	-	Computational Fluid Dynamics
B/L	-	Width To Length Ratio
H_1	-	Untextured Inlet
H_0	-	Untextured Outlet
L	-	Length
L_1	-	Texture Length
ABS	-	Acrylonitrile Butadiene Styrene
FEA	-	Finite Element Analysis
a	-	Axis
w	-	Angular Velocity
E	-	Angular Acceleration
Ra	-	Measurement Of Average Roughness
AM	-	Additive Manufacturing
CO2	-	Carbon Dioxide
PPE	-	Personal Protective Equipment
STL	-	Standard Triangle Languange
FFT	-	Fast Fourier Transform
rpm	-	Revolution Per Minute
Hz	-	Hertz
EDS	-	Energy-Dispersive X-Ray Spectroscopy

UNIVERSITI TEKNIKAL MALAYSIA MELAKA

LIST OF APPENDICES

اونيۈرسيتي تيكنيكل مليسيا ملاك
UNIVERSITI TEKNIKAL MALAYSIA MELAKA

CHAPTER 1

INTRODUCTION

1.1 Background

Since the mid-nineteenth century, ball thrust bearings, also known as axial ball bearings, have been in use. The ball thrust bearing is designed to facilitate axial movement while decreasing friction between two elements in contact with each other. Sven Winquist, a Swedish inventor, produced one of the earliest known designs of a ball thrust bearing in 1907. Winquist's design had two sets of races: one for the balls to run on and another for the balls to hold the assembly together. This invention evolved into the double-row, self-aligning ball bearing, which was widely utilized in automotive and industrial applications. During World War II, the ball thrust bearing witnessed considerable advancements as the demand for high-performance bearings for airplanes and other military gear skyrocketed. The development of new materials and manufacturing procedures enabled the production of more accurate and long-lasting ball thrust bearings. Ball thrust bearings are now employed in a variety of applications such as automotive, aerospace, and industrial machinery. They have become an important component in many types of equipment and are intended to carry both radial and axial stresses, making them appropriate for a wide range of applications. In this research, we are optimizing the geometry of the ball thrust bearings.

Optimize, according to the Cambridge Advanced Learner's Dictionary & Thesaurus, implies making something as good as possible. In structural optimization, the optimized geometry in the study title is classed as topological optimization. Topology optimization uses the algorithm to change the density of structure while controlling the stiffness contribution and make changes to the dimension of CAD model to obtain desired structural properties (Robert and Peter, 2016). Optimization with a few simple structures where the film thickness takes a few distinct values can minimize the coefficient of friction torque in the new bearing geometry (Kalle, 2020).

The aim of this research is to create the different geometry (circle, triangular, square, rectangular) holes on the outer ring to see the improvement of reducing the contact area between ball bearing and outer ring. The contact pressure on rolling elements is dependent on the length of the contact surface. When the optimized geometry is properly constructed, it is predicted to significantly improve the bearings' stability properties. However, conventional bearing geometries are based on a fixed logarithmic spiral curve, and there is no literature on how to effectively change the groove geometry to drastically improve the bearing characteristics (Hashimoto, 2008).

In the words of Wikipedia, CATIA or know as computer-aided three-dimensional interactive application is a multi-platform software suite for computer-aided design (CAD), computer-aided manufacturing (CAM), computer-aided engineering (CAE), 3D modeling and product lifecycle management (PLM), developed by the French company Dassault Systèmes. Software CATIA V5 has been used to manufacture prototypes in designing and optimizing CAD models. After that the design will be printed out by Selective Laser Sintering (SLS) as a sample. SLS is an additive manufacturing process that employs a laser as the power and heat source to sinter powdered material (usually nylon or polyamide), autonomously targeting the laser at places in space defined by a 3D model and binding the material together to form a solid structure. In this case, Nylon PA12 is selected for prototyping model. Nylon PA12 has strong impact strength, great chemical resistance, low specific density, outstanding barrier characteristics, and ideal impact strength at lower temperatures, as well as excellent dimensional stability for 3D printing.

SIMSOLID is also being used in this case. SIMSOLID is a next-generation simulation program created for structural analysis on complicated assemblies and designs by engineers and designers. So, in SIMSOLID software, simulate the performance of the new design to get forces and reaction pressure on various connections (contacted surfaces during operation). Meanwhile, a rotating shaft powered by an accelerometer, a surface roughness tester, and a scanning electron microscope machine are used for physical simulation. As a result, prototypes' vibration analysis, surface roughness, wear analysis, and chemical composition are all documented.

1.2 Problem Statement

According to MARKET RESEARCH REPORT, the worldwide bearings market was valued at USD 118.23 billion in 2020 and is predicted to increase to an 8.6% CAGR during the forecast period. Bearings are components that bear a load while in contact with or moving relative to another element. Bearings allow for movement between a machine's stationery and mobile parts, reducing friction and machine wear and tear. The product is available in ball, roller, ball thrust, roller thrust, and tapered roller thrust bearings. Ball bearings are the most prevalent and are utilized in a broad variety of applications. Bearings nowadays must withstand tremendous loads, high speeds, and a variety of environmental conditions (corrosive, humidity, temperature, and so on). This may cause an increase in the market value of bearings in the future. As a result, bearing performance is crucial to meeting functional requirements. Friction issues, such as wear and overheating, are the most typical causes of bearing failures.

Friction is the force that prevents one solid item from slipping or rolling over another. Frictional forces, such as the traction required to walk without slipping, can be useful, but they can provide a significant amount of resistance to motion (Adam, 2018). There are a few types of friction which are dry friction, fluid friction, lubricated friction, skin friction, and internal friction. As two surfaces move relative to each other, friction between them turns kinetic energy into thermal energy (that is, it converts work to heat). The interactions between temperature and power loss of components within an application are complicated, and these elements are interdependent with many others, such as bearing sizes, loads, and lubrication conditions (SKF).

According to Amonton's second law, the friction of an item is governed by the qualities of the surface with which it comes into contact (Pranay, 2019). The magnitude of the friction force experienced between two dry solid bodies across a surface of contact is proportional to the size of the normal force between them. Plus, rolling friction is an important consideration in bearing design and performance. It is the rolling motion resistance that occurs between the rolling components and the bearing races. Rolling friction influences the load capacity, durability, and overall efficiency of the bearing. Consequently, to overcome bearing friction, it is critical to analyze the influence of the contact area during rotational motion. Another than that, the Nylon PA12 material properties are used as prototype material suitable for future material in manufacturing bearing. This is because Nylon PA12 has strong impact strength, great chemical resistance, low specific density, outstanding barrier characteristics, and ideal impact strength at lower temperatures, as well as excellent dimensional stability for 3D printing (WAZP, 2021). One study has investigated the mechanical characteristics and wear resistance of nylon PA12 in ball bearing applications in another investigation. According to the findings of the study, nylon PA12 has great stiffness and exceptional wear resistance, making it appropriate for use in ball bearings that

UNIVERSITI TEKNIKAL MALAYSIA MELAKA

operate at high speeds and under severe loads (Zhang, 2018). It also offers damping noise and vibration which can increase reliability lifetime and reduce the noise. Finally, use of selective laser sintering (SLS) 3D printing offers a capacity to construct complicated geometries that would be difficult or impossible to fabricate using existing technologies. SLS is great for custom bearings that require precise shapes, sizes and reduce friction because it can build elaborate patterns, internal chambers, and fine features with high precision and accuracy.

1.3 Objective

The objectives of this project are stated as below:

1. To fabricate a new optimized geometry of thrust bearing.
2. To test the develop bearing according to vibration testing.
3. To investigate the tribological behavior of the developed bearing.

1.4 Scope

The scope of this research are as follows:

1. Fabricating the new optimized geometry bearing using CAD/CAE; A simulation is run by utilizing SIMSOLID and a prototype bearing is printed using the SLS process.
2. Testing the developed bearing by computerized vibration analyzer to validate the performance of the newly designed bearing in comparison to the previous type (PT 500.04).
3. Investigating new bearing's tribological behavior is assessed using a profilometer (surface roughness tester- SJ401) and surface morphological analysis (SEM).

اونيۏرسيتي تيكنيكل مليسيا ملاك
UNIVERSITI TEKNIKAL MALAYSIA MELAKA

CHAPTER 2

LITERATURE REVIEW

2.1 Introduction

According to JTEKT, bearings play an important function in many machineries and equipment by allowing for smooth rotation and decreasing friction. They are essential components found in vehicles, airplanes, generators, home appliances, and a variety of other gadgets. Bearings allow these devices to run quickly and effectively by supporting the spinning shafts within them.

Bearings' primary role is to reduce friction and increase rotational smoothness. When a shaft rotates, it experiences resistance from the supporting components. Bearings are installed between the spinning shaft and the supporting portion to minimize friction and hence energy consumption. This function is critical because it guarantees that the machinery performs optimally. Furthermore, bearings safeguard the supporting elements and ensure the spinning shaft's precise placement. Bearings operate as a barrier between the shaft and its supporting components during operation, avoiding damage caused by these forces. Furthermore, they guarantee that the spinning shaft remains in the right position, allowing the machine to perform consistently over long periods of time.

The operation of many machineries would be significantly hampered without bearings. Bearings may appear to be basic mechanical components, yet their importance cannot be emphasized. They are commonly recognized as the machine industry's backbone because of their crucial function in ensuring smooth rotation, decreasing friction, and protecting important components. Therefore, bearings are an essential and irreplaceable element of modern machinery, enabling us to benefit from the convenience and reliability of countless devices that we rely on in our daily lives.

2.1.1 The development of bearing

In different periods of time, the engineers were using knowledge and creativity to create a new idea of bearing to improve the function and quality.

Table 2.1 Evolution of Bearing in Different Period, source (Dean, n.d)

Year	Descriptions	
2600 BC		The Ancient Egyptians employed roller bearings to aid in the movement of enormous stone chunks used in the construction of the Pyramids.
40 BC		An early known example of a hardwood ball bearing was used to support a revolving table. This sample was discovered in the wreckage of a wrecked Roman ship in Lake Nemi, Italy.

UNIVERSITI TEKNIKAL MALAYSIA MELAKA

1500 AD	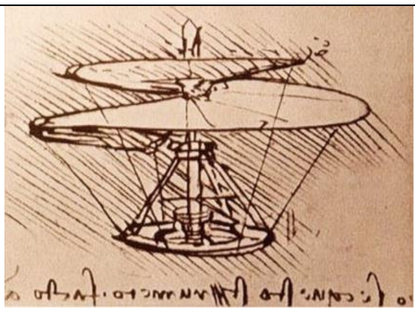	Leonardo da Vinci employed ball bearings in his blueprint drawings and early concept design of a helicopter. This is the earliest documented usage of bearings in aeronautical design.
17TH CENTURY	For the first time, Galileo explains a caged bearing.	
1740	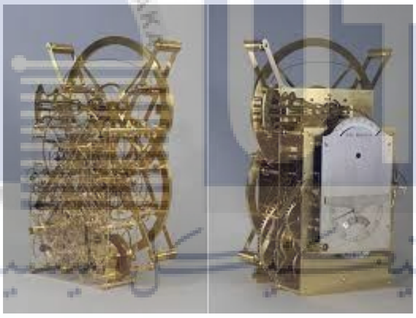	The first caged roller bearing for H3 maritime timekeeping is invented by John Harrison. He had overlooked that he was using the identical bearing in a modern regulated clock.
1794	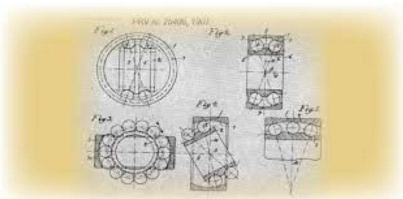	Philip Vaughn of Carmarthen, Wales, was given the first patent for the ball race. His concept included a ball that ran down a groove in an axle assembly.

UNIVERSITI TEKNIKAL MALAYSIA MELAKA

1869		Jules Suriray, a Parisian bicycle mechanic, wins the first patent for a radial ball bearing, which he installed on the winning bike of the world's first cycling race in Paris.
1898	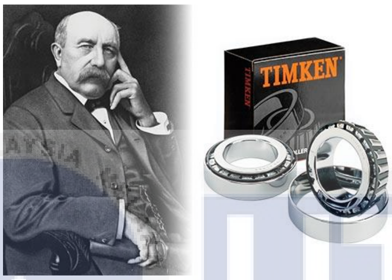	Timken Tapered Roller Bearings receive their first patent. Henry Timken launched his firm the next year.
1907	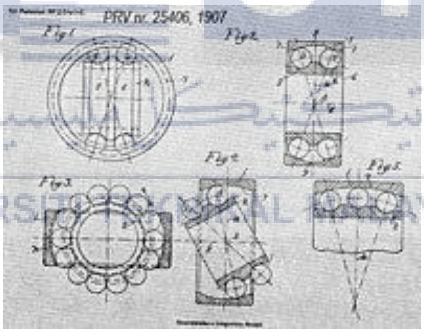	Sven Wingquist of SKF invents new self-aligning ball bearings. This established a new design standard, and inventions such as the wire race bearing in 1934 and the vee groove bearing in 1968 arose as a result.
1917		During World War I, US bearing producers decided to organise an informal cooperative to help with bearing

UNIVERSITI TEKNIKAL MALAYSIA MELAKA

		manufacturing. This resulted in the formation of The American Bearing Manufacturers Association (ABMA).
1960		Elasto-hydrodynamic theory describes how bearings and gear's function, which has led to breakthroughs in grinding accuracy and ultrasonic technology.
1980		Robert Schroeder created the first bimaterial plain bearing here. Schroeder founded Pacific Bearing.
2000		Ball and roller bearings are now employed in a wide range of industrial applications, from automobile wheel bearings to ultra-high-speed bearings used in dentistry drills and everything in between.

UNIVERSITI TEKNIKAL MALAYSIA MELAKA

2.1.2 General types

Bearings come in a variety of sorts that are adapted to specific demands, allowing us to manage the degrees of freedom of a component. They serve an important function in restricting movement and guaranteeing stability, making them vital in a wide range of applications across industries.

Table 2.2 Types of Bearing

Type		Description
Plain bearing		• It is the simplest form of bearing. It just has a bearing surface and no rolling components. The shaft is spinning inside the bearing hole. It offers sliding friction that is larger than rolling friction. Shaft spinning inside the bearing surface is an example.
Rolling element bearing	 	• A rolling-element bearing is a type of bearing that supports a load by sandwiching rolling elements (such as balls or rollers) between two concentric, grooved rings known as races. The relative motion of the races permits the rolling parts to roll with very little rolling resistance and very little slippage.

UNIVERSITI TEKNIKAL MALAYSIA MELAKA

Linear bearing		• The linear bearing has balls or rolling components between two races and is used to provide linear motion to any component. A sliding door, drawer in a cabinet, and so forth are basic examples of linear bearings.
Magnetic bearing	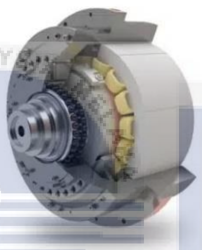	• Magnetic bearings employ the notion of Magnetic Levitation to maintain moving elements in the air. It is a common bearing since the spinning element has no speed limit. There are two types of magnetic bearings: active and passive. In the Active version, we employ an electric magnet that turns on when the shaft travels out of place to return it to the centre. In the passive kind, we employ permeant or fixed magnets, which are challenging to build.

UNIVERSITI TEKNIKAL MALAYSIA MELAKA

Fluid bearing		• These are cutting-edge bearings that are rapidly replacing metal bearings. The fluid is subjected to two-element contact, which lowers friction. Due to fluid pressure, two components never come into touch. It is less loud and vibrates less than conventional metal bearings.
Jewel bearing		• A simple bearing with the spindle spinning in a jewel-lined pivot hole. delivers reduced friction, extended life, and high dimensional precision. It is commonly used in mechanical watches.
Composite bearing		• A composite bearing is a type of bearing that uses a combination of materials to improve performance. It typically comprises of a resin matrix reinforced with fibres, as well as lubricants and other friction-reducing additives. This combination of components improves the bearing's longevity, load capacity, and efficiency.

UNIVERSITI TEKNIKAL MALAYSIA MELAKA

2.1.2.1 Thrust ball bearing.

The single-row deep groove ball bearing chose from among the numerous varieties of ball bearings. For increased performance and functionality, we particularly insert a thrust ball bearing (as illustrated in Figure 2.1) into the rolling element system in our prototype model. In our design, this mix of bearing types allows for efficient rotation and smooth operation.

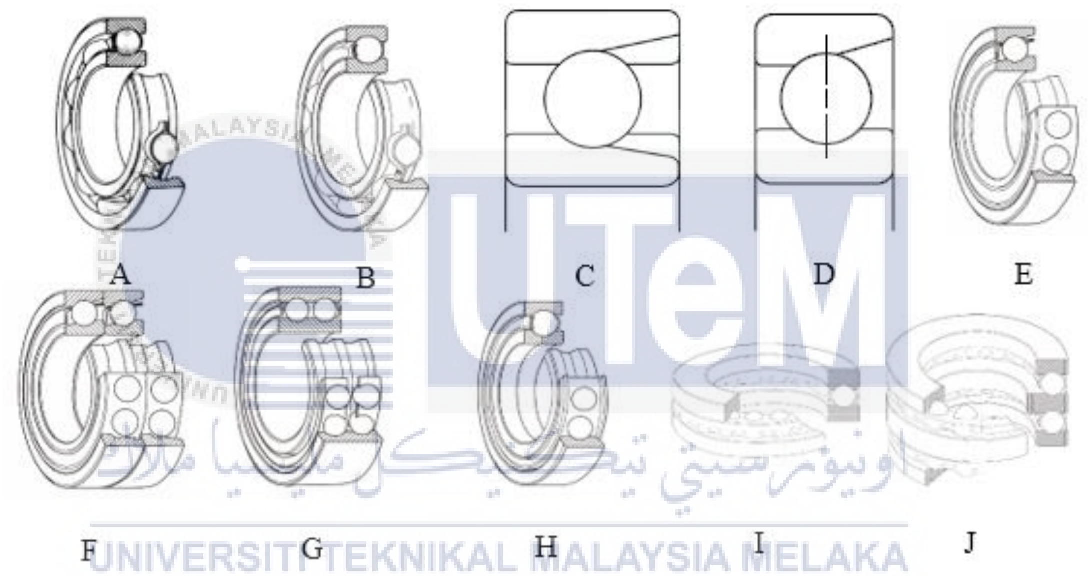

UNIVERSITI TEKNIKAL MALAYSIA MELAKA

Figure 2.1 Types of Ball Bearings

Table 2.3 Features for Types of Ball Bearings, source (NSK.com, n.d.)

Types of bearing	Name	Features
A	Single-Row Deep Groove Ball Bearings	• Support radial and axial loads. Single-row DGBBs can withstand both radial and axial stresses.

		• Proven performance. DGBBs are the most common type of bearing and have been utilised in many applications.
B	Extra Small Ball Bearings and Miniature Ball Bearings	• A diverse selection. A variety of types are available for both general and specialised purposes. • Various protective arrangements. There are three options: open, sealed, and shielded.
C	Maximum Ball Bearings	• High radial load capacity. Because they include more balls than deep groove ball bearings, maximum ball bearings can withstand high radial stresses. Due to the ball filling slots, they are not appropriate for axial stresses. • Standard dimensions Shared boundary dimensions (BL2/Series 62, BL3/Series 63) allow for simple replacement.

UNIVERSITI TEKNIKAL MALAYSIA MELAKA

D	Magneto Bearings	• Design is unique. Magneto bearings have a shorter inner ring groove than deep groove ball bearings, and the outer ring groove has a shoulder on just one side (counter-bored outer ring). • Easy-to-mount. A detachable outer ring aids with installation.
E	Single-Row Angular Contact Ball Bearings (Pressed Steel Cages & Machined Brass Cages)	• Support both radial and axial loads These bearings can withstand radial and axial stresses in a single direction and have typical contact angles of 30° or 40°. • A range of contact angles Larger contact angles are preferable for axial loads, whereas lower contact angles are better for high-speed spinning. • The internal clearance of two opposing bearings is changed. Pressed steel cages are commonly utilised, although polyamide resin cages are frequently employed for high-precision bearings with contact angles less than 30°.

UNIVERSITI TEKNIKAL MALAYSIA MELAKA

F	Matched Angular Contact Ball Bearings	• Flexible arrangements The way the bearings are joined defines angular ball bearing sets. Bearings can be positioned with their outer ring front faces aligned (face-to-face/DF), back faces aligned (back-to-back/DB), or both in the same direction (tandem/DT). • Support axial and radial loads DF and DB configurations can withstand radial and axial loads in both directions. DT configurations are utilised for heavy axial loads in a single direction. • High precision Precision class setups are frequently utilised with machine tool main spindles. In this situation, a preload is applied based on operating circumstances to alter the internal clearance. They also employ a unique fit.
G	Double-Row Angular Contact Ball Bearings	• Design that is limited Double-row angular contact ball bearings are made up of a single inner and outer ring

UNIVERSITI TEKNIKAL MALAYSIA MELAKA

		and allow an integrated back-to-back mounting of two single-row ACBBs. • Axial loads must be supported. ACBBs with two rows can withstand axial (thrust) loads in both directions.
H	Four-Point-Contact Ball Bearings	• Simple to use. The outer ring of these specialised single-row angular contact ball bearings can be divided from the inner ring's two halves by a plane perpendicular to the shaft centre. • Axial load capacity is very high. Four-point-contact bearings with a contact angle of 35° are well-suited for pure or combination loads with a high axial load. • Compact A single bearing can replace a face-to-face or back-to-back bearing system.
I	Single-Direction Thrust Ball Bearings	• Design expertise The balls are contained in a cage, and the grooved aligning seat washer guides them. • Components with specific functions

اونيورسيتي تيكنيكل مليسيا ملاك
UNIVERSITI TEKNIKAL MALAYSIA MELAKA

		Washers attached to the shaft are referred to as "shaft washers," whereas washers attached to the housing are referred to as "housing washers" (fixed rings). • Axial loads must be supported. Thrust ball bearings with a single direction of rotation can withstand axial stresses in just one direction.
J	Double-Direction Thrust Ball Bearings	• Specialised design The balls are held in place by a cage, which is guided by a grooved aligning seat washer. • Dedicated components Washers attached to the shaft are known as "shaft washers," whereas those linked to the housing are known as "housing washers." • Support axial loads in both directions Both ways thrust ball bearings can resist axial loads in both directions. Thrust ball bearings with aligning seat washers reduce mounting errors.

UNIVERSITI TEKNIKAL MALAYSIA MELAKA

2.1.3 Bearing properties

Bearing development has been driven by the necessity to satisfy distinct industrial needs under a variety of operating situations. Several features were considered during this procedure, including corrosion and chemical resistance, cost-effectiveness, lightweight design, and durability. These qualities guarantee that bearings can work successfully in a variety of settings and give optimal performance while meeting specific industry requirements.

Table 2.4 Bearing Properties

Properties	Description
Carbon steel	Carbon steel is distinct from stainless steel in that it contains up to 2.1% carbon by weight. The larger the carbon concentration, the more powerful the bearing. However, it becomes less ductile, has a lower melting point, and cannot work at high speeds or with huge loads. The advantages of employing carbon steel bearings are their low cost and toughness.
Chrome steel	Because of its low cost, high hardness level, and quieter working volume, chrome steel bearings are one of the most popular types of bearing components and materials. Despite its name, a chrome steel bearing contains very little chromium. The advantages of adopting a chrome steel bearing end with the high hardness, high load capacity, low decibel, low cost, and wide accessibility. However, it requires lubrication and is not resistant to corrosion or chemicals.

UNIVERSITI TEKNIKAL MALAYSIA MELAKA

Stainless steel	Stainless steel is the last steel material utilised to make industry-ready bearings. The composition has less carbon than carbon steel bearings, but more chromium than chrome steel bearings. A stainless-steel bearing is more effective, accurate, robust, and long-lasting than most other bearing kinds. The only disadvantages are the heavier content, the requirement for lubrication, and the higher expenses.
Ceramic	Ceramic bearings are designed to be very non-corrosive and long-lasting, with two ceramic rings and a fluorine resin retainer. Due to the non-magnetic requirements of the machinery, this material was chosen above stainless steel and its variations. The benefits of employing a ceramic ball bearing include high hardness, anti-corrosion, durability, lightweight, high-temperature resistance, low density, and minimal maintenance owing to the lack of lubrication.
Polymer plastic	Many non-metallic materials are also utilised to create ball and roller bearings due to their lightweight properties, among other things. The following plastics and polymers are utilised in the bearing industry: Nylon Silicone Nitrate Phenolic Teflon (PTFE) Nitrile Rubber

UNIVERSITI TEKNIKAL MALAYSIA MELAKA

	Polymer plastic bearings offer large temperature ranges and inherently low friction capabilities due to its porous composition, requiring no lubrication. Other advantages of employing polymer plastic bearings include corrosion, chemical, and rust resistance, as well as a lightweight body with high strength that may be utilised in a variety of industrial machinery.
Hybrid	Hybrid bearings are manufactured with best practice in mind. Using high radial and axial strength of steel for the rings and bearing grade silicone nitrate to manufacture the rolling elements, it provides electrical insulation. With this, hybrid bearing types feature the benefits of high wear resistance, varied industry application scenarios, higher speed capabilities than most and non-conductive components for temperature rises or RCF.

UNIVERSITI TEKNIKAL MALAYSIA MELAKA

2.1.3.1 Polymer Plastic (Nylon PA 12)

For the prototype, Polymer Plastic (Nylon PA 12) was utilized. It is a versatile multipurpose plastic with a wide range of additive uses. It is popular in the 3D printing area due to its excellent performance in flexibility without fracture, toughness, tensile, and impact strength.

Table 2.5 Properties for Nylon 12, Nylon 12 GF, And Nylon 11

Specification	Nylon 12	Nylon 12 GF	Nylon 11
Ultimate Tensile Strength	50 Mpa	38 Mpa	49 Mpa

Tensile Modulus	1850 Mpa	2800 Mpa	1573 Mpa
Elongation at Break (X/Y)	11%	4%	40%
Elongation at Break, Z (%)	6%	3%	N/A
Notched IZOD	32 J/m	36 J/m	71 J/m
Heat Defection Temp. @ 1.8Mpa (°C)	87	113	46
Heat Deflection Temperature (HDT) @ 0.45Mpa	170 °C	171 °C	182

2.1.4 Manufacturing of Bearing

UNIVERSITI TEKNIKAL MALAYSIA MELAKA

Bearings can be made in a variety of ways, depending on their individual design needs. Casting, machining, forging, precise grinding, and other techniques are used to make bearings with a variety of forms, sizes, and performance characteristics to suit different applications and industries.

Table 2.6 Reference Research on Geometry Optimization

Type of bearing	Manufacturing process	Description
Metal bearing	• Machining • Heat treatment	Steel bar is heated and chopped before being pressed and moulded into inner and outer rings. Following that, the turning operation to eliminate extra material

	• Grinding • Die • Press molding	for the inner and outer rings follows the designs. The inner and outer rings are then heat treated to harden them. Later, proceed to the grinding procedure to achieve precise finish tolerances and surface finishes. Later, the steel balls or rollers are died punched, then run through a grinder to eliminate bumps before being shaped by another machine. While the cages are made using press moulding. Finally, all the pieces are being put together.
Ceramic bearing	• Hot isostatic pressing (HIP)	Apply high-pressure hot gas uniformly in all three directions of the furnace to build intricate structures from ceramic particles. This method decreases metal porosity and increases the density of various ceramic materials.
Plastic bearing	• Injection molding	Because of the large temperature differential between the material melt and the tool-surface temperature, the material in contact with the tool surface cools quickly throughout the injection moulding process as the mould tool fills.
	• CNC machining	CNC machining is a typical subtractive manufacturing technology that begins with a solid

UNIVERSITI TEKNIKAL MALAYSIA MELAKA

	block of material and removes material until the desired final form is obtained.

2.1.5 Addictive Manufacturing

Additive manufacturing, often known as 3D printing, is a revolutionary method that includes constructing a product layer by layer with specialized software and equipment. It provides a variety of object-creation procedures, including VAT Photopolymerization, Material Jetting, Binder Jetting, Material Extrusion, Powder Bed Fusion, Sheet Lamination, and Directed Energy Deposition. To make our bearing, we used the Powder Bed Fusion process, namely Selective Laser Sintering (SLS). This approach includes utilizing a laser to selectively fuse powdered components together, resulting in a long-lasting and precise product. SLS and other additive manufacturing techniques have opened new opportunities for customized, complicated, and efficient manufacturing processes in a variety of sectors.

Table 2.7 Powder Bed Fusion

Type	Description
Powder Bed Fusion	Powder bed fusion is an additive manufacturing technology that includes melting and fusing powdered material together using a thermal energy source such as a laser or electron beam. A tiny coating of powder is deposited on a build plate to begin the process. The thermal energy source selectively melts the powder to generate a solid layer in the appropriate shape. After that, another layer of powder is placed, and the procedure is continued until the entire shape is constructed. Powder bed fusion includes several techniques such as selective laser melting

اونيۇرسيتي تيكنيكل مليسيا ملاك
UNIVERSITI TEKNIKAL MALAYSIA MELAKA

	(SLM), selective laser sintering (SLS), electron beam melting (EBM), and direct metal laser sintering (DMLS). Powder bed fusion is frequently performed in a warmed chamber filled with inert gas, establishing a controlled environment, to get high-quality results. This helps to avoid oxidation and guarantees that the material keeps its desirable qualities during the melting and solidification processes. Although powder bed fusion is ideal for making prototypes and visual models, it often takes longer to process than other additive manufacturing processes. Powder bed fusion is widely used in sectors like as aviation, notably for the manufacture of jet engine components. The technology allows for the creation of complicated shapes and elaborate structures with outstanding mechanical qualities. Powder bed fusion's capabilities are expanding and finding greater applications in sectors other than aviation, because to developments in materials and process optimisation.

UNIVERSITI TEKNIKAL MALAYSIA MELAKA

2.2 Low Friction of Thrust Bearing

Friction is a force that resists the inverse direction or propensity of motion between two surfaces in contact. When two objects come into contact and move relative to each other, there is typically resistance or opposition to their motion induced by the interaction of their surfaces. Friction is the term for this resistance to motion.

Friction may occur between solid objects, fluids (such as air or water), or even gases. However, once we refer to friction, we often consider the force that exists between two solid surfaces. It is caused by the imperfections on the surfaces, which interlock and impede motion between them. Friction is caused by electromagnetic forces between the atoms and molecules of the two surfaces in contact.

2.2.1 A Review of types of Friction

There are several types of friction based on the contact state.

Table 2.8 Type of Friction

Type	Description
Dry Friction	A force that resists the lateral motion of two solid surfaces in contact. Dry friction is further classified as static friction between non-moving surfaces and kinetic friction between moving surfaces. Dry friction, apart from atomic or molecular friction, is caused by the interaction of surface characteristics known as asperities.
Fluid Friction	The friction between moving layers of a viscous fluid.
Lubricated Friction	An instance of fluid friction in which a lubricating fluid separates two solid surfaces.
Skin Friction	Drag is the force that resists the movement of a fluid across the surface of a body.
Internal Friction	The force resisting motion between the components making up a solid substance when it undergoes deformation.

UNIVERSITI TEKNIKAL MALAYSIA MELAKA

2.2.2 Dry Friction

Dry friction is the resistance of two solid surfaces in contact with lateral motion. Static friction ("stiction") between non-moving surfaces and kinetic friction (also known as sliding friction or dynamic friction) between moving surfaces are the two regimes of dry friction.

$$F_f \leq \mu F_n, \tag{2.1}$$

F_f is the amount of friction that each surface has on the other. It runs parallel to the surface and in the opposite direction as the net applied force.

μ is the coefficient of friction, which is an empirical feature of the materials in contact.

F_n is the normal force exerted by one surface on the other that is oriented perpendicular (normal) to the surface.

Table 2.9 Laws of Dry Friction

Law	Description
Amonton's First Law	The frictional force grows in proportion to the applied load.
Amonton's Second Law	The frictional force exists regardless of the visible area of contact.
Coulomb's Law of Friction	The sliding velocity has no effect on kinetic friction.

UNIVERSITI TEKNIKAL MALAYSIA MELAKA

2.2.2.1 Sliding Friction and Rolling Friction

When an object slides across a surface, sliding friction develops; sliding friction is weaker than static friction. Dry friction laws are used.

Rolling friction occurs when a wheel, ball, or cylinder rolls freely on a surface, such as in ball or roller bearings. The loss of energy involved in object deformation is the main cause of friction in rolling. Sliding friction coefficients are sometimes 100 to 1,000 times larger than rolling friction coefficients for equivalent materials. Historically, this benefit was supplied by the move from sledge to wheel.

2.2.3 Coefficient of Friction

The coefficient of friction (COF) is a measurement of the degree of friction between two surfaces. A low coefficient of friction means that the force required for sliding is less than the force necessary when the coefficient of friction is large. Furthermore, COF is equal to the ratio of the friction force (F) between two bodies and the force (L) that is causing them to collide.

$$\mu = \frac{F}{L} \tag{2.2}$$

2.2.4 Normal force

The normal force is defined as the net force that compresses two parallel surfaces together and has a perpendicular direction to the surfaces and its direction is perpendicular to the surfaces (Figure 2.2).

$$Fn = mg \tag{2.3}$$

m is the mass of object in kg,

g is the gravitation ($9.81ms^{-2}$)

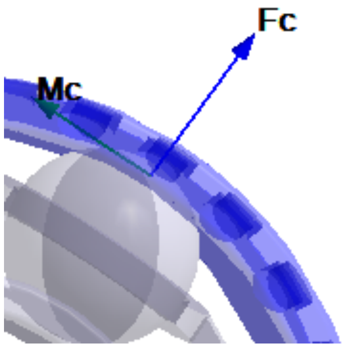

Figure 2.2 Normal Force on The Ball Bearing

2.3 Geometry

Geometry is the study of the forms, proportions, qualities, and connections of figures and spaces. It comes from the Greek words "geo" (Earth) and "metron" (Measurement). The 4 common geometries applied in this research are circle, triangle, rectangular and square.

Figure 2.3 Common Goemetry

2.3.1 Geometry Optimization

UNIVERSITI TEKNIKAL MALAYSIA MELAKA

Geometry optimization in design refers to the process of determining the best form or configuration of an object or system to fulfil design requirements. Geometry optimization is also used in a framework to boost application performance. Several research projects on geometry optimization have been conducted to highlight the discovery and future development prospects.

Table 2.10 Reference Research on Geometry Optimization

No.	Title	Conclusion
1	High-speed structural optimisation of ball bearings with three-point contact	The ball makes separate contact with the two outer raceways to share the excessive centrifugal force of the ball and suppress the difference between the inner-ball contact angle and the outer-ball contact angle, thereby extending bearing fatigue life and slowing the weakening of overall bearing stiffness. However, it also causes the ball motion to be limited by three raceways (two outside and one inner), increasing frictional losses.
2	Geometry Optimization of Textured 3-D Micro-Thrust Bearings	The improvement in W* (non-dimensional load bearing capacity) for infinite width sliders when comparing ideally textured sliders to optimally smooth sliders is 7.5 percent. Large load capacities and low friction coefficients are maintained throughout a wide variety of convergence ratio values.

UNIVERSITI TEKNIKAL MALAYSIA MELAKA

3	The influence of weights and speeds interacting on the dry sliding behaviour of fused filament fabrication Different interior geometry of 3D-printed acrylonitrile butadiene styrene pins	In several sliding circumstances, pins with an internal triangular flip have the best wear resistance and the lowest COF values. Furthermore, when subjected to a high normal load, all pins with different internal geometries demonstrated the lowest COF and wear rates, regardless of sliding speed. However, regardless of their normal loads, rectangular and circular constructions exhibited enhanced wear resistance when the sliding speed was increased.

UNIVERSITI TEKNIKAL MALAYSIA MELAKA

2.3.1.1 Approach for Enchancing the Durability of the Inner Geometry of Spherical Ball Bearings.

According to Zhao (2020), The inner raceway offset distance before and after bearing optimization. The bearing's outer racetrack is stationary, while the inner raceway is offset under load, with the position of the inner raceway's curvature center before and after optimization. The purpose of this study is to look at the effect of inner geometry on the durability and reliability of ball bearings. It is concerned with determining how modifications in the interior design might affect their performance in terms of production processes and competitive advantages.

The purpose of optimization is to lower the contact pressure where the rolling element encounters the outer and inner rings. The structural specifications of single-row four-point ball bearings are listed below.

Table 2.11 Structural Parameters of Single-Row-Four-Point Ball Bearings, source (Zhao, 2020)

Parameters	Value
Ball diameter, D_w (mm)	12.7
Bearing pitch diameter, D_{pw} (mm)	545
Ball number, Z	101
Nominal contact angle, (°)	30
Inner raceway curvature coefficient, f_i	0.54
Outer raceway curvature coefficient, f_o	0.525
Clearance, g_o (mm)	0

2.3.1.2 Textured Three-Dimensional Micro-Thrust Bearings Geometry Optimization

UNIVERSITI TEKNIKAL MALAYSIA MELAKA

In this study, the geometry of three-dimensional micro-thrust bearings is optimized over a wide range of convergence ratios (Papadopoulos, 2011). The bearings are depicted as microchannels with a smooth moving wall (rotor) and a stationary wall (stator) with partial periodic rectangular texturing.

The goal of optimization is to enhance the bearing load carrying capacity. The flow field is approximated using the numerical solution of the Navier-Stokes equations for incompressible isothermal flow, and the bearing load capacity and friction coefficient are calculated using the results. The design of the textured channel was influenced parametrically over a range of width-to-length ratios, B/L. The convergence ratio, k- (HI - Ho) /Ho. The results are acquired by CFD simulations.

When compared to smooth sliders, the use of optimal texture patterns greatly increases bearing load capacity, especially at low convergence ratio values. The load carrying capacity of small-width optimum sliders (B/L up to roughly 1.0) is greater than that of corresponding optimal step bearings.

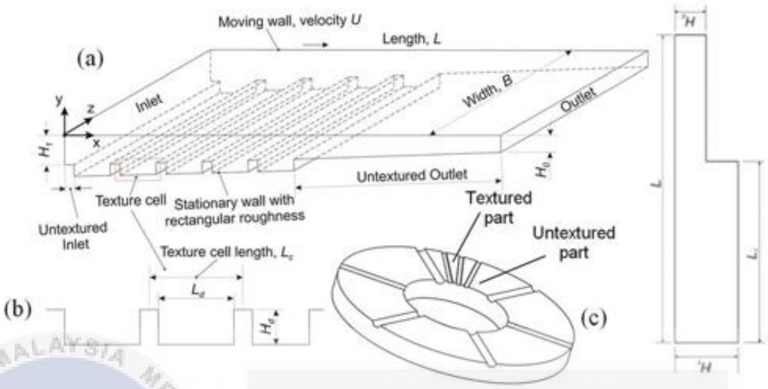

Figure 2.4 Three-Dimensional Parametric CAD Model, source (Papadopoulus, 2011)

Table 2.12 Geometric Properties of Optimum Step Bearings for Various B/L Ratios

Width to length ratio, B/L	Optimum step bearing		
	H_1/H_0	L_1/L	W*
0.5	1.7	0.52	0.027
1.0	1.73	0.58	0.074
1.5	1.75	0.63	0.107
2.0	1.77	0.65	0.128
Inf	1.85	0.72	0.206

UNIVERSITI TEKNIKAL MALAYSIA MELAKA

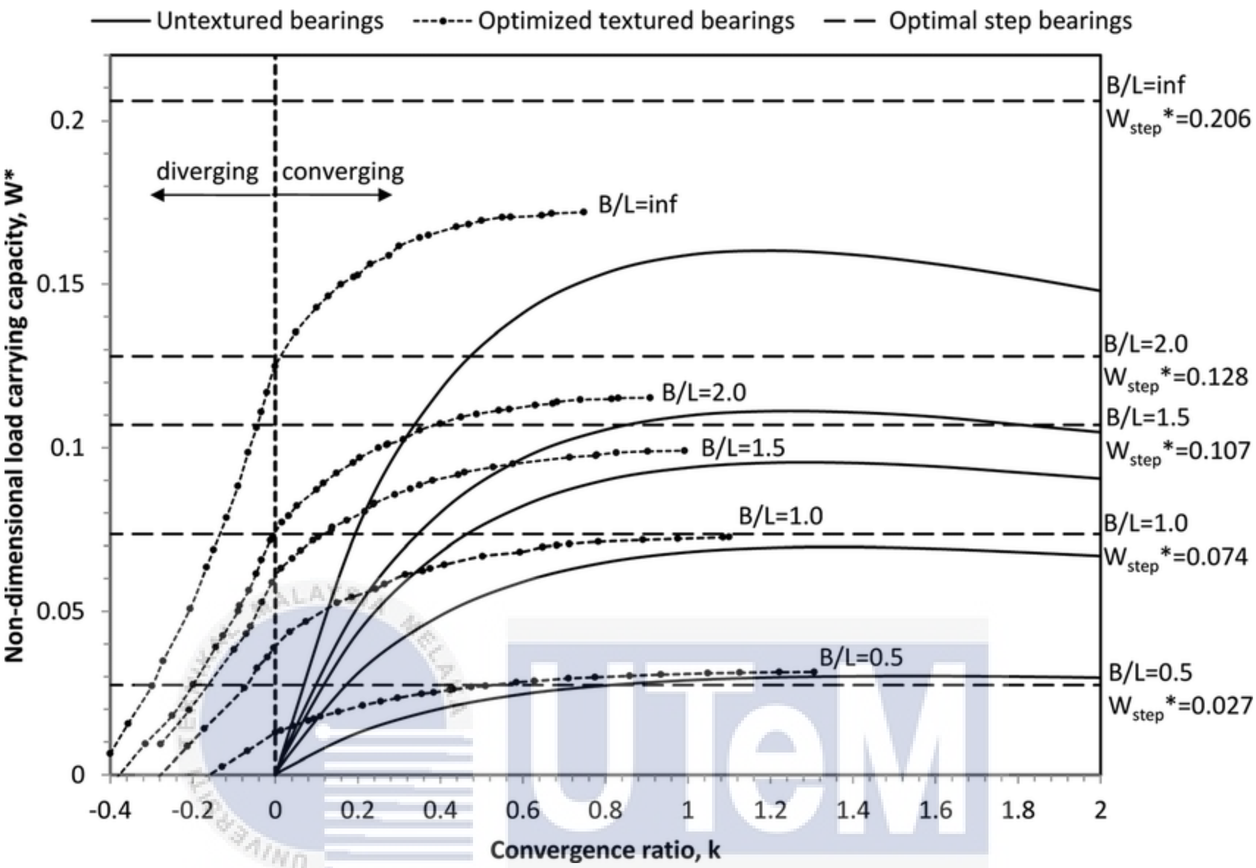

Figure 2.5 Optimization Results, source (Papadopoulus, 2011)

2.3.1.3 Integrative results of dry sliding behavior of the 3D-printed acrylonitrile butadiene styrene (ABS) pins with different geometrics.

UNIVERSITI TEKNIKAL MALAYSIA MELAKA

The primary goal of Abdollah's (2020) research is to evaluate the dry sliding behavior of 3D-printed acrylonitrile butadiene styrene (ABS) pins with varied interior geometry. The study focuses on using fused filament manufacturing technologies to create these pins and testing their performance under various typical loads and sliding speeds.

The study's goal is to find the best interior shape for improving the mechanical characteristics of 3D-printed ABS pins. A DUCOM pin-on-disc tribometer, which enables controlled sliding trials, is used to investigate the dry sliding behavior. Mechanical property testing is also performed using an Instron compression test machine and a Shimadzu micro hardness tester.

The study intends to acquire insights into the impact of different interior geometries on the performance of 3D-printed ABS pins during dry sliding circumstances by analyzing the outcomes of these tests. The final objective is to find the best structure for improving the mechanical characteristics of the pins, which might have potential uses in a variety of sectors that demand high-performance materials. The tribological and mechanical parameters of the 3D-printed ABS pin with various internal geometries have no statistically significant association. The best wear resistance and lowest COF values are found in pins having an interior triangular flip.

UNIVERSITI TEKNIKAL MALAYSIA MELAKA

Figure 2.6 Internal Geometries Structure of Pins, source (Abdollah, 2020)

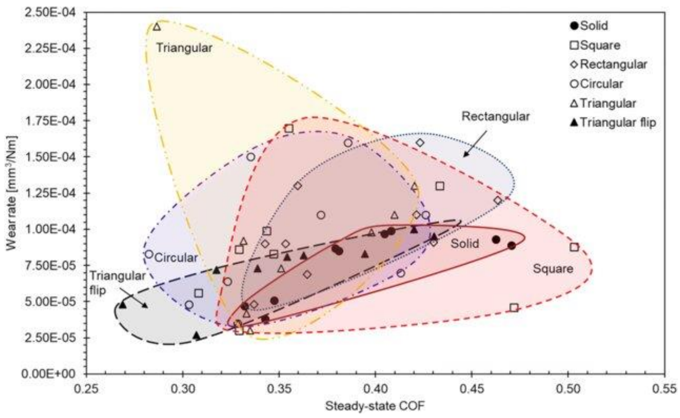

Figure 2.7 Distribution of COF Values and Wear Rates for the 3D Printed ABS Pins, source (Abdollah, 2020)

2.4 Simulation and Bearing Quality.

In Chapter 3.4, it was described how to use the SIMSOLID simulation platform to identify the designed structure and run simulations. This platform enables the analysis of contact response and contact forces on various connections within the structure. We can obtain valuable results about the behavior of the structure under different conditions by inputting the necessary parameters and running the simulation. Furthermore, we mentioned testing bearing prototypes with bearing performance testing equipment equipped with accelerometers and speed sensors. This equipment allows you to evaluate the performance of your bearings by measuring vibration data at various speeds. We analyzed the behavior of the bearings and assessed their effectiveness and reliability in practical applications by recording this data.

2.4.1 Simsolid

SIMSOLID is a comprehensive structural simulation software that provides comprehensive statics, dynamics, and thermal analyses. SIMSOLID's innovative technique of conducting studies without the necessity for meshing distinguishes it from typical finite

UNIVERSITI TEKNIKAL MALAYSIA MELAKA

element analysis (FEA) methods, making it more efficient and less skill intensive. SIMSOLID, unlike FEA, uses fully featured solid geometry models directly, eliminating the time-consuming processes of geometry simplification and mesh generation. This method enables engineers to swiftly examine complicated CAD models without losing accuracy. Additionally, SIMSOLID includes a range of simulation analysis tools, including limitations that may be applied directly to the CAD model, thus boosting its adaptability and efficacy in engineering research (Table 2.13).

Table 2.13 Constraints Applied to Structure, source (SIMSOLID Fast Start Training, 2019)

Function	Descriptions
Immovable 	An immovable support enforces zero translational displacements in all directions. It is applied to one or more of the models' faces.
Hinge 	Hinge supports allow a component to freely rotate around the centre of a cylinder face while preventing movement in both the radial and axial axes. Hinges can only support complete or partial cylindrical faces. Concave or convex cylindrical faces are conceivable.
Inertia Loads (Rotational Inertia) 	Loads of rotational inertia are applied to a rotation axis. Choose a curved cylinder edge to find the rotation axis. If necessary, use the Flip axis button to change the direction of the axis. Drag the ball and arrows to get close to the origin point, then change the text values on the dialogue. Once the object is in position, just define the acceleration along the axis

UNIVERSITI TEKNIKAL MALAYSIA MELAKA

	[a], angular velocity [w], or angular acceleration [E] as desired, then click OK to close the window.
Slider 	A sliding support imposes zero displacement in normal to the surface direction orientations. Tangential displacements have no boundaries. A sliding support can be used to define symmetry planes.

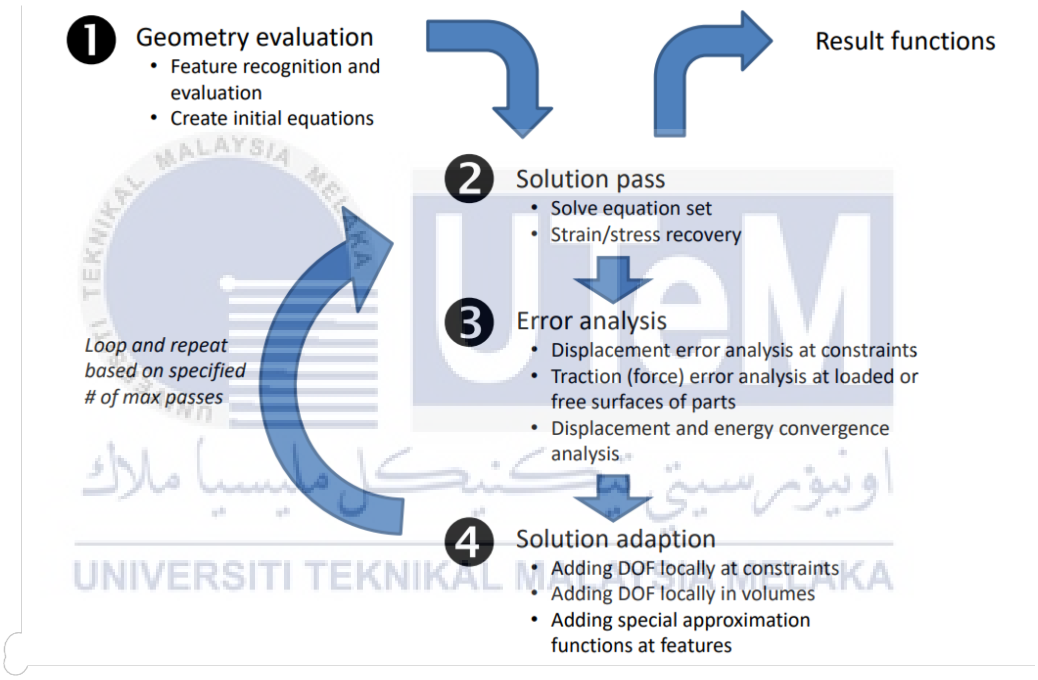

Figure 2.8 SIMSOLID Simulation Process, source (SIMSOLID Fast Start Training, 2019)

2.4.2 Vibration Analysis.

Vibration analysis is a technique for identifying abnormal vibration events and analyzing the overall condition of a component, machinery, or structure by monitoring the levels and patterns of vibration signals inside it. It is a technique for monitoring vibration levels and analyzing vibration patterns. It's commonly done directly on the vibration signal's time waveforms, as well as the frequency spectrum obtained by applying the Fourier Transform to the time waveform.

As a result, it is highly desirable to integrate frequency spectrum analysis with time domain analysis in real-world applications, particularly in rotating equipment. A sophisticated machine with numerous components generates a mixture of vibrations, which is a combination of vibrations from each rotating component. As a result, assessing the status of critical components such as gears, bearings, and shafts in large rotating equipment using just time waveforms is difficult. The frequency components associated with each component may be investigated using frequency analysis, which decomposes time waveforms and explains the repetitiveness of vibration patterns. Furthermore, the well-known fast Fourier transform (FFT) technique enables quick and efficient frequency analysis as well as the building of different digital noise filters. In this investigation, the vibration data was acquired using a PT 500.04 Computerized Vibration Analyzer - G.U.N.T. Hamburg.

2.5 Surface Validation

The Scanning Electron Microscope (SEM) and Surface Roughness Tester are critical tools for detecting and analyzing prototype surface conditions. The scanning electron microscope (SEM) uses electron beams to produce high-resolution pictures of the sample's surface, allowing for thorough investigation of its microstructure and topography. This aids with the detection of any faults, irregularities, or structural traits that may impair performance. The Surface Roughness Tester, on the other hand, quantitatively assesses the roughness of the surface, delivering numerical values that represent the texture and smoothness. This data assists in assessing the quality of the prototypes and ensuring they fulfil the specified requirements. Researchers may acquire significant insights into surface qualities by using this equipment, allowing for improvements and optimizations in the design and production processes.

2.5.1 Surface Roughness Tester

A surface roughness tester is a tool used to evaluate the quality of a surface. It is well understood that rough surfaces wear faster and have greater friction coefficients than smooth surfaces. As a result, roughness is a good signal for forecasting the performance of mechanical parts since defects on the surface act as locations for breakage or corrosion onset. The measurement of average roughness (Ra) is very important in evaluating the performance of bearings with varying geometries. Engineers can acquire insights into the behavior and durability of bearings by accumulating such data, assisting in the assessment and enhancement of their performance.

2.5.2 SEM

SEMs are used in a variety of industrial, commercial, and research situations. SEMs are used in this work to perform wear analysis on prototypes after bearing performance testing. This research enables a thorough assessment of the prototypes' surface properties and wear patterns. Furthermore, the study intends to analyze the dependability of 3D printed prototypes by comparing their chemical composition, texture, and a variety of other aspects. Using SEMs and examining these factors, researchers can acquire insights into the performance and durability of prototypes, assisting in the development of production methods and materials employed.

UNIVERSITI TEKNIKAL MALAYSIA MELAKA

CHAPTER 3

METHODOLOGY

3.1 An Overview of Methodology

This chapter presents a complete and extensive overview of the methodological procedure used throughout the experiment. The main goal of this explanation is to ensure that the research goal is met. Throughout the chapter, numerous critical components are discussed, beginning with a detailed description of the bearing design, and progressing through an exploration of the SIMSOLID simulation used in the study. In addition, the chapter goes into the manufacturing technology used in SLS 3D printing, offering insight on the complexities of this approach. Furthermore, it includes a detailed evaluation of the bearing's performance through rigorous testing, as well as a complete analysis of the acquired data and its subsequent results. The chapter then goes on to explain the approach used for surface validation, with the goal of gaining significant insights into many factors such as surface roughness, wear patterns, textural characteristics, material orientation, and chemical composition. This explanation offers a full discussion of the methodologies and processes used to examine and confirm the surface's integrity and quality.

UNIVERSITI TEKNIKAL MALAYSIA MELAKA

3.1.1 Flow Chart

Figure 3.1 represents a few aspects of the procedure used in this study. The flow chart depicts all the operations involved in evaluating the performance of the new optimized geometry bearings.

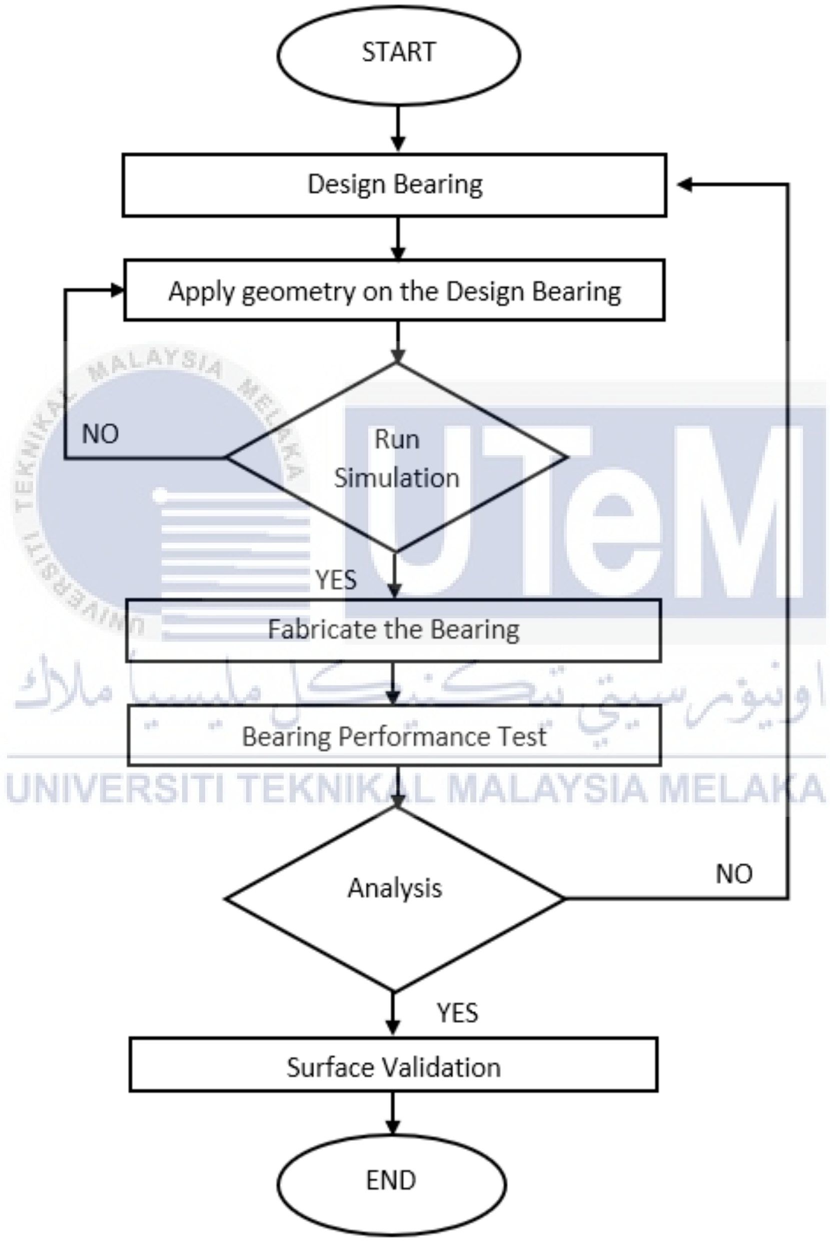

Figure 3.1 Flow Chart

3.2 Texture Design Preparation

Obtaining a reference bearing typically requires a few stages that identify the application's specific requirements. Load capacity, speed, temperature, and climatic variables were all taken into consideration. Once the application requirements have been identified, the type of bearing can be determined. There are several types of bearings accessible in industry, including ball bearings, roller bearings, needle bearings, and others. Once the bearing type has been determined, the manufacturer's bearing specifications must be obtained. This specification will include details like load capacity, speed rating, and other critical metrics. Furthermore, the geometry of the bearing part or assembly is defined for CAD model design. This is accomplished by employing several equipment, including vernier calipers from the reference bearing. The constraints are then imposed to verify that the part or assembly fits the specified design criteria. Dimensions, angles, and other geometric connections were among the constraints. Additional features such as fillets, chamfers, and holes were also added to the model. As a result, testing and refinement are used to guarantee that it fits the design criteria. SIMSOLID's simulation tool is used for this. The model was improved and changed until it met all the requirements. Finally, when the CAD model was completed, production drawings were created to provide specific information about the bearing, such as dimensions, tolerances, and other critical factors.

UNIVERSITI TEKNIKAL MALAYSIA MELAKA

3.2.1 Reference Bearing Selection

At the beginning, a discussion was held, and experiment equipment (Figure 3.2 A&B) was chosen in the vibration laboratory with several considerations to proceed with the bearing performance testing. The ball bearing in (Figure 3.3 A) supports the shaft during rotation. The structural data as the reference model gathered using visual observations, vernier calipers, and series code on the bearings (Figure 3.3 B & Table 3.1).

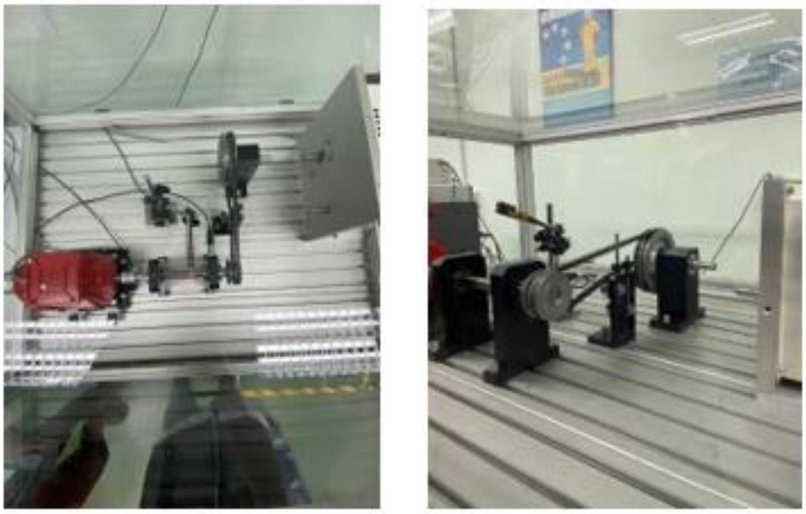

A B

Figure 3.2 A. Bearing Performance Testing Experiment Equipment Top View, B. Bearing Performance Testing Experiment Equipment Left View

UTeM
UNIVERSITI TEKNIKAL MALAYSIA MELAKA

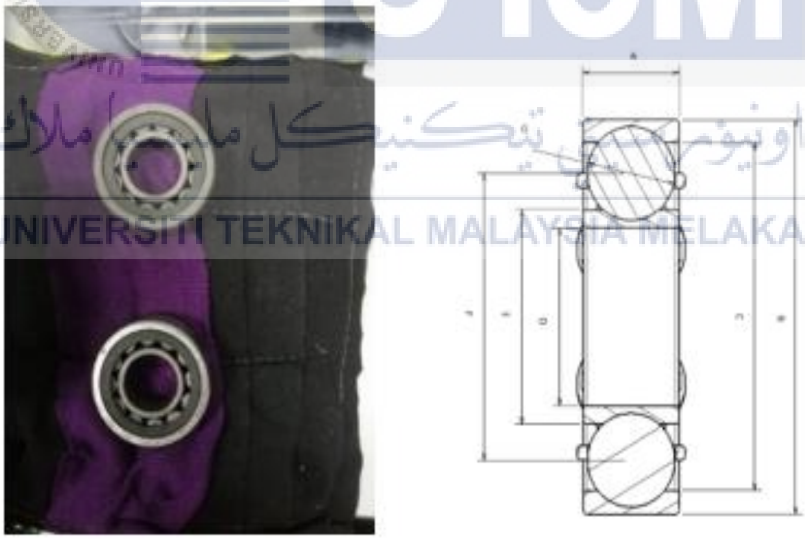

A B

Figure 3.3 A. Cylinder Roller Bearing, B. Bearing 2D Structure Diagram with Labels

Table 3.1 Structure Data for Roller Bearing

Label	A	B	C	D	E	F	G
Dimension (mm)	16	50.2	47	24	26.5	32.7	12.7

3.2.2 CATIA V5R21

The thrust ball bearing is constructed in four parts: the thrust ball bearing, the bearing's cage, the outer ring, and the inner ring (Figure 3.4). With the bearing data collected, we began to design the new optimized CAD model bearing using CATIA V5R21 software. We began by selecting the component design in the mechanical design portion of the software interface to begin creating the part of our bearing. Sketch, Shaft, Pad, Pocket, Chamfer, Edge fillet, Trim, and Circular Pattern are the most often developed tools utilized in the CAD model.

First, use the sketch function to create 2D geometry in the various planes formed by the axes X, Y, and Z. Then, using the shaft and pad functions, we can convert it to a 3D object of the desired shape. Furthermore, the pockets on the 3D bodies, such as the bearing's cage and the geometric shape applied to the outer ring, were created using the pocket function. Aside from that, use the chamfer and edge fillet functions to smooth the edge and reduce friction and impact forces during the rotation motion of the bearing. Finally, a circular pattern is used to generate multiple clones of the selected structure. For instance, the square pattern on the outer ring, the holes in the bearing's cage, and the varying geometry on the outside ring.

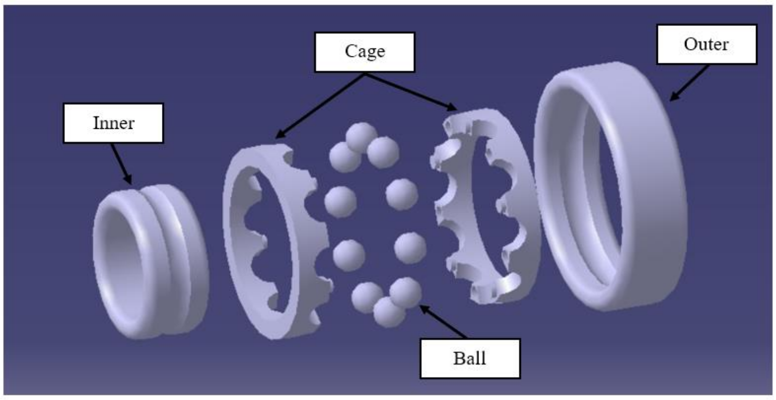

Figure 3.4 Bearing’s Parts

3.3 Impose Geometry on Bearing Design

The diverse geometry holes formed by the pocket and circular pattern functions were discussed in chapter 3.2.2. For the first, follow the appropriate dimensions (Table 3.2) to generate the 2D geometry on either plane. Then, continue with the circular pattern by using the pocket function to make geometry holes at the outer ring. Following the specific numbers and angles (Table 3.3), the circular pattern is used to create multiple holes around the outer ring.

UNIVERSITI TEKNIKAL MALAYSIA MELAKA

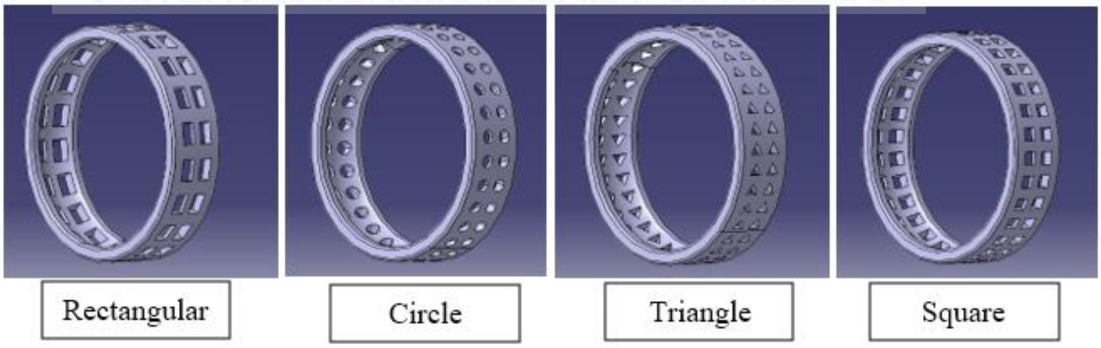

Figure 3.5 Different Geometry on The Outer Cage

Table 3.2 Dimension of Geometry Applied

Geometry	Square	Circle	Rectangular	Triangle
Dimension (mm)	3*3	3	5*3	3
Gap between geometry (mm)	2	2	2	2

Table 3.3 Total Number of Different Geometry and Angle Applied

Geometry	Square	Circle	Rectangular	Triangle
Total number	30	30	20	36
Angle (°)	12	12	18	10

3.4 Simulation Process

SIMSOLID software was performing simulations on the CAD models created in the previous chapter. Initially, the CAD models were imported into SIMSOLID from CATIA V5R21. Then, on the CAD model design, detect structure errors (Figure 3.6) and manually create the connection (Figure 3.7). If there is any overlapping, the bearing will be printed as a faulty product rather than a functional bearing. Following that, the material was applied to the CAD models' part and the performance simulation results in non-linear structure analysis were simulated. Then, apply the immovable function to the outer ring surface, the hinge and rotational inertia to the inner ring, and the slider to both sides of the inner ring. Finally, run all analyses to record all the results in reaction/contact force and response (Figure 3.8).

UNIVERSITI TEKNIKAL MALAYSIA MELAKA

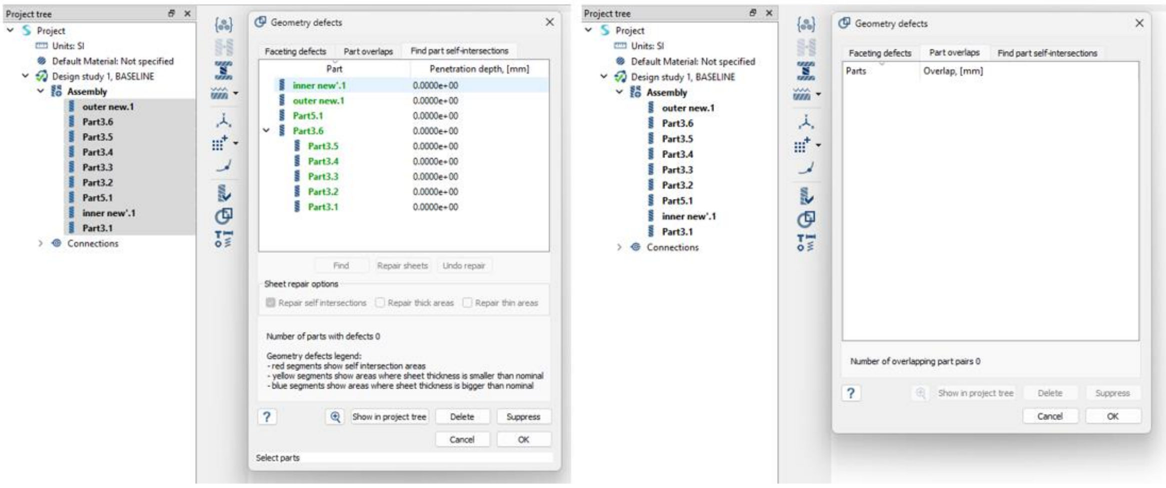

Figure 3.6 Interception and Overlap Results in The Bearing Design

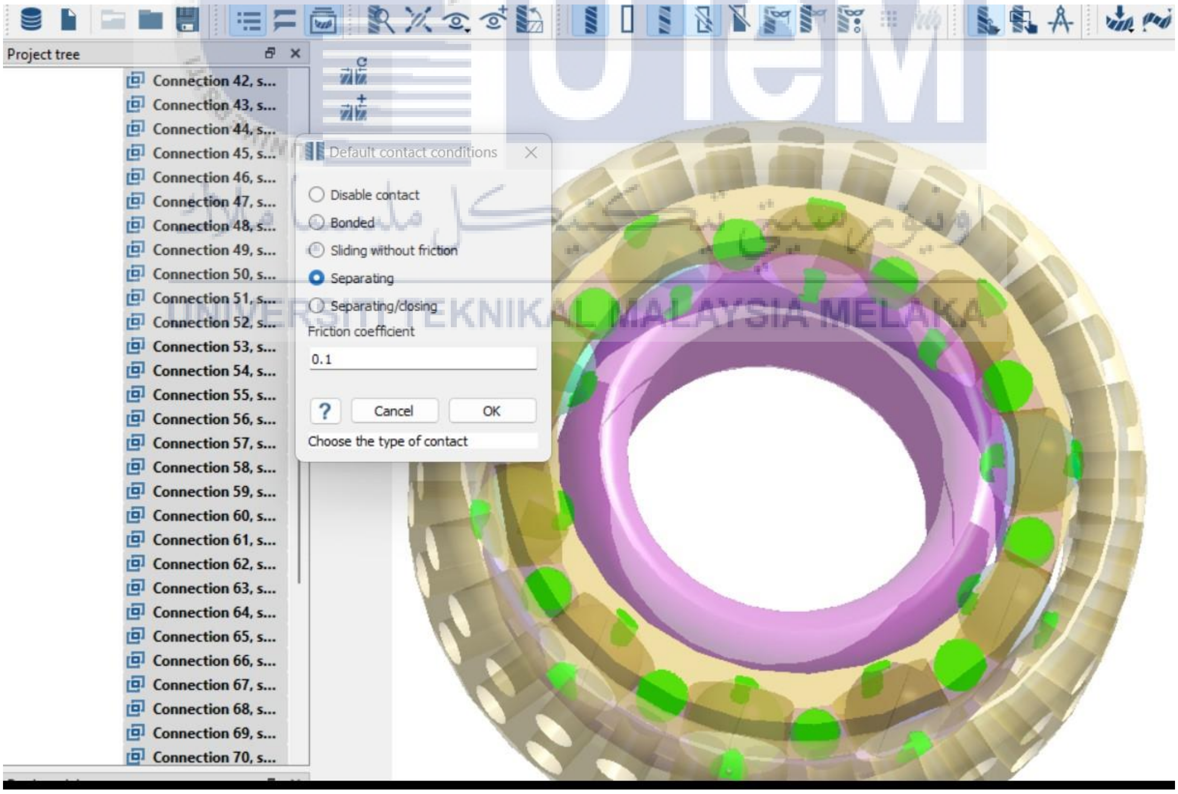

Figure 3.7 Create and Set Up the Connections

UNIVERSITI TEKNIKAL MALAYSIA MELAKA

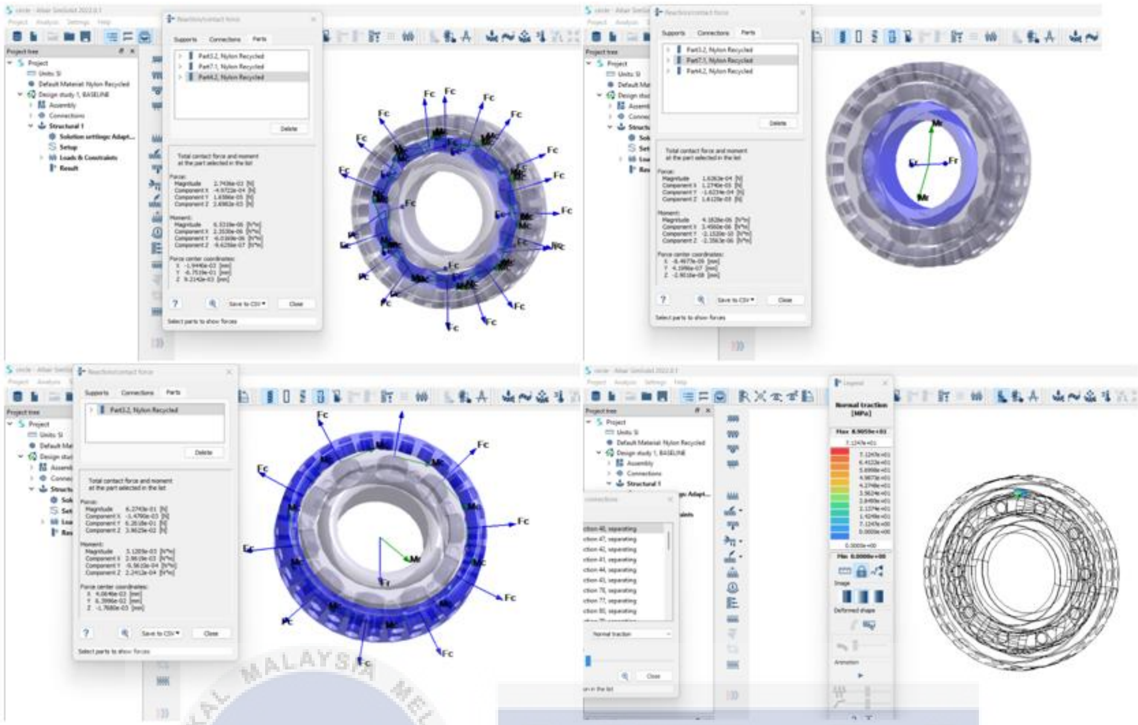

Figure 3.8 Reaction/Contact Force and Respond Result

3.5 Fabrication Process

Fabrication process done by using SLS 3D printing to fabricate the new optimized bearing. Selective Laser Sintering (SLS) is an additive manufacturing process that sinters layers of powder material to build three-dimensional objects. This chapter introduces equipment and the fabrication process flow in SLS 3D printing.

3.5.1 SLS 3D Equipment

Additive manufacturing (AM) techniques provide the efficiency of bottom-up construction of 3D structures by selectively adding material based on CAD data. These approaches have gotten quicker, cheaper, more cost-effective, sophisticated, and higher in resolution and quality. AM has the potential to increase the productivity of many industrial sectors while also providing as a significant resource for aerospace, automotive, and biomedical engineering. Metals, ceramics, polymers (thermoplastics, thermosets,

UTeM
UNIVERSITI TEKNIKAL MALAYSIA MELAKA

hydrogels), and some composite materials, such as magnetic particles suspended in polymer sand cells, can all be employed today. However, the suitable AM technology must be chosen by considering aspects such as the kind of product, material qualities, volume, manufacturing time, and cost.

This study focuses on a specific sort of 3D printing machine, the Farsoon FS402P Selective Laser Sintering (SLS) technology model. The benefits of employing this SLS machine include robust components for functional testing or low-volume manufacturing, as well as a cheap cost with applications in a wide variety of sectors such as aerospace, automotive, medical consumer items, and electronics. Since SLS involves the fabrication of pieces with no support, the design options are practically limitless. In contrast to traditional melting with high shear mixing and fluidity, SLS technology does not compact during processing, making it an important 3D printing approach to produce porous segregated structures. SLS employs a CO2 laser as a heat source to fuse the powders under pressure-free circumstances. Figure 3.9 shows that components in 3D SLS Printing Technology Model follow with its function.

UNIVERSITI TEKNIKAL MALAYSIA MELAKA

Figure 3.9 SLS 3D Printing Equipment

Table 3.4 SLS 3D Printing Descriptions

Equipment	Descriptions
Nitrogen Generator Equipment	Provide nitrogen to the Farsoon SS402P during prototyping to reduce the oxygen concentration.

Farsoon SS402P	In the powder tank, the powder is melted using a laser to make the pieces.
Powder Breakout Station	Station for separating the printed cake, collecting, and cleaning the components. It also recycles and filters the extra powder.
Media Blasting Cabinet	To remove the final powder residue from the pieces, use compressed air and an abrasive medium. Finally, use compressed air to clean up.
Powder Mixer Machine	Using both fresh and recycled powder.
PPE	Prevent powder pollutants from entering the eyes, skin, and respiratory system.

3.5.2 Printing Process

UNIVERSITI TEKNIKAL MALAYSIA MELAKA

The operation setup comprised of three major steps: (i) pre-process stage (Figure 3.10 A-B), (ii) 3D printing process stage (Figure 3.10 C-D), and (iii) postprocess stage (Figure 3.10 E-F). The SLS 3D printer includes four major chambers: a feeder chamber, a construction chamber, a collector chamber, and a powder overflow chamber with levelling roller (Figure 3.11). The volume and weight of the substance were computed at the first stage. The key constant parameters for the SLS 3D printer were established according to the setup during the 3D printing process stage. During the post-processing step, the material block was taken from the SLS Effect of Polyamide-12 Material Compositions on Mechanical Properties 63 machine-building chamber and transported to the sieve machine, as shown in Figure 3.12 (Process 6).

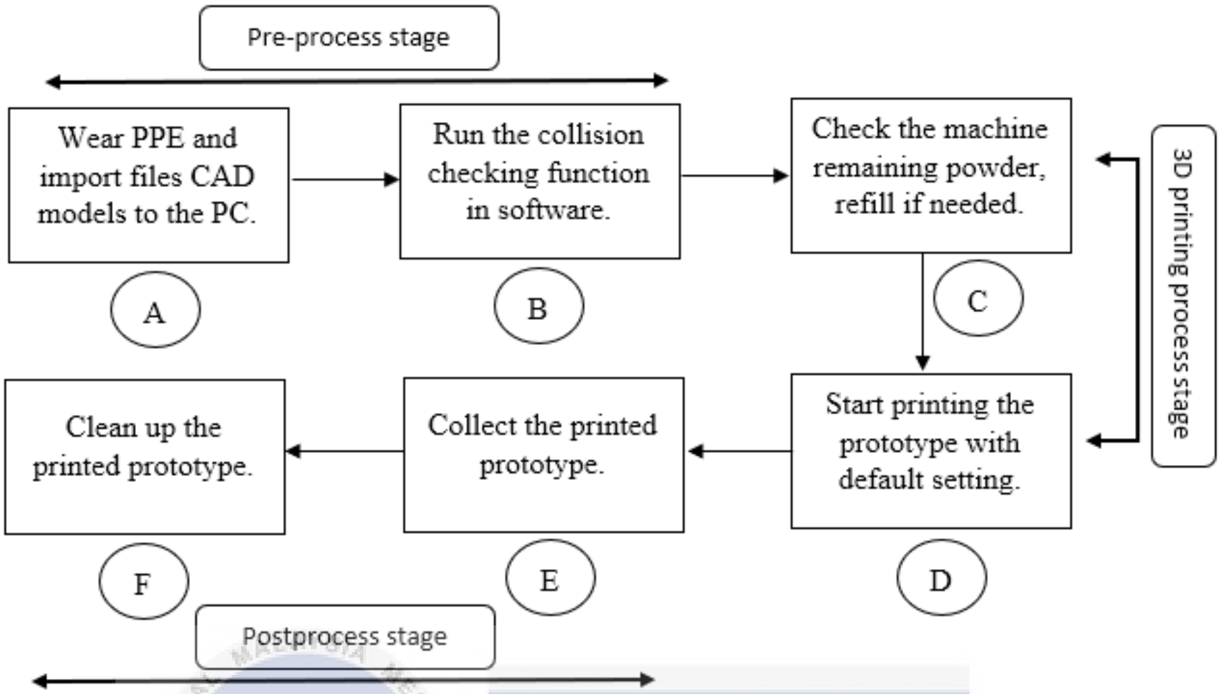

Figure 3.10 SLS 3D Printing Process Flow

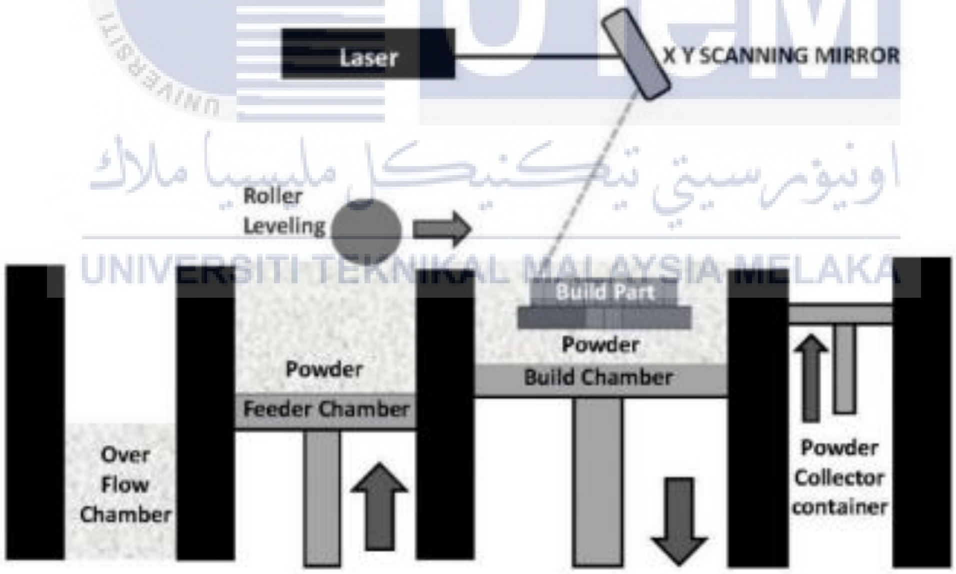

Figure 3.11 SLS Process for Farsoon FS402P, source (Rafi, 2022)

UTeM
UNIVERSITI TEKNIKAL MALAYSIA MELAKA

UNIVERSITI TEKNIKAL MALAYSIA MELAKA

Figure 3.12 Prototyping Process in SLS 3D Printing

Table 3.5 Prototyping Process Descriptions

Process	Description
1	Before beginning, put on PPE and load STI files into the BuildStar software.
2	To decrease powder waste, adjust the bearing position and fill the horizontal vacant area. Check for colliding pieces within the arrangement and make any adjustments.

3	The software will determine the amount of powder required for the prototypes we set up, ensuring that there is enough powder in the tank.
4	Navigate to the MakeStar programme and locate the file for the prototypes layout that we saved in the BuildStar software. Examine the default settings for laser power, printing thickness, and so on. Then, click Start Printing, and the time required to complete the prototypes will be calculated. Click Yes to print the prototypes, and the machine will begin increasing the temperature and decreasing the oxygen level by introducing nitrogen gas in accordance with the specifications.
5	After cooling, remove the printed cake from the Farsoon SS402P and place it in the Powder Breakout Station. Then, activate the filter functions and shatter the printed cake. Gather the prototypes and clean them up with a brush.
6	Using high compressed air, clean the prototypes in the media blasting cabinet.

UNIVERSITI TEKNIKAL MALAYSIA MELAKA

3.6 Performance Test Process

A bearing performance test is a mechanical test that is used to evaluate the performance of bearings. The goal of the test is to determine a bearing's capacity to tolerate varying loads and speeds over time. To guarantee accuracy and consistency of results, the test is often performed under controlled laboratory settings. This chapter explains the experiment equipment, procedure and the result needed.

3.6.1 Experiment Process

The drive unit enables rotational motion to the shaft, which is supported by two cylindrical roller bearings and an unbalanced rotor mounted on the shaft's end. The bearing performance testing equipment is depicted in Figure 3.13 and Table 3.6.

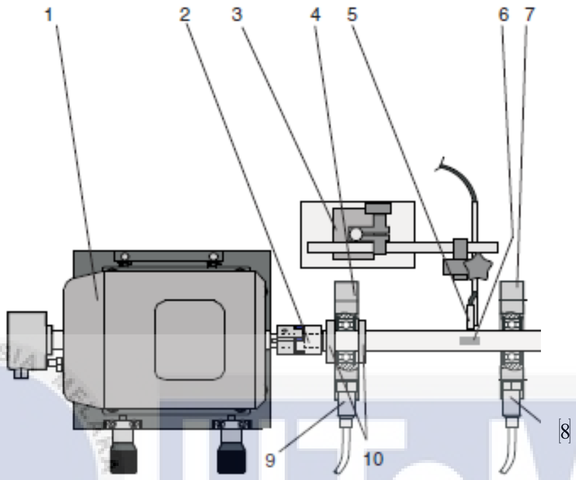

Figure 3.13 Bearing Performance Testing Equipment

Table 3.6 Bearing Performance Testing Equipment Components

No	Equipment
1	Drive unit
2	Elastic claw coupling
3	Magnetic clamp
4,7	Bearing housing
5	Speed sensor
6	Reflective mark
8,9	Accelerometer
10	Shaft collars

UNIVERSITI TEKNIKAL MALAYSIA MELAKA

3.6.2 Vibration Test

In the PT 500.04 Computerised vibration analyzer - G.U.N.T Hamburg, two types of vibration data are collected: the fast Fourier transform spectrum (Figure 3.14) and the envelope analysis (Figure 3.15).

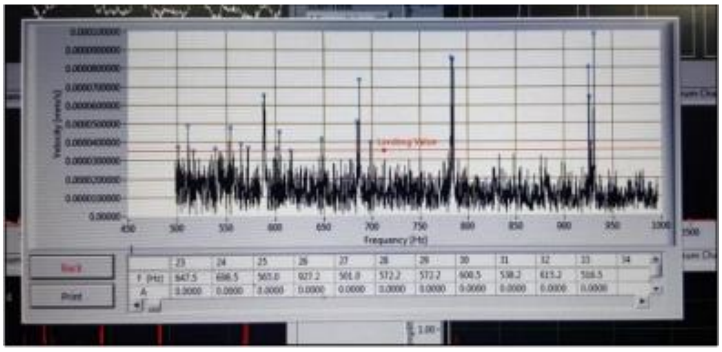

Figure 3.14 Fast Fourier transform (FFT) spectrum

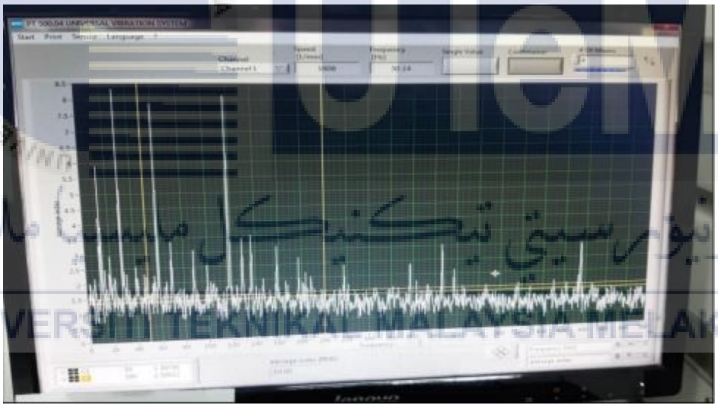

Figure 3.15 Envelope Analysis

UNIVERSITI TEKNIKAL MALAYSIA MELAKA

3.6.3 Experiment Procedure

The initial step in starting the experiment is to launch the PT500.04 program on a personal computer (PC). Once the software is launched, the parameters must be tweaked. As shown in Figure 3.16, the scan rate should be adjusted to 8 k/s, the scan length to 4 seconds, the mode to Velocity, and Channel B to Channel 2. Following the software setup, the reference bearing should be replaced with the cylindrical roller bearing prototype situated in bearing housing no.7, as shown in Figure 3.13. The prototype is then firmly secured to the shaft. During this procedure, it is critical to maintain adequate alignment and stability.

After the setup is complete, the motor and data recording for envelope analysis are started. After a 3-minute run-in time to stabilize the system, this study is done at a motor speed of 1000rpm. The envelope analysis gives important insights into the amplitude fluctuations of the vibration signal, allowing for the discovery of any potential flaws or irregularities within the bearing. The rotor is then given an extra element of imbalance by randomly inserting a screw (static setting). Following that, the FFT spectrum analysis is performed at three distinct motor speeds: 500rpm, 1000rpm, and 1500rpm. This analysis allows for a more detailed examination of the frequency components present in the vibration signal, providing insights into the effects of the imbalance on the system dynamics.

To broaden the scope of the inquiry, the preceding trials will be performed, but this time with the linked and dynamic settings indicated in Figure 3.17. The outcomes of these settings will offer more information on the system's behavior and response to various operating circumstances. Finally, the entire experiment described in the preceding paragraph will be performed with four more prototypes: Triangle, Square, Circle, and Rectangle, to investigate the influence of optimized geometry roller bearing prototypes. The goal of this enlarged study is to analyze the performance and features of the various bearing geometries under the stated experimental settings, allowing for a thorough comparison and assessment of their efficacy.

UNIVERSITI TEKNIKAL MALAYSIA MELAKA

Figure 3.16 PT500.04 FFT Spectrum Settings

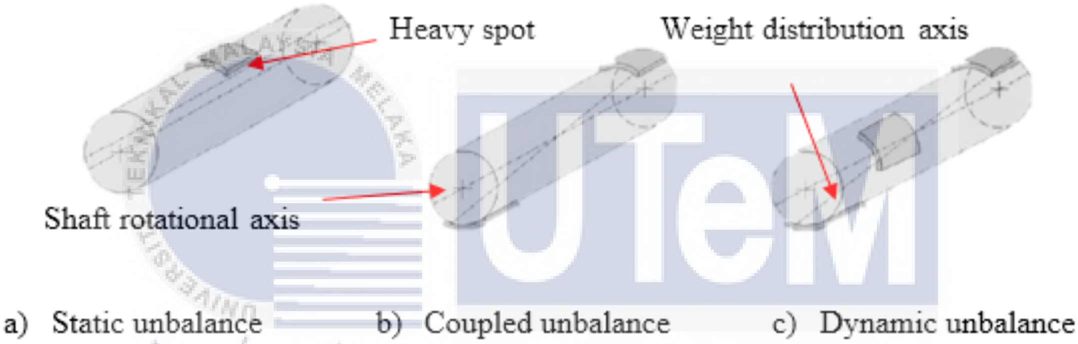

Figure 3.17 Unbalanced Rotor Settings with Weights

اونيۏرسيتي تيكنيكل مليسيا ملاك
UNIVERSITI TEKNIKAL MALAYSIA MELAKA

3.7 Analysis Data

Two unique methodologies are used in this experimental study to test and analyze the performance and features of the bearings under consideration. The first approach, envelope analysis, is a useful tool for finding and diagnosing possible bearing issues. Envelope analysis detects and localizes several sorts of bearing problems, including those in the inner race, outer race, ball bearings, and the cage, by evaluating the amplitude fluctuations in the vibration signal. This approach is critical in determining the overall health and functionality of the bearing.

The second approach used, in addition to envelope analysis, is FFT spectrum analysis. This approach examines the frequency domain of the vibration signal and offers critical information about the performance and behavior of various bearing shapes. It is feasible to compare and assess the performance of various bearing geometries under the given experimental conditions by observing the peaks in the FFT spectrum. The magnitude and distribution of these peaks are crucial indications of the dynamic response and bearing characteristics. This data is useful for evaluating the efficacy and appropriateness of various bearing designs, allowing researchers and engineers to make educated judgements about their application in real-world circumstances.

This experimental study seeks to get a full knowledge of bearing performance, problem diagnosis capabilities, and comparative assessment of different bearing geometries by utilizing both envelope analysis and FFT spectrum analysis. These analytical tools give vital insights into the dynamic behavior and health state of bearings, allowing for more informed decision-making and improving overall bearing system dependability and efficiency.

UNIVERSITI TEKNIKAL MALAYSIA MELAKA

3.7.1 Envelope Analysis

Envelope analysis is a signal processing technique used to detect defects in bearings and gears. Small hits in the high frequency area are usually the first symptom of bearing problems. Thus, the findings in the vibration characteristic and the damaged index (RMS) were examined. The flaws can then be recognized when anomalous peaks arise at frequency (Table 3.7). Then, compare the envelope analysis findings to classify the excellent prototype (Figure 3.18).

Table 3.7 PT500.12 Roller Bearing Faults Kit Manuals (Damage and Speed Frequencies)

Damage Frequencies			
n	Outer ring	Inner ring	Ball
n rpm	f_o (Hz)	f_i (Hz)	f_k (Hz)
500	40.4	59.6	41.7
1000	80.8	119.2	83.4
1500	121.1	178.9	125.1

Frequencies of speeds			
n	Inner Ring	Cage	Ball
n rpm	f_N (Hz)	fc, (Hz)	f_r (Hz)
500	8.3	3.5	20.8
1000	16.7	6.9	41.7
1500	25.0	10.1	62.5

UNIVERSITI TEKNIKAL MALAYSIA MELAKA

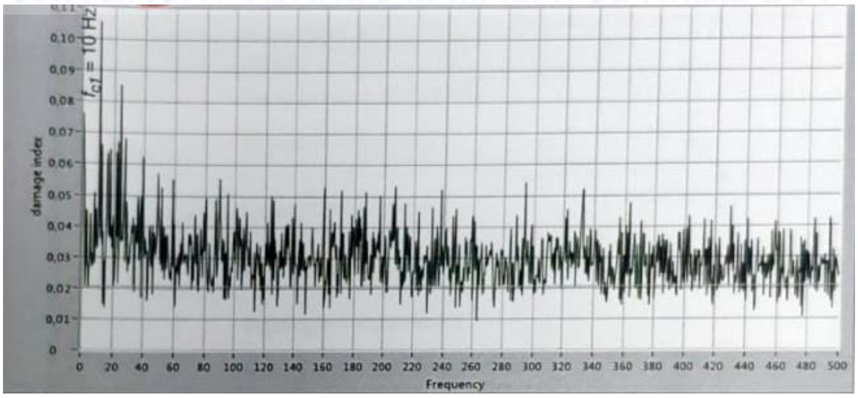

Figure 3.18 No Defect Bearing 's Envelope Analysis Results

3.7.2 Fast Fourier Transform (FFT) Spectrum.

According to Wikipedia, FFT is a method that computes a sequence's discrete Fourier transform (DFT) or inverse (IDFT). Fourier analysis translates a signal from its native domain (typically time or space) to a frequency domain representation and vice versa. The DFT is created by dividing a series of values into components with distinct frequencies (Wikipedia, 2022). Essentially, the FFT spectrum provides a simplified perspective of the vibrations that occur at different frequencies for all the components in the system. So, record and calculate the average vibrations from 10 peaks locations, and then examine the vibration trend on the FFT spectrum.

3.8 Surface Validation

At first, we used scanning electron microscopy (SEM) to cut our prototypes into smaller pieces so that the measurement process would go more smoothly. In addition, scanning electron microscopy is used to thoroughly analyse the surface's state. Through the use of this comprehensive approach, the surface's quality, texture, and overall condition may be thoroughly studied, yielding valuable insights.

UNIVERSITI TEKNIKAL MALAYSIA MELAKA

3.8.1 Scanning Electron Microscopy (SEM)

Scanning Electron Microscopy (SEM) is a cutting-edge imaging technology utilized in scientific research and materials analysis. It produces high-resolution photographs of a sample's surface, allowing researchers to examine and analyze microstructures at the nanoscale. SEM produces comprehensive pictures of surface morphology, topography, and composition by focusing an electron beam onto the sample and detecting the resultant signals. It has remarkable imaging capabilities, enabling the analysis of fine features and elemental composition by energy-dispersive X-ray spectroscopy (EDS). SEM is used in a variety of scientific areas, providing qualitative and quantitative analysis, and recent improvements have expanded its possibilities even further. To summarize, SEM is a powerful technique for studying the microstructures and characteristics of many materials.

3.8.1.1 Sample Coating Process

To minimize charging of the surface, to induce the emission of secondary electrons so that the specimen conducts uniformly, and to provide a homogenous surface for analysis and imaging, it is usually necessary to coat the sample with a thin coating of gold or gold-palladium alloy.

Figure 3.19 Quorum SC7620 Mini Sputter Coater/Glow Discharge System

UNIVERSITI TEKNIKAL MALAYSIA MELAKA

3.8.1.2 Magnification Setting

Observe and capture surface wear using the low magnification setting. A high magnification setting is used to examine the texture, orientation of materials, and chemical composition.

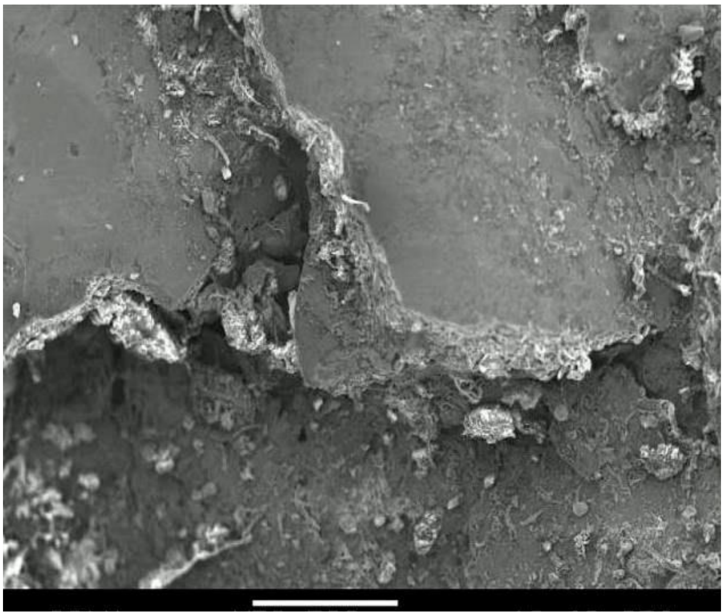

Figure 3.20 SEM Image

UTeM
اونيورسيتي تيكنيكل مليسيا ملاك
UNIVERSITI TEKNIKAL MALAYSIA MELAKA

CHAPTER 4

RESULT AND DISCUSSION

4.1 Introduction

This chapter aims to clarify and discuss the results obtained from the performed vibration testing, and SEM. To improve the clarity of the assessment process, special attention is given to organizing the results of the vibration testing into a methodical ranking system. By using a hierarchical system, the outcomes become more easily attainable and provide a more distinct comprehension of the comparative intensities of vibration reactions. Moreover, the incorporation of surface roughness and SEM outcomes enhances a thorough evaluation, offering a diverse viewpoint on the analyzed materials or systems. The purpose of this systematic arrangement and display of data is to simplify the understanding of intricate findings and enable well-informed decision-making within the study's framework.

4.2 SIMSOLID simulation

This section compiles all data on contact force and contact response for various components. The purpose is to facilitate later analysis (Table 4.1). Table 4.2 displays the ranking score, which corresponds to the findings reported in Table 4.1. The placement of the findings remains consistent if they share the same value. Placements are typically ranked on a scale of 1 to 5, however sometimes they may be decreased owing to comparable outcomes. The score given corresponds to the ranking. In the final placing, priority is given to performance stability when the overall ranking score is equal. Altair's official statement confirms that SIMSOLID's correctness has been validated by comparisons with established reference solutions in many common solution domains.

Table 4.1 Overall Simulation Result

No.		Max. Displacement Magnitude (mm)				
		Circle	Rectangular	Solid	Square	Triangle
a)		2.98e-5	2.98e-5	2.77e-04	3.3e-2	2.92e-5
			Force (N)			
b)	Outer ring	4.01e-5	1.53e-4	5.68e-6	1.1e-4	2.04e-4
c)	Lock	5.83e-7	5.83e-7	5.81e-7	5.88e-7	5.81e-7
d)	Inner ring	4.01e-6	4.01e-6	4.01e-6	4.00e-6	4.01e-6
			Moment (Nm)			
e)	Outer ring	5.69e-7	2.82e-6	9.76e-7	6.14e-7	1.44e-6
f)	Lock	1.45e-6	1.99e-6	1.4e-6	8.4e-7	1.66e-6
g)	Inner ring	2.2e-6	1.3e-6	1.71e-7	2.03e-6	2.88e-6

Table 4.2 Overall Simulation Ranking

Geometry	Ranking Score							Total	F.P
	a)	b)	c)	d)	e)	f)	g)		
Circle	1	2	2	2	1	3	4	15	2
Rectangular	1	4	2	2	5	5	2	21	4
Solid	2	1	1	2	3	2	1	12	1
Square	4	3	3	1	2	1	3	17	3
Triangle	3	5	1	2	4	4	5	24	5

UNIVERSITI TEKNIKAL MALAYSIA MELAKA

4.3 Envelope Analysis

Two outcomes are reported in this section: the damage index and the prototype defects that were detected during vibration testing. Both results are significant.

4.3.1 Prototypes defects

The frequency table in APPENDIX 4 displays various common mistakes that have been detected. An underlying assumption in this research is that the observed deformations in the components occurred during the rolling motion, with a size difference of about 100-fold. Notably, while comparing the tensile modulus, it is discovered that prototypes made of polyamide PA12 have a modulus of 1.85 GPa, whereas the stainless-steel metal bearing has a modulus of 203 GPa.

Given the significant disparity in material characteristics, notably modulus, the envelope analysis frequencies used in this experiment may not be optimum suited for detecting mistakes. The large difference in deformability between the nylon PA12 and stainless-steel components shows that the frequency patterns associated with the two materials may not be well aligned with the selected analytical technique. As a result, additional procedures or changes may be required to improve the sensitivity and accuracy of error identification in this experimental environment.

4.3.2 Damage Index

Figure 4.1 displays a graph that illustrates the relationship between the damage index and different speeds. The graph exhibits a progressive upward trend. Burdzik's research, titled "Research on the Influence of Engine Rotational Speed to the Vibration Penetration into the Driver through Feet - Multidimensional Analysis," reveals a heightened inclination for vibrations with root mean square (RMS) values ranging from 1500 to 3000 rpm. The damage index has escalated due to the impact of velocity and structural relaxation. Conversely, the graph illustrates that square geometry yields more consistent results, even in the presence of the structure's loosening issue. As the speed exceeds 1200 rpm, the contrast in damage index values for different geometries becomes more noticeable. To summarize, there is a clear correlation between speed and the damage index, and the structural loosening issue leads to a noticeable increase in the damage index for most of the geometric elements. In Figure 4.1 (b) show the ranking of geometry for each speed to declare which greater.

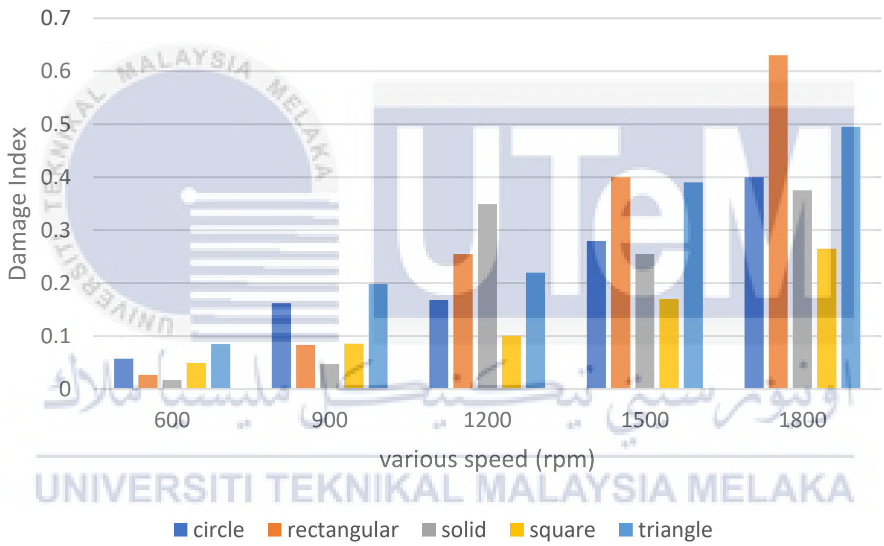

UNIVERSITI TEKNIKAL MALAYSIA MELAKA

(a)

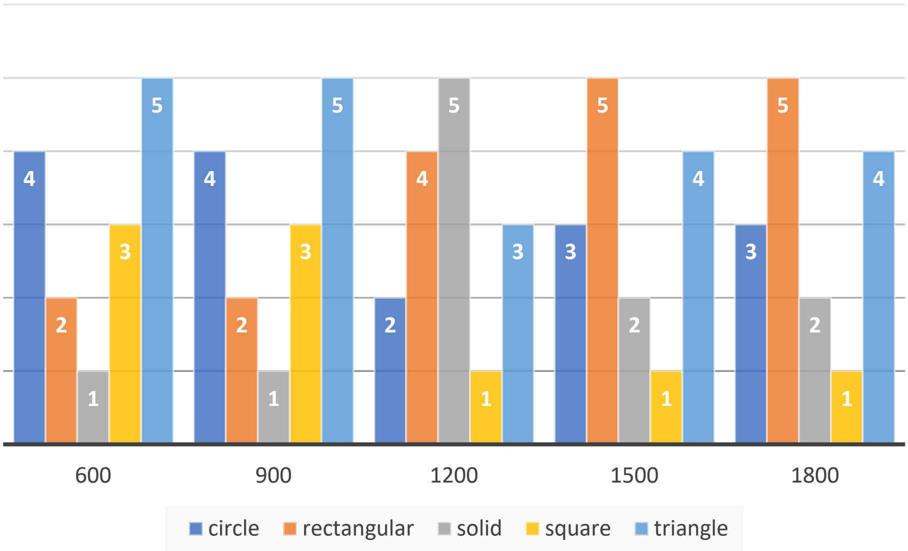

(b)

Figure 4.1 (a) Damage Index results in specific geometry for, (b) Ranking results of specific geometry for each speed

4.3.3 Comparing Damage with Previous Roller Bearing in Various Speed

This section examines the outcomes of vibrations induced by various geometries and compares them to the previous findings obtained using the roller bearing technique. The comparison is based on factors such as ranking, specific speed, and experimental conditions.

UNIVERSITI TEKNIKAL MALAYSIA MELAKA

4.3.3.1 Vibration Testing Results Comparison with Previous Roller Bearing in 600 rpm.

Figure 4.2 illustrates the vibration outcomes at a velocity of 600 rpm. The thrust ball bearing is represented by the blue line, while the roller bearing is represented by the red line. Upon visual examination, it is evident that both bearings demonstrate satisfactory performance at this velocity. When examining the thrust ball bearing, significant differences in the damage index may be found across various geometries. More precisely, the solid geometry displays outstanding performance by having the lowest damage index value, but the triangular geometry shows less than ideal performance by having the highest damage index among all the geometries. In contrast, the roller bearing has a more uniform graph, where most geometries provide comparable values for the damage index. The rectangle geometry is particularly noteworthy due to its much higher damage index, setting it apart from the other geometries. Table 4.3 presents a thorough evaluation of each shape, emphasizing their individual performances and kinds of bearings. The rankings are based on the information obtained from Figure 4.2. Significantly, while operating at a speed of 600 rpm, the thrust ball bearing proves to be more efficient than the roller bearing, especially in three specific geometries that exhibit the lowest damage index values. This research highlights the subtle performance differences across various shapes within each kind of bearing, providing useful insights into the efficiency of thrust ball and roller bearings at the given speed.

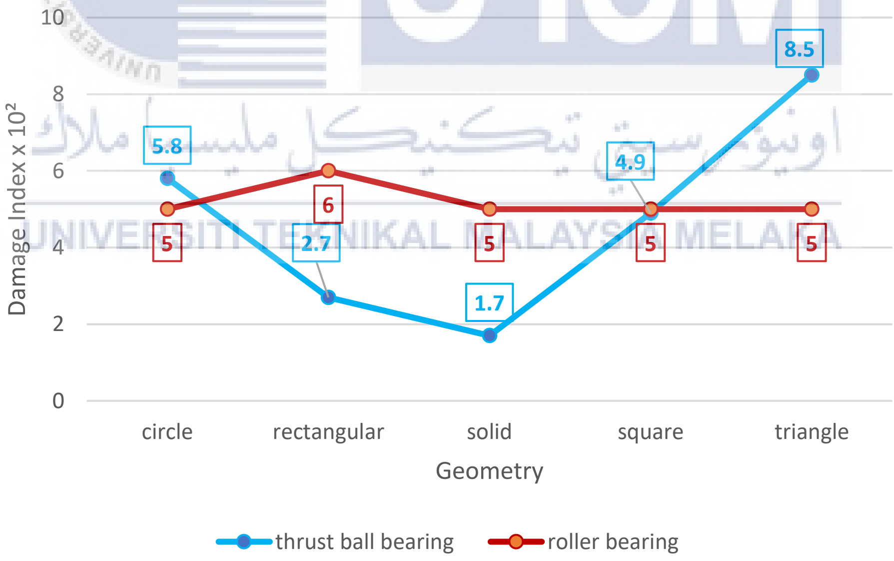

Figure 4.2 Comparison of result thrust ball bearing and previous roller bearing at 600 rpm

Table 4.3 Ranking of bearing type for specific geometry at 600 rpm

Geometry					Result
Circle	Rectangular	Solid	Square	Triangle	
Roller bearing	Thrust ball bearing	Thrust ball bearing	Thrust ball bearing	Roller bearing	Thrust ball bearing

4.3.3.2 Vibration Testing Results Comparison with Previous Roller Bearing in 900 rpm

Figure 4.3 illustrates the vibration results at a speed of 900 rpm, where the thrust ball bearing is shown by the blue line and the roller bearing is indicated by the red line. Upon visual examination, it is evident that both bearings are performing well at this velocity. Upon closer inspection, it becomes evident that there are significant variances in the damage index across various geometries of the thrust ball bearing. More precisely, solid geometry excels in terms of performance, with the lowest damage index value. Conversely, the triangle shape demonstrates suboptimal performance, with the greatest damage index compared to all other geometries. Conversely, the roller bearing has a graph that is more uniform, since various shapes provide similar values for the damage index. The rectangle and triangle geometries stand out due to their exceptional performance since they both have the lowest damage index and set themselves apart from other forms. On the other hand, the circular shape exhibits the greatest damage index, which suggests that the performance at this speed is not ideal. Table 4.4 provides a thorough assessment of each shape, highlighting their distinct performances and their correlation with the two kinds of bearings. The ranks are determined based on the knowledge acquired from Figure 4.3. Significantly, while operating at a velocity of 900 revolutions per minute, the roller bearing that was previously mentioned demonstrates superior efficiency compared to the thrust ball bearing, particularly in three specific configurations that display the lowest values for the damage index. The effectiveness of thrust ball and roller bearings at the given speed is highlighted by this study, which also highlights the subtle changes in performance across different shapes within each kind of bearing.

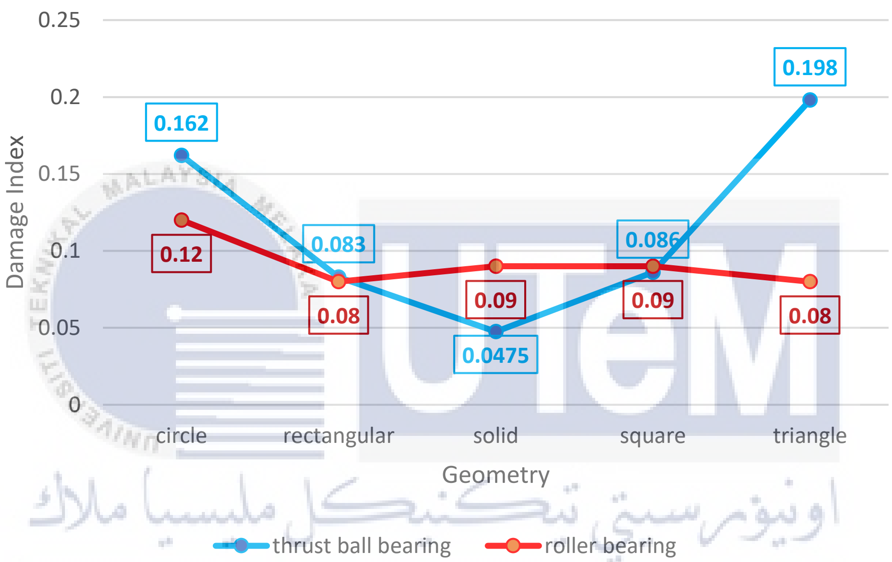

UNIVERSITI TEKNIKAL MALAYSIA MELAKA

Figure 4.3 Comparison of result thrust ball bearing and previous roller bearing at 900 rpm

Table 4.4 Ranking of bearing type for specific geometry at 900 rpm

Geometry					Result
Circle	Rectangular	Solid	Square	Triangle	
Roller bearing	Roller bearing	Thrust ball bearing	Thrust ball bearing	Roller bearing	Roller bearing

4.3.3.3 Vibration Testing Results Comparison with Previous Roller Bearing in 1200 rpm

Figure 4.4 provides a thorough summary of vibration findings acquired at a velocity of 1200 rpm, with the thrust ball bearing shown by the blue line and the roller bearing by the red line. Upon first examination, both bearings demonstrate good performance at this velocity. However, following further examination, significant discrepancies in the damage index may be seen across various geometries of the thrust ball bearing. More precisely, the square shape stands out as the best performer, with the lowest damage index value. Conversely, the solid shape demonstrates worse performance, as it records the greatest damage index among all geometries at this velocity. Unlike the thrust ball bearing, the roller bearing graph has a more uniform pattern, where different shapes provide comparable values for the damage index. The roller bearing's solid and triangular geometries are notable for their remarkable performance, characterized by the lowest damage index and setting them apart from other shapes. In contrast, the round shape has the greatest damage index, suggesting suboptimal performance at this velocity. To get a more comprehensive examination of the performance of each shape and its relationship with the two kinds of bearings, please refer to Table 4.5. The ranks are determined based on the knowledge acquired from Figure 4.4. Remarkably, while rotating at a speed of 1200 revolutions per minute, the roller bearing outperforms the thrust ball bearing in terms of efficiency. Three specific configurations of the roller bearing provide the lowest values for the damage index, indicating greater performance in these settings.

اونيورسيتي تيكنيكل مليسيا ملاك
UNIVERSITI TEKNIKAL MALAYSIA MELAKA

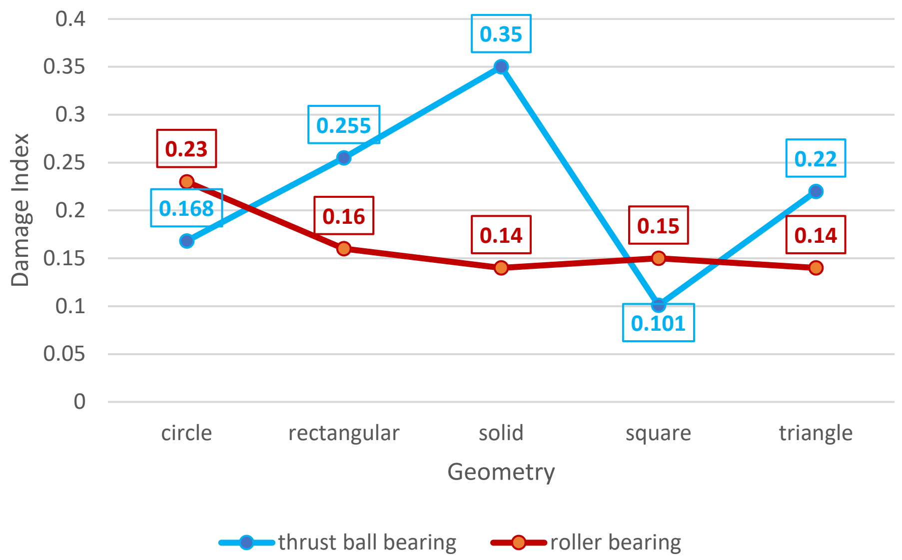

Figure 4.4 Comparison of result thrust ball bearing and previous roller bearing at 1200 rpm

Table 4.5 Ranking of bearing type for specific geometry at 1200 rpm

Geometry					Result
Circle	Rectangular	Solid	Square	Triangle	
Thrust ball bearing	Roller bearing	Roller bearing	Thrust ball bearing	Roller bearing	Roller bearing

UNIVERSITI TEKNIKAL MALAYSIA MELAKA

4.3.3.4 Vibration Testing Results Comparison with Previous Roller Bearing in 1500 rpm

Figure 4.5 shows a full picture of the shaking results at 1500 rpm. The blue line shows how well the thrust ball bearing worked, and the red line shows how well the roller bearing worked. From what we can see so far, both bearings seem to be working well at this speed. But when you look more closely, you can see that the damage index is very different for different roller bearing shapes. To be more specific, the triangle shape stands out as the best because it has the lowest damage index value. In comparison, the circle geometry doesn't work as well; at this speed, it has the highest damage score of all the shapes. This difference in function shows how sensitive the roller bearing is to different shapes. The thrust ball bearing curve, on the other hand, shows a more different pattern, with the damage index values being similar for different forms. When it comes to performance, the thrust ball bearing's square shape stands out because it has the lowest damage index and is different from other forms. On the other hand, the damage score for the rectangular shape is the largest, which means it doesn't work as well at this speed. Table 4.6 for a full breakdown of how well each shape works and how it relates to the two types of bearings. The rankings are based on what we can learn from Figure 4.5. When the speed of spinning is 1500 turns per minute, the roller bearing is more efficient than the thrust ball bearing. The roller bearings with the lowest damage index numbers are in three unique designs. This means they work better in these settings.

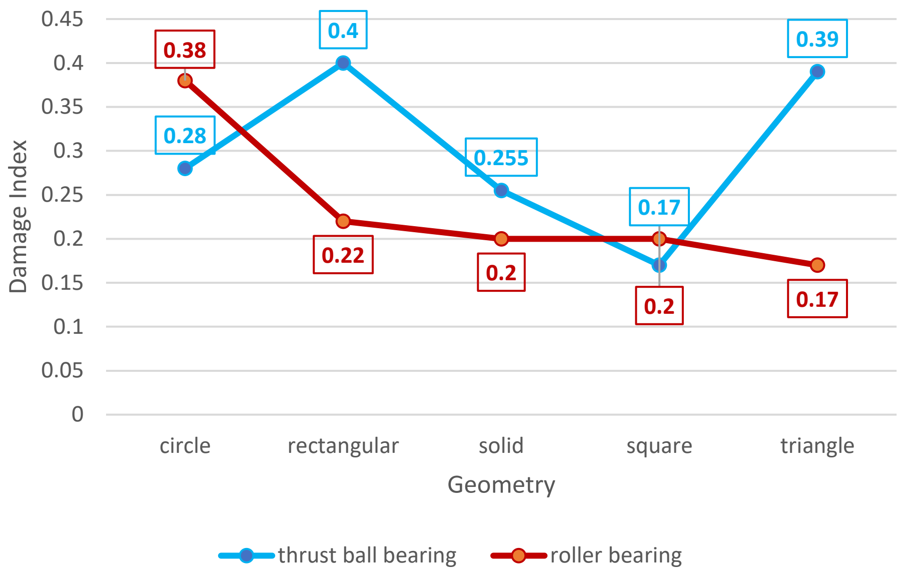

Figure 4.5 Comparison of result thrust ball bearing and previous roller bearing at 1500 rpm

Table 4.6 Ranking of bearing type for specific geometry at 1500 rpm

Geometry					Result
Circle	Rectangular	Solid	Square	Triangle	
Thrust ball bearing	Roller bearing	Roller bearing	Thrust ball bearing	Roller bearing	Roller bearing

UNIVERSITI TEKNIKAL MALAYSIA MELAKA

4.3.3.5 Vibration Testing Results Comparison with Previous Roller Bearing in 1800 rpm

A complete visualization of the shaking results at 1800 rpm is shown in Figure 4.6. The performance of the push ball bearing is shown by the blue line, and the performance of the roller bearing is shown by the red line. From what we've seen so far, both bearings seem to work well at this spinning speed. However, a closer look shows that the damage index is very different for roller bearings of different sizes. The uniform shape stands out as the best because it has the lowest damage index value. The circle geometry, on the other hand, doesn't work as well; at this speed, it does the most damage of any shape. This range of values shows how sensitive the roller bearing is to different geometric shapes. On the other hand, the thrust ball bearing curve shows a more stable pattern, with damage index values that stay the same for all forms. In particular, the thrust ball bearing's square shape stands out for its better performance, it has the lowest damage index and is different from other shapes. In contrast, the rectangular shape has the biggest damage score, which means it doesn't work as well as it could at this spinning speed. Glance at Table 4.7 for a full explanation of how well each shape works with the two types of bearings. The rankings are based on what we can learn from Figure 4.6. The roller bearing is surprisingly more efficient than the thrust ball bearing when it comes to 1800 spins per minute. The roller bearings with the lowest damage index numbers come in three different styles, which means they work better in these specific setups. When the surface was under more force at 1800 rpm, the wear mechanism worked more, which changed the hardness of the surface and caused the acceleration to drop suddenly. If the state of the surface roughness stays the same, the link between speed and acceleration is a straight line. It is found that the acceleration is greater when the surface is rougher

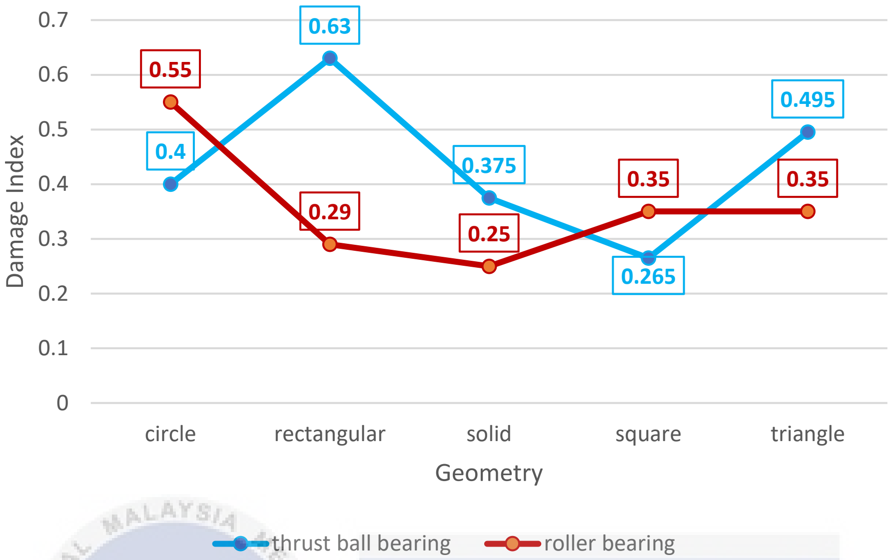

Figure 4.6 Comparison of result thrust ball bearing and previous roller bearing at 1800 rpm

Table 4.7 Ranking of bearing type for specific geometry at 1800 rpm

Geometry					Result
Circle	Rectangular	Solid	Square	Triangle	
Thrust ball bearing	Roller bearing	Roller bearing	Thrust ball bearing	Roller bearing	Roller bearing

4.3.3.6 Comparing Damage Index at Low Speed

Low-speed bearings are specifically engineered to operate at their best performance when the rotational speed is maintained at a relatively low level. These bearings are advantageous in mechanical systems and machines where accurate motion is necessary but the rotational speed is not high. Low-speed bearings have applications in various industrial

UNIVERSITI TEKNIKAL MALAYSIA MELAKA

equipment such as gearboxes, conveyor systems, slow-speed motors, and specific industrial machines. When used in these manners, bearings provide seamless and controlled rotation, ensuring the proper functioning of the equipment. Low-speed bearings prioritise durability, load-carrying capabilities, and resilience over high-speed bearings due to their reduced exposure to rotational force. Longevity and efficiency are improved by the use of materials, lubrication systems, and protective measures that are specifically tailored to suit the unique demands of low-speed operations. Figure 4.7 displays the vibration outcome shown in graph (a) for the thrust ball bearing and graph (b) for the roller bearing. The majority of data in roller bearings exhibit stability at low speeds, but the values for thrust ball bearings show slight variations. This issue may be attributed to the geometric characteristics and the contact area between the ball bearing and the outer ring. The roller bearing has a comparatively greater contact area with the outer surface. In addition, some geometries exhibit a minimum damage index for thrust ball bearings and a maximum damage index when compared to roller bearings. The shape of the bearing directly impacted its performance.

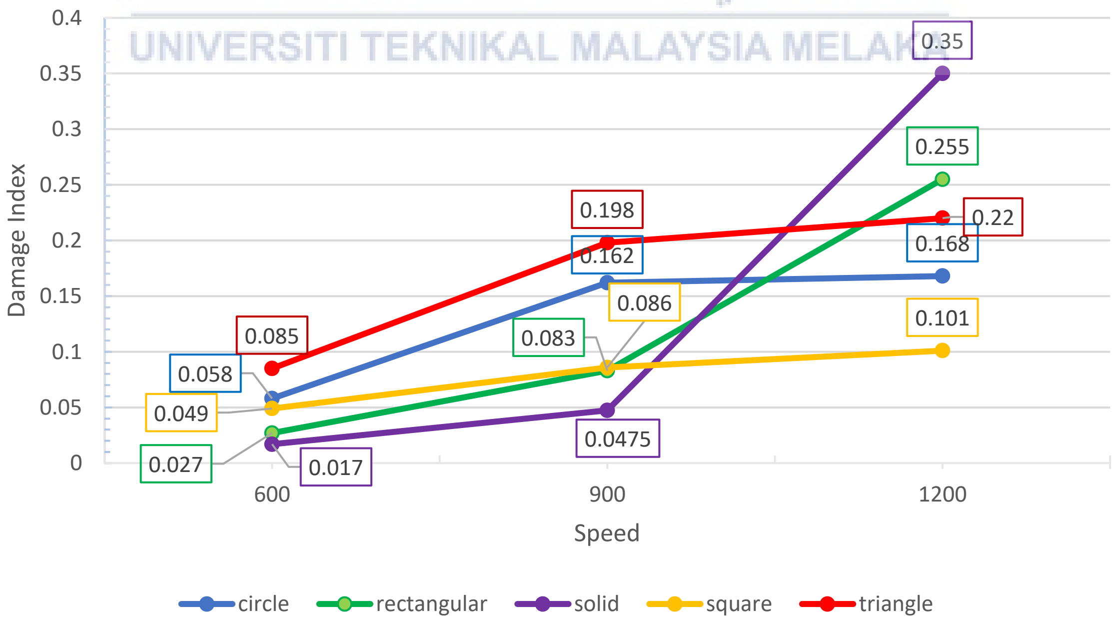

(a)

UNIVERSITI TEKNIKAL MALAYSIA MELAKA

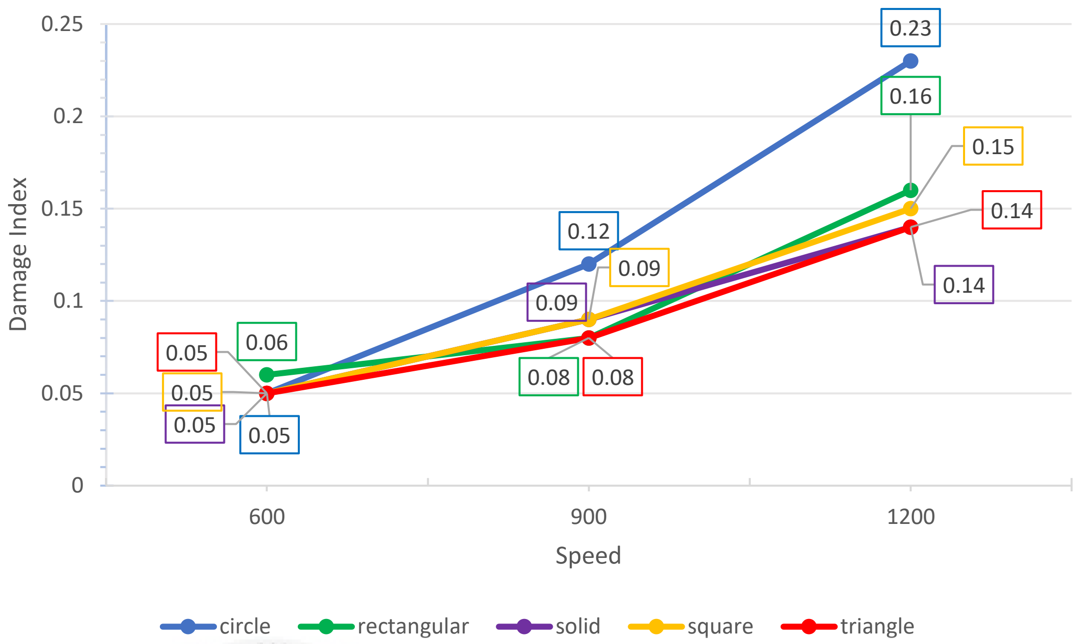

(b)

Figure 4.7 Comparing Damage Index at low speed, (a) Thrust ball bearing, (b) Roller bearing

4.3.3.7 Comparing Damage Index at High Speed

Applications needing fast rotational motion, usually characterized by speeds above standard bearing limitations, are well-suited for high-speed bearings, which are specifically designed components. Aerospace, automobile, and precision equipment are just a few of the many sectors that rely on these bearings. Some frequent examples of high-speed applications are turbochargers in car engines, aviation engine components, and machine tool spindles. Reducing friction, dissipating heat, and designing precisely to endure high rotating speeds are all factors that went into making these bearings. Machinery that operates at high speeds relies on high-speed bearings for best performance and durability in these harsh settings. These bearings are engineered with advanced materials, lubrication systems, and complicated designs. Figure 4.8 shows the results of the vibration analysis for the thrust ball bearing (a) and the roller bearing (b). The thrust ball bearings' values fluctuate substantially

UNIVERSITI TEKNIKAL MALAYSIA MELAKA

depending on the geometry while traveling at high speeds. Except for the circular shape, the value of the roller bearing is quite comparable. Although roller bearings perform well at these speeds, thrust ball bearings with a square shape perform much better.

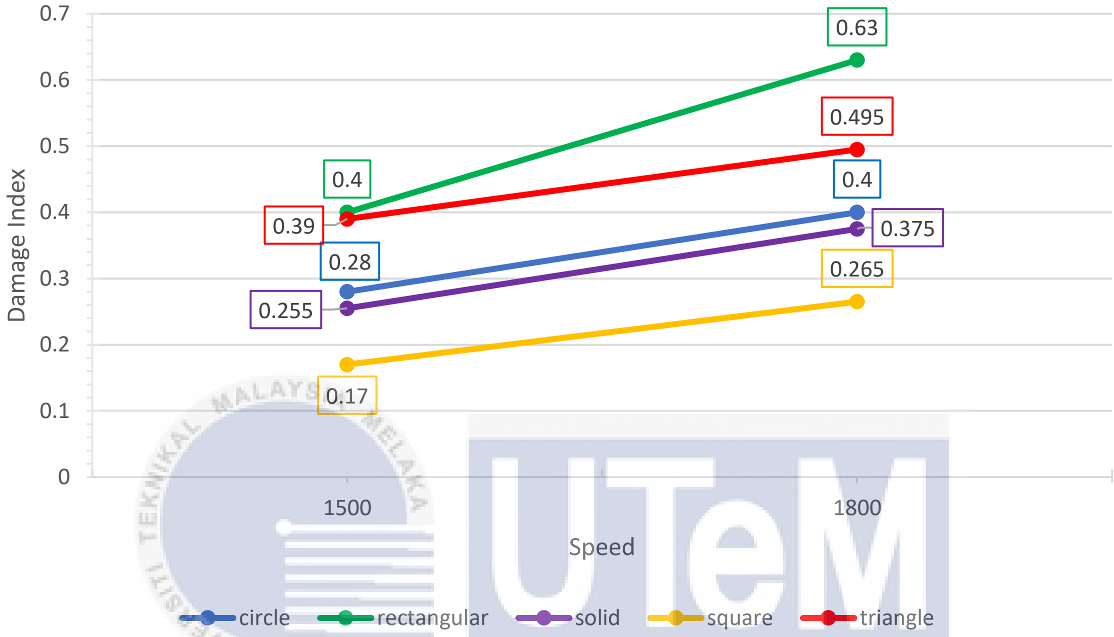

(a)

UNIVERSITI TEKNIKAL MALAYSIA MELAKA

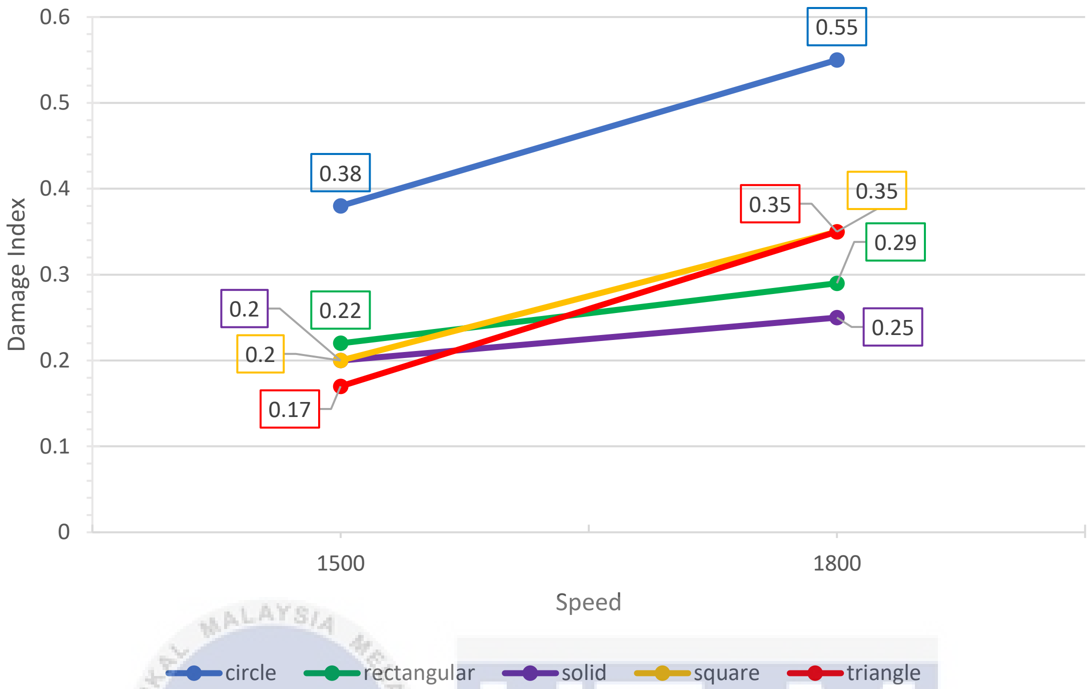

(b)

Figure 4.8 Comparing Damage Index at high speed, (a) Thrust ball bearing, (b) Roller bearing

4.3.3.8 Overall Results for Damage Index

The data shown in Table 4.8 provide a detailed investigation of bearing performance, considering different speeds and geometries. The data indicates that roller bearings consistently exhibit superior performance compared to thrust ball bearings at speeds of 900, 1200, and 1500 rpm. This suggests a prevailing inclination for roller bearings when evaluating the overall effectiveness of bearings under various operating situations. The damage index, a vital measure for evaluating the condition and efficiency of bearings, consistently shows a preference for roller bearings across the designated speed range. Through a more detailed analysis of the specific characteristics of each bearing's shape, a subtle and intricate pattern becomes apparent. Thrust ball bearings provide exceptional performance across all measured speeds due to their square design. In contrast, roller bearings demonstrate best performance when arranged in a triangular configuration. This insight is very helpful for engineering applications as it provides guidance for selecting bearing types based on considerations of both speed and shape. It implies that while selecting a bearing, one should not only take into account the general type, but also the particular geometric arrangement that is suitable for the desired operating circumstances. The selection of materials is a crucial determinant of these outcomes. The roller bearings are made of nylon P12, whilst the thrust ball bearings are made of a mix of nylon P12 and steel. The choice of material has a considerable influence on performance, since plastic demonstrates lesser friction in comparison to steel. This discovery highlights the significance of material science in bearing design, emphasising the need to take into account not only the bearing type and shape, but also the materials used to guarantee the best possible performance in various operating situations. Overall, the interaction between the kind of bearing, its shape, and the choice of materials is crucial in attaining excellent performance throughout different speed ranges.

Table 4.8 Comparing all speed data results

Speed	Geometry					Result
	Circle	Rectangular	Solid	Square	Triangle	
600	■	●	●	●	■	●
900	■	■	●	●	■	■
1200	●	■	■	●	■	■
1500	●	■	■	●	■	■
1800	●	■	■	●	■	●

Roller bearing = ■ Thrust ball bearing = ●

UNIVERSITI TEKNIKAL MALAYSIA MELAKA

4.4 Frequency spectrum (FFT)

The results of vibrations induced by various geometries are discussed in this part. The results are broken down into the following categories: acceleration, ranking, specific speed, and experiment condition.

4.4.1 Frequency Spectrum for Thrust Ball Bearing Results

Figure 4.9 presents two important representations, which are as follows: In Figure 4.9 graph (a), the acceleration for each shape is shown, and in Figure 4.9 graph (b), the ranking of these geometries according to their performance is displayed. Upon doing an analysis of the acceleration findings shown in Figure 4.9 graph (a), it becomes apparent that the majority of geometries have a value that is steady. One geometry that sticks out, however, is the square geometry, which exhibits a little acceleration increase in conjunction with the increase in speed. According to this discovery, the square geometry exhibits a behaviour that is distinct from that of the other geometric shapes. As we go on to Figure 4.9 graph (b), which presents the ranking of average performance for each geometry, a major disparity becomes apparent. In terms of average performance, the triangular geometry is found to be the most successful, presenting the greatest overall performance. On the other hand, the rectangle geometry is shown to have the least favourable overall performance. This experiment leads to the conclusion that, among the geometries that were tested, the triangle geometry excels in terms of average performance, while the rectangular geometry lags behind. This indicates that there is a significant variation in the performance characteristics of various geometric shapes under the conditions of the experiment.Based on the material combination, the friction coefficient for dry surfaces after the breakaway might rise or fall with sliding speed (Harnoy, 2002). The friction coefficient f increases with the roughness at a higher range of roughness, above 10 mm, due to an increase in the interaction between the surface asperities (Rabinovitz, 1965).

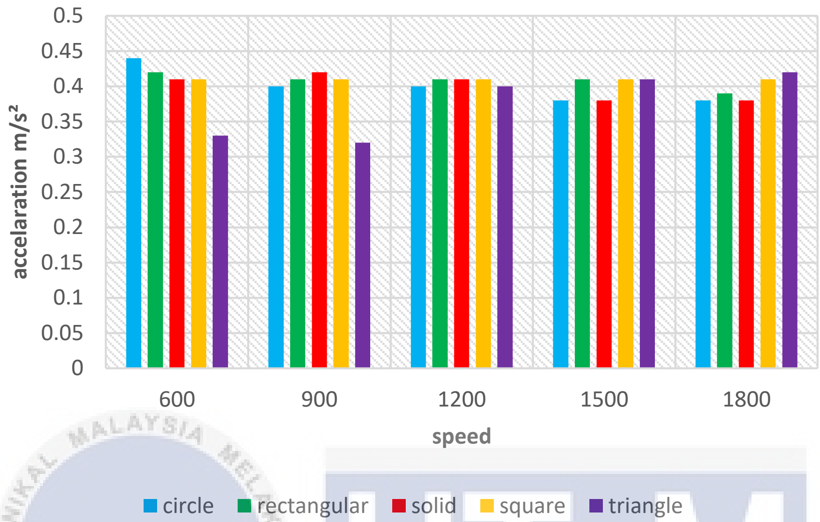

(a)

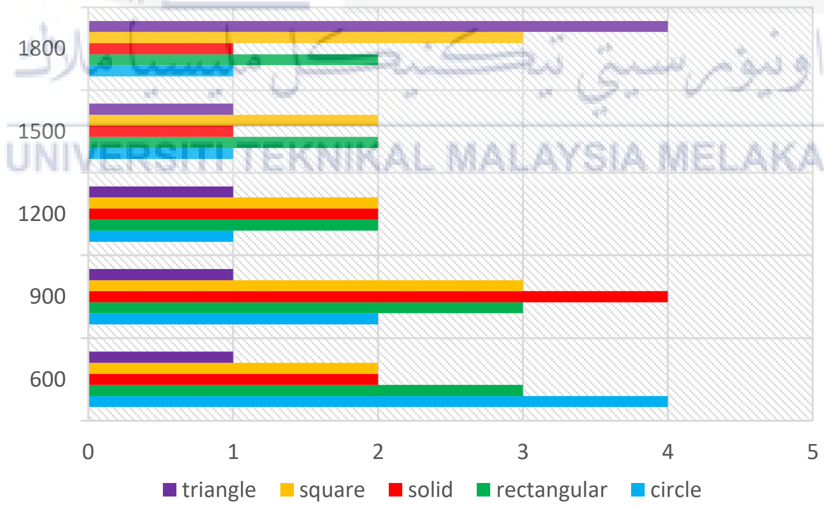

(b)

Figure 4.9 (a) Accelaration results for various speed; (b)Ranking for various speed

UNIVERSITI TEKNIKAL MALAYSIA MELAKA

4.4.2 Comparing the Results of Frequency Spectrum with Previous Roller Bearing

Significant variations in performance characteristics between thrust ball bearings and roller bearings are seen in Figure 4.10, which compares acceleration at different speeds. The thrust ball bearing experiences much higher acceleration at 600 rpm graph (a), whereas the roller bearing has much less acceleration. Graphs (b), (c), and (d) show that at 900, 1200, and 1500 rpm, respectively, the same pattern continues, with noticeable differences at lower speeds. In all cases, the roller bearing performs better, showing reduced acceleration values regardless of the geometry. It should be noted that the thrust ball bearing keeps the acceleration relatively constant throughout all geometries. The thrust ball bearing has smaller error bars compared to the roller bearing, suggesting less stability and more susceptibility to outside influences. In addition, the disparity in acceleration between the two kinds of bearings becomes less noticeable when looking at the data at 1800 rpm graph (e). Both roller and thrust ball bearings have similar acceleration values; however, thrust ball bearings, especially those with square or triangular geometries, display somewhat lower acceleration. Keep in mind that the roller bearing's error bars are always big, no matter the speed, which means it's more vulnerable to outside influences and unknowns. Consistent with Fernandez's findings, the results highlight the significant effect of structural loosening on vibration outcomes, particularly when small external excitation pressures are present. The observed discrepancies in acceleration findings may be attributed, in part, to the fact that the experiment used several kinds of bearings, which introduce varying contacting surfaces, friction, and gap widths. Furthermore, the thorough examination of acceleration data at different speeds demonstrates that roller bearings outperform thrust ball bearings when it comes to reducing acceleration. With narrower error bars suggesting improved dependability, the thrust ball bearings demonstrate steady performance across diverse

UNIVERSITI TEKNIKAL MALAYSIA MELAKA

geometries. These notable variations underline the importance of Fernandez's findings about the effect of looseness on vibration amplitudes and the bearing type/structural integrity relationship in determining vibration characteristics.

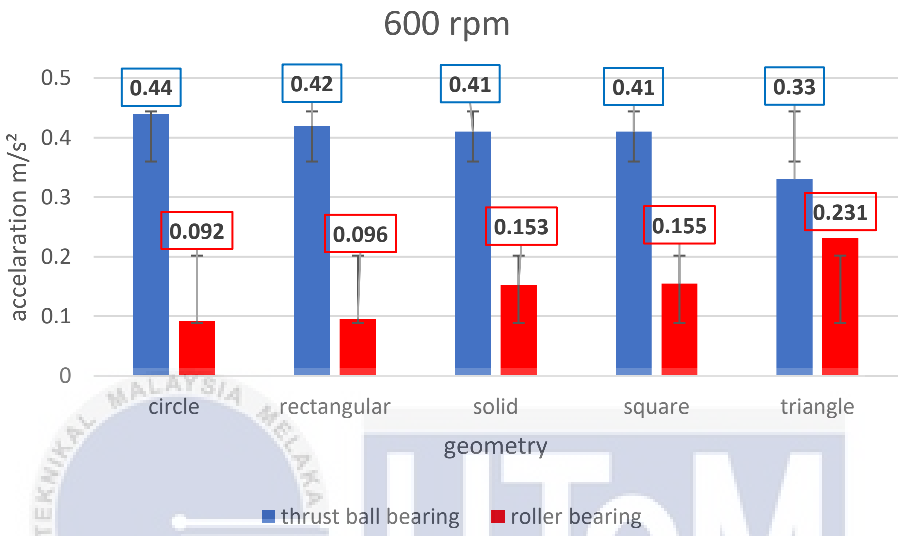

(a)

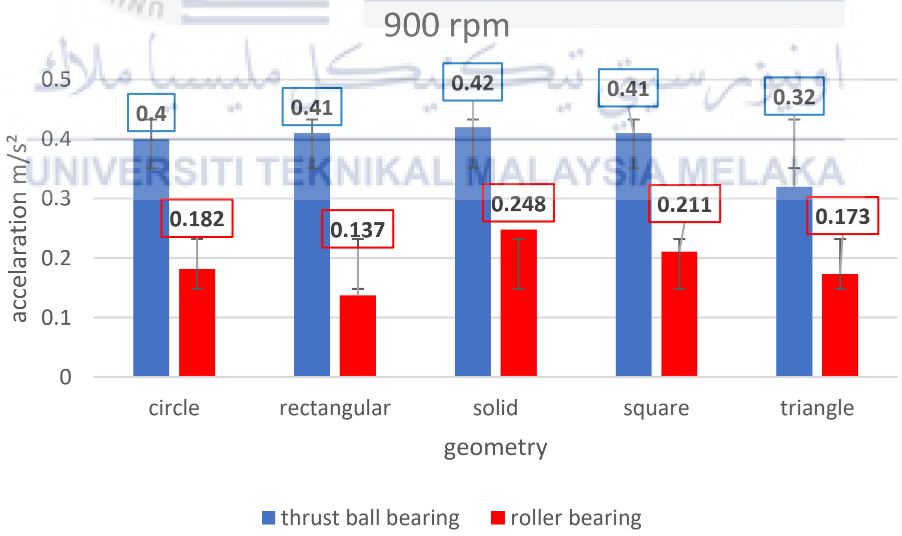

(b)

UNIVERSITI TEKNIKAL MALAYSIA MELAKA

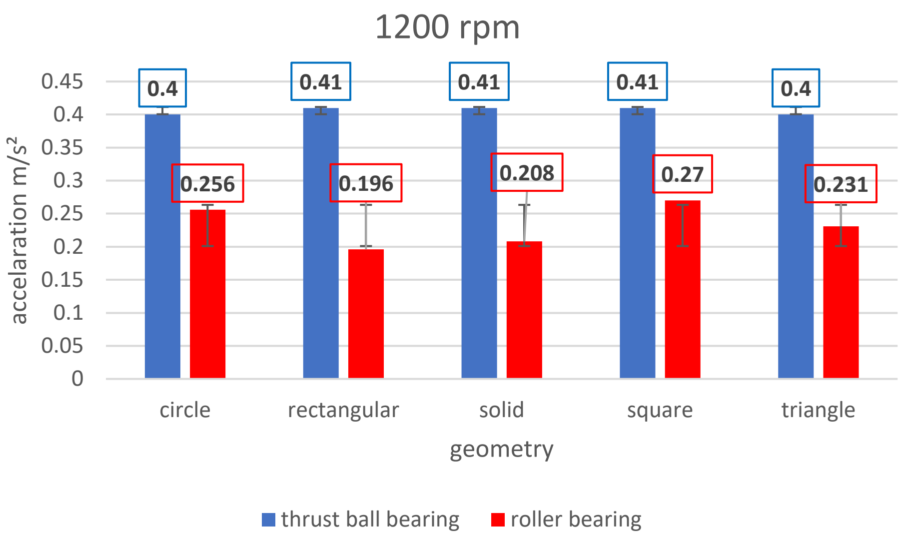
1200 rpm
accelaration m/s²
0.45
0.4
0.35
0.3
0.25
0.2
0.15
0.1
0.05
0
0.4
0.256
0.41
0.196
0.41
0.208
0.41
0.27
0.4
0.231
circle
rectangular
solid
square
triangle
geometry
thrust ball bearing
roller bearing

(c)

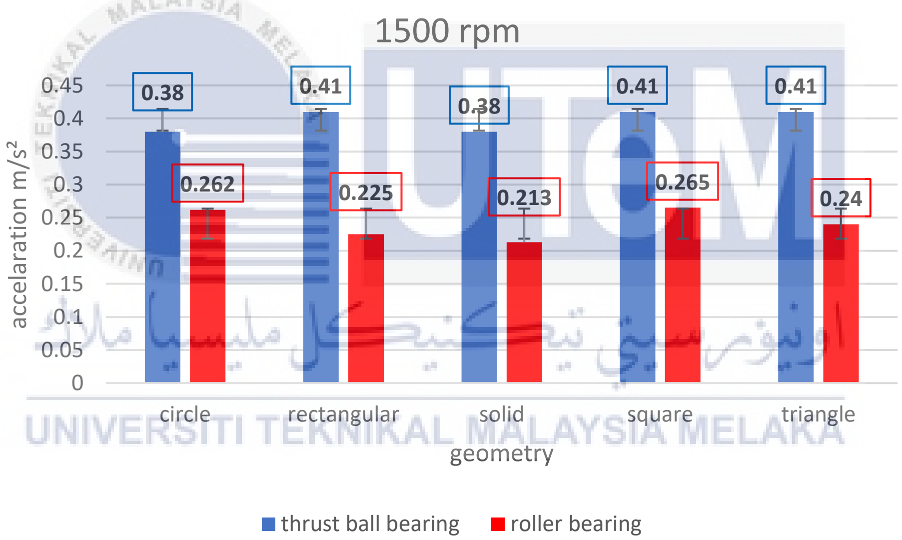
1500 rpm
accelaration m/s²
0.45
0.4
0.35
0.3
0.25
0.2
0.15
0.1
0.05
0
0.38
0.262
0.41
0.225
0.38
0.213
0.41
0.265
0.41
0.24
circle
rectangular
solid
square
triangle
geometry
thrust ball bearing
roller bearing

(d)

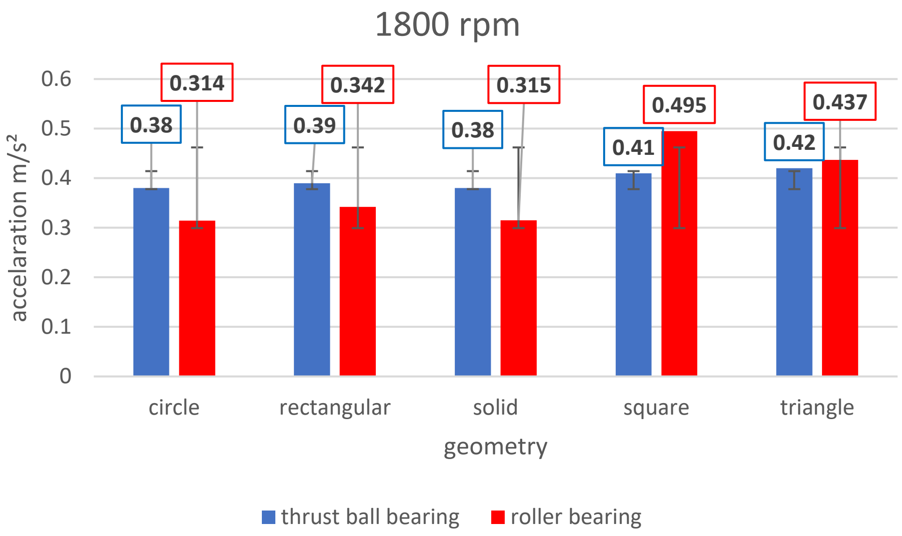

Figure 4.10 Frequency spectrum comparing results, (a) Result for speed 600 rpm, (b) Result for speed 900 rpm, (c) Result for speed 1200 rpm, (d) Result for speed 1500 rpm, (e) Result for speed 1800 rpm.

4.5 SEM

Within the extremely tiny surface area that is generated by the little particles, the overall surface of the circular geometry is seen to be quite rough in the image that is shown in Figure 4.11. The spacing between the melted particles is rather large, and there are some particles that are independent of one another, as seen in Figure 4.11 (b).

UNIVERSITI TEKNIKAL MALAYSIA MELAKA

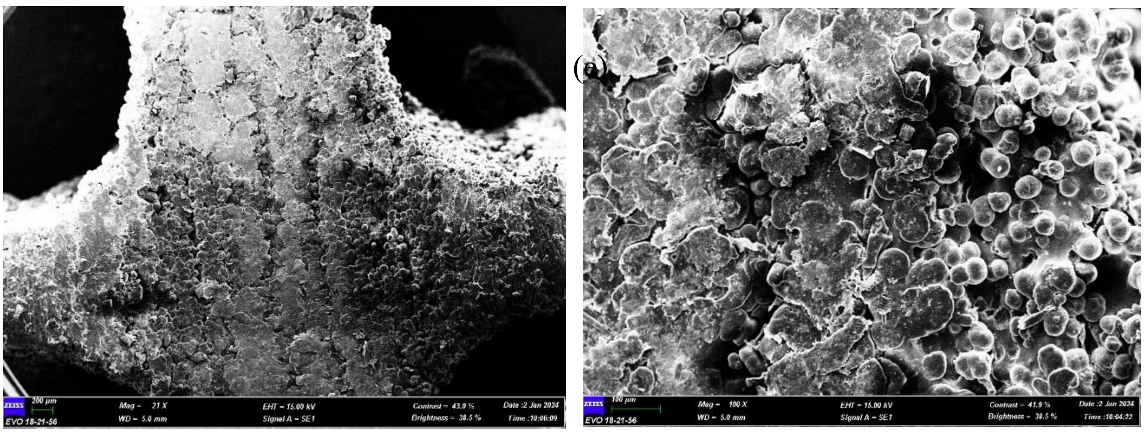

(a) (b)

Figure 4.11 (a) Circle Geometry's SEM; (b) Zoomed Circle Geometry's SEM

Within the context of Figure 4.12, figure an illustrates how the overall surface of the square geometry is rough on the little surface area that is generated by the small particles. This indicates that the surface is more smooth than the circular geometry alone, as seen in Figure 4.12 (b), which shows that the space between the melted particles is very short. However, there are a large number of independent particles with unpredictable shapes.

.

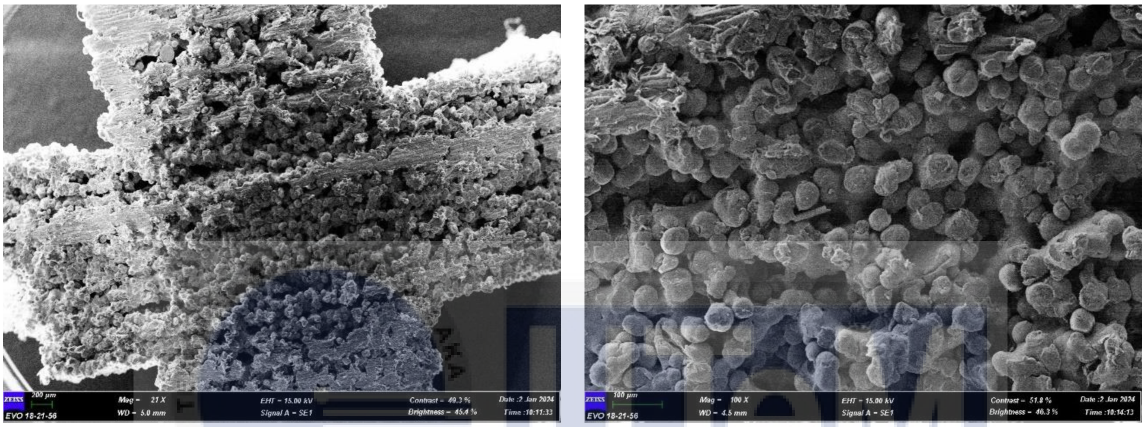

(a) (b)

Figure 4.12 (a) Square Geometry's SEM; (b) Zoomed Square Geometry's SEM

Within the medium surface area that is generated by the tiny particles, the overall surface of the solid geometry is shown to be somewhat rough in image a, which can be seen in Figure 4.13. The distance between the melted particles is rather tiny, as seen in Figure 4.13 (b); yet there are a great number of independent particles that have an irregular form.

UNIVERSITI TEKNIKAL MALAYSIA MELAKA

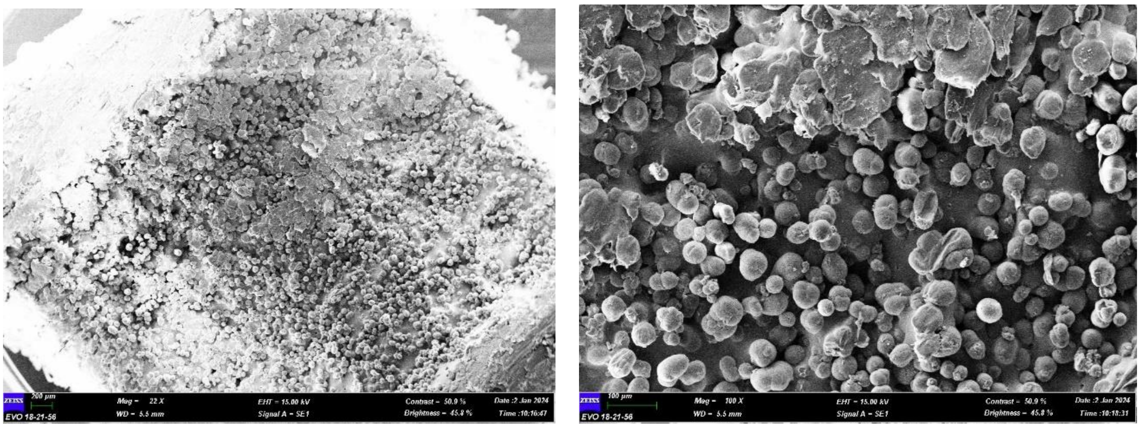

(a) (b)

Figure 4.13 (a) Solid Geometry's SEM; (b) Zoomed Solid Geometry's SEM

On the extremely tiny surface area that is generated by the little particles, the overall surface of the rectangular is shown to be quite rough according to image an in Figure 4.14. Figure 4.14 (b) demonstrates that the distance between the melted particles is rather large, and that there are some particles that are independent of one another.

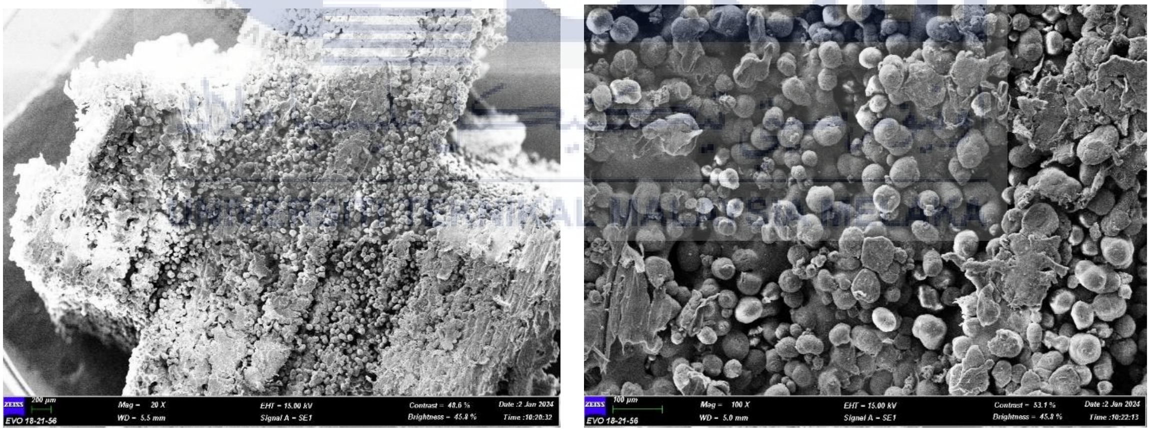

(a) (b)

Figure 4.14 (a) Rectangular Geometry's SEM; (b) Zoomed Rectangular Geometry's SEM

A smooth and flat surface is generated by the melted particles, as seen in image an of Figure 4.15. The overall surface of the triangle is smooth. This indicates that the surface is smoothest when compared to square geometry because the spacing between the melted particles is short, the area of the melted particles is enormous, and there are fewer independent particles. These are the characteristics that are shown in Figure 4.15 (b).

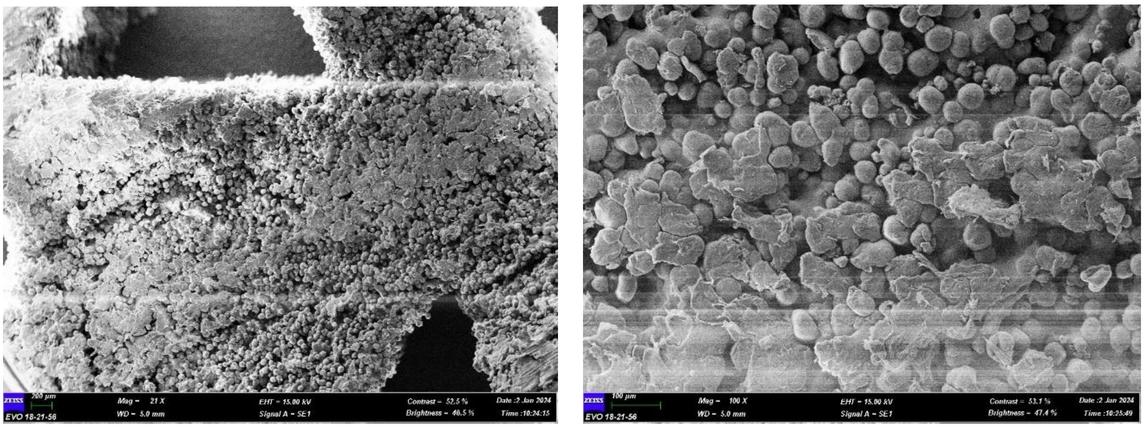

(a) (b)

Figure 4.15 (a) Triangular Geometry’s SEM; (b) Zoomed Triangular Geometry’s SEM

4.6 Overall Result & Discussion

Surface imperfections, surface deformation, and pressure are the only factors that affect rolling friction and sliding friction, as shown in Table 4.9. There is a clear correlation between an increase in surface roughness and an increase in both kinds of friction. According to "An Experimental Study on the Relation Between Friction Force and Real Contact Area," a study conducted by Liang et al., the relationship between friction force and real contact area is significantly affected by rough topographies. Vibrations caused by high friction levels impair the performance of bearings. Vibration testing is significantly related to surface roughness rankings, according to the data. The stress transferred from the roller to the surface of each outer ring has changed due to various design improvements that reduced the contact area (Figure 4.16). The localized stress grows in relation to the shrinking contact area. In addition, Liang et al. conclude that, under loading, the friction force is directly proportional to the normal load multiplied by the actual contact area.

Table 4.9 Factors that Affects the Rolling Friction and Sliding Friction

<table>
<tr><th rowspan="2">Remain Constant</th><th colspan="2">Friction</th></tr>
<tr><th>Rolling</th><th>Sliding</th></tr>
<tr><td>x</td><td colspan="2">Surface Irregularities</td></tr>
<tr><td>x</td><td colspan="2">Surface Deformation</td></tr>
<tr><td>✓</td><td colspan="2">Material</td></tr>
<tr><td>✓</td><td colspan="2">Weight (Shaft)</td></tr>
<tr><td>✓</td><td>Ball diameter</td><td>-</td></tr>
<tr><td>✓</td><td>Surface Adhesion</td><td>-</td></tr>
<tr><td>✓</td><td>Thickness, Shape, and Orientation on Rolling Object</td><td>-</td></tr>
<tr><td>x</td><td>-</td><td>Pressure</td></tr>
</table>

اونيۏرسيتي تيكنيكل مليسيا ملاك
UNIVERSITI TEKNIKAL MALAYSIA MELAKA

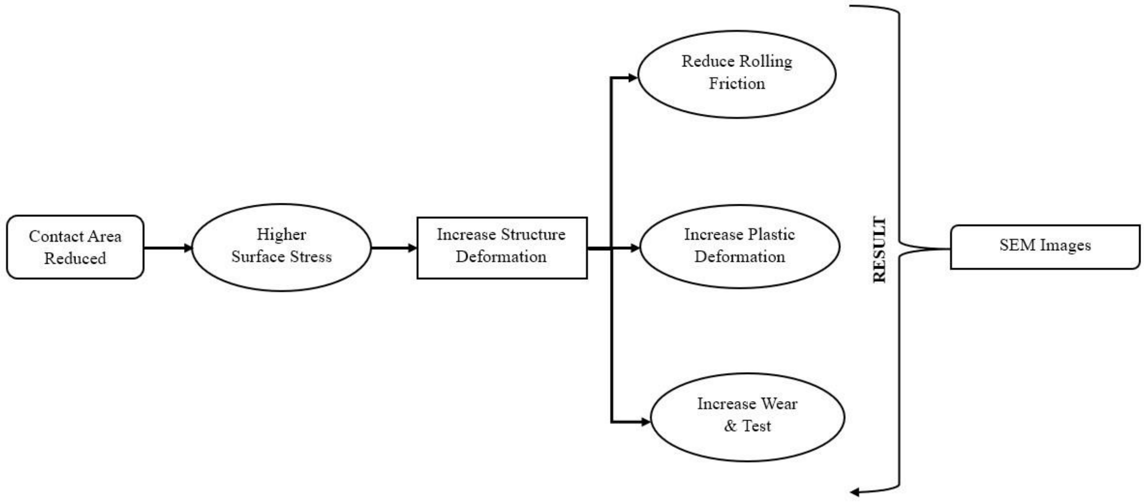

Figure 4.16 Optimized Design Impact

4.6.1 Plastic Deformation

During the motion of the outer ring, there is a noticeable increase in the structural deformation that occurs as a result of the severe stress and quick velocity that are applied to the surface of the ring. In the event that the applied stress exceeds the elastic limit of the material, plastic deformation will reveal itself. As a result of the research conducted by Liang and colleagues, the true contact area decreases in a consistent manner throughout the process of unloading, yet it demonstrates a nonlinear drop until it completely disappears. Furthermore, it is discovered that the plastic deformation that occurred during the loading period is absolutely irreversible. The picture of the rectangular shape obtained using scanning electron microscopy (SEM) provides a striking demonstration of how plastic deformation transforms the powder, which was originally circular, into a more expansive flattened area (Figure 4.17). This is supported by the fact that the rectangular shape is a rectangle.

It is of the utmost importance to note that the rectangular structure, as it has been defined clearly, is subjected to the maximum stress because of the small contact surface it has. Consequently, when comparing plastic deformation across a variety of geometries, the rectangle stands out as the shape that has the most broad flat surface area among all forms.

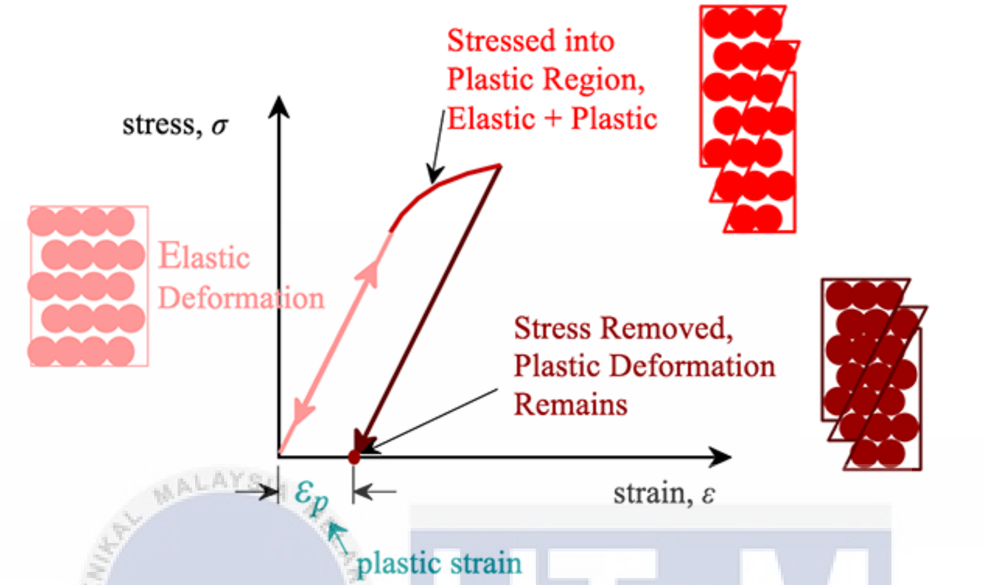

Figure 4.17 Plastic Deformation

Note. Stress-strain curve [Image], by Figure 7.10(a), Callister & Rethwisch 5e, 2018, (https://www.e-education.psu.edu/matse81/node/2104).

اونيۏرسيتي تيكنيكل مليسيا ملاك
UNIVERSITI TEKNIKAL MALAYSIA MELAKA

4.6.2 Friction

Within the scope of this discussion, the frictional forces that are most prominent are rolling friction and sliding friction. The material qualities of the 3D-printed bearing product remain the same; nevertheless, there is a significant difference in the composition. The outer ring and cage are made from fresh PA12 powder, while the other components are made from recycled PA12 powder. This is a considerable differential. Abrasion, adhesion, and fatigue are the three processes that have been recognized as being responsible for wear, according to the results of extensive study. During the inspection of the powder particles using scanning electron microscopy (SEM) that comes before the vibration testing, abnormalities in the powder particles are shown to have a circular shape (Figure 4.18).

The dynamics of rolling friction indicate a decrease that may be ascribed to the dissipation of energy that results from deformation, which is an exceptionally intriguing phenomenon. The entire travel time of the elastic deformation state decreases due to a lower contact area, which in turn restricts the amount of the deformation. This occurs despite the fact that the rolling element experiences a greater degree of distortion during the process. For the purpose of minimizing the influence of plastic deformation on the wear mechanism, this decrease in the total travel time during elastic deformation helps to limit the amount of plastic distortion seen. The book "Modern Approach to Maintenance in Spinning" provides evidence in favor of this assertion by highlighting the fact that sliding friction occurs when one surface glides over another, which results in a greater contact area and, as a consequence, increased resistance. Rolling friction, on the other hand, cuts down on friction by minimizing surface contact, which in turn reduces resistance.

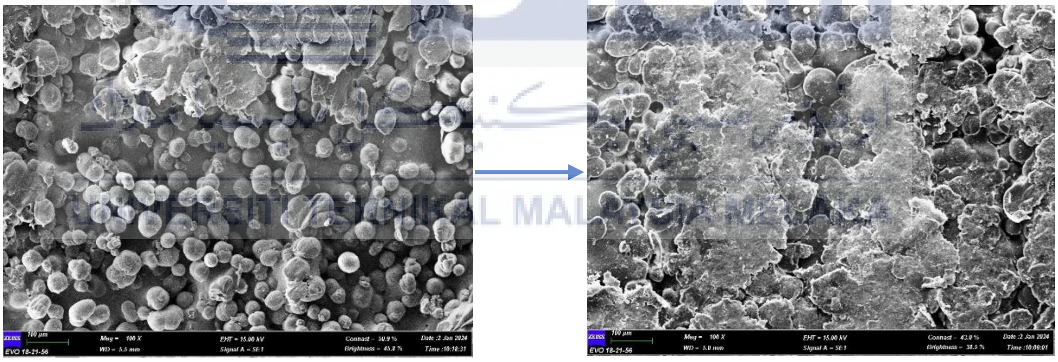

(a) (b)

Figure 4.18 Surface Microstructure of the SLS Mold Before Experience Stress; (a) Before vibration testing; (b) After vibration testing

4.6.3 Wear Mechanism

When comparing virgin and recycled powder products, the hardness value of the former is higher, according to Mohammad Rafi Omar and others. Due to its construction from virgin powder, the outer ring will rip away any surface flaws on the bearing roller. The reason being the wear mechanism is to blame. Because of the action of both abrasion and adhesion, the abrasive will eventually stick to the outer ring's surface. When one substance is transferred to another, whether it's hard or soft, the process is called material transfer. By rolling out a softer material, the roller does more than just smooth out the surface; it also helps fill in any microstructure gaps.

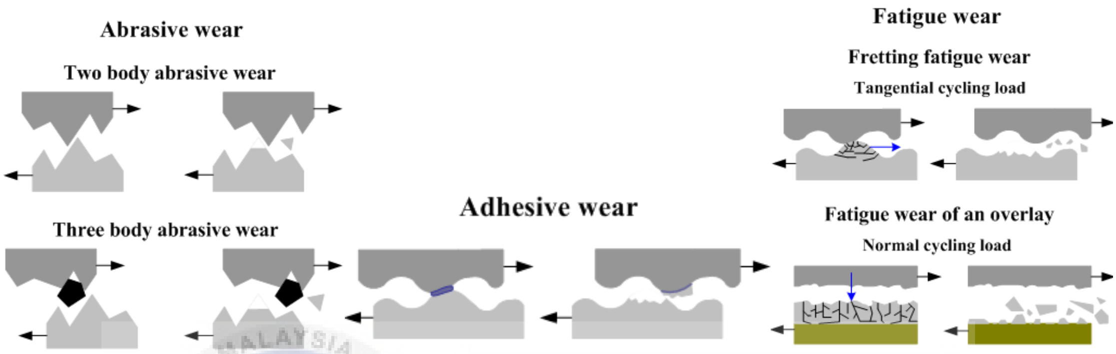

Figure 4.19 wear Mechanism

Note. Adhesive wear, Abrasive wear, and Fatigue wear [Image], by Dmitri Kopeliovich, 2021, (https://www.substech.com/dokuwiki/doku.php?id=mechanisms_of_wear#:~:text=Wear%20i s%20the%20removal%20of,the%20bearing%20and%20the%20crankshaft.).

4.6.4 Overall Result

UNIVERSITI TEKNIKAL MALAYSIA MELAKA

A detailed study of a variety of characteristics is shown in Table 4.10, which contains parallel data for scanning electron microscopy (SEM), surface roughness testing, and vibration testing. It is interesting to note that the SIMSOLID simulation presents a unique viewpoint, since the ranking of the simulation demonstrates an inverse correlation. A lower force equates to a better ranking in SIMSOLID, which is the fundamental measure that revolves around the forces that are hitting the structure. Figure 4.19 provides an insightful explanation of this one-of-a-kind ranking relationship, which stands in contrast to other testing methodologies.

An overarching assumption is taken into consideration once the findings have been combined. According to the information that is presented in Chapter 4.3.1, the real metal product has a tensile modulus that is one hundred times more resistant, which successfully prevents plastic deformation. Therefore, the forces that are operating on the structure are the primary factors that contribute to the wear process. The potential influence of surface deformation and roughness is pushed to the background. Because of this, the SIMSOLID simulation is used to determine and rank the bearing design that is optimum, hence offering a unique way to optimization.

Table 4.10 Comparing All Result Ranking

Geometry	Circle	Rectangular	Solid	Square	Triangle
SIMSOLID Simulation	2	4	1	3	5
Vibration Testing	3	4	2	1	5
SEM	5	3	2	4	1

UNIVERSITI TEKNIKAL MALAYSIA MELAKA

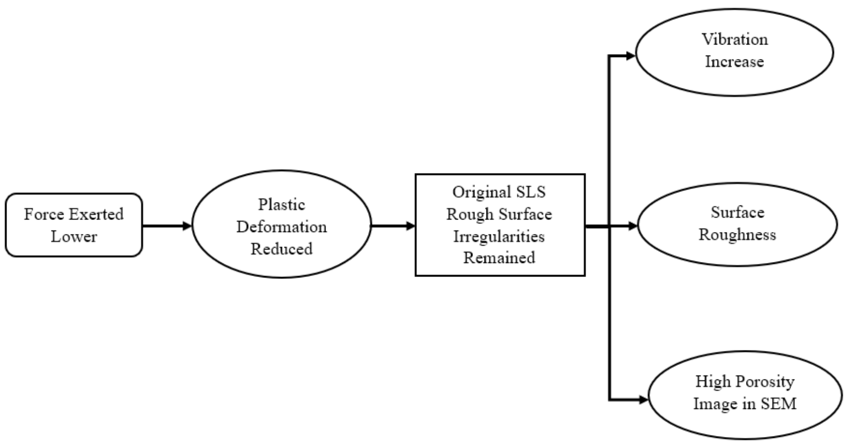

Figure 4.20 Inverse Ranking Relationship of SIMSOLID Simulation Result to Others

CHAPTER 5

CONCLUSION AND RECOMMENDATION

5.1 Conclusion

A new bearing that has a shape that has been optimized has been successfully envisioned in this ground-breaking work. To materialize the prototypes that were painstakingly constructed in Catia V5 and confirmed using SIMSOLID simulations, the cutting-edge Farsoon Technologies 3D SLS Printer SS402P was an essential component. In addition to the manufacturing process, a sophisticated test rig was used to rigorously evaluate the performance of the newly produced bearing, comparing it to the one that was already in existence. An extensive dataset for in-depth study has been provided because of the experimental data that was acquired, which has shown distinguishing traits across a multitude of speeds. In addition, a comprehensive investigation of the tribological behavior of the produced bearing has been carried out based on the findings of the experiment. A thorough examination and discussion has been conducted on the most important factors, which include plastic deformation, friction (both rolling and sliding), and the wear process. Surprisingly, the results of the tests not only fulfilled the expectations that were set for them, but they also positively reinforced one another, which increased the credibility of the conclusions. Since a detailed analysis of the results, the optimum geometric bearing configurations have been rated. The square design has emerged as the top performance, closely followed by the solid, circle, rectangle, and triangle configurations. From a

UNIVERSITI TEKNIKAL MALAYSIA MELAKA

fundamental standpoint, it is undeniably clear that decreasing the surface's contact area has a transformational effect on the performance of the bearing. This research not only presents a bearing design that is revolutionary, but it also offers a comprehensive approach for evaluating and contrasting the performance of various geometrical configurations. As a result, it establishes a new benchmark in the field of bearing invention and analysis.

5.2 Recommendation

Incorporating the reaction-response graph function into the vibration data collecting technique is one way to improve it. This function will result in a curve that is more nuanced and will reflect the distinctive response of acceleration/amplitude vs speed. There are obstacles involved in identifying faults in the damage frequencies using envelope analysis. As a result, a new experiment is required to investigate the possibility of defects in the bearing product. Since the validity of our experiment findings is limited to nylon material and steel ball bearings, it is very necessary to evaluate bearings made of metal with a particular emphasis on geometric performance assessment. When looking for an alternative, it is necessary to investigate various materials that can provide higher performance. In addition, it is essential to take into consideration alterations to the outer race to prevent lubricant from escaping onto the racetrack. This will ensure that the hydrodynamic lubrication phenomena inside the system remains stable.

UNIVERSITI TEKNIKAL MALAYSIA MELAKA

5.3 Future Prospect

Bearings play a crucial role in the functionality of various machines, facilitating smooth rotation and reducing friction between moving parts. The continuous evolution of bearing designs is essential for enhancing overall machine performance. The recent advancements in force distribution analysis have highlighted the potential of optimized bearing designs to revolutionize the bearing market in the future. While the performance gains may seem, marginal compared to existing models, the key lies in improving factors such as bearing life. The optimized designs demonstrate a more efficient force distribution, hinting at longer-lasting bearings that can withstand the rigors of extended usage, ultimately leading to increased reliability and reduced maintenance requirements in diverse machinery applications. The testing findings, especially those related to nylon geometries, may be used to optimize plastic and nylon-like bearings. Engineers may improve bearing designs or build new ones with comparable qualities by understanding nylon geometry. This understanding may increase equipment performance by making bearings stronger and more durable for certain applications. Adopting optimal designs might advance the bearing market and fulfill the expectations of industries that require efficient and durable equipment.

UNIVERSITI TEKNIKAL MALAYSIA MELAKA

REFERENCES

Papadopoulos, C. I., Efstathiou, E. E., Nikolakopoulos, P. G., & Kaiktsis, L. (2011). Geometry optimization of textured 3-D micro - Thrust bearings. *Proceedings of the ASME Turbo Expo*, *3*, 801–810. https://doi.org/10.1115/GT2011-45822

Wasilczuk, M. (2013). *Should we seek further improvement of fluid film bearings-what for and how? Increasing durability of bearings in wind turbine gearboxes View project Should we seek further improvement of fluid film bearings-what for and how? Faut-il encore chercher à améliorer les paliers à film fluide-pourquoi et comment?* https://www.researchgate.net/publication/258319102

Nordin Mohamad Norani, M., Ilman Hakimi Chua Abdullah, M., Fadzli Bin Abdollah, M., Amiruddin, H., Redza Ramli, F., Tamaldin, N., Abdullah, R., Rafi Omar, M., Kejuruteraan Mekanikal, F., & Teknologi Kejuruteraan Mekanikal, F. (2022). *Internal structure part friction deviation between SLS and FFF 3D-printed methods*.

tribonet. (2019). *Laws of Friction | Tribology | Tribonet*. https://www.tribonet.org/wiki/laws-of-friction/

SKF. (n.d.). https://www.skf.com/my/products/rolling-bearings/ball-bearings/thrust-ball-bearings

Chang, Zhou, et al. "Optimization of the Grinding Process to Improve the Surface Integrity of Bearing Raceways." *Optimization of the Grinding Process to Improve the Surface Integrity of Bearing Raceways*, vol. 91, no. 9-12, 12 Feb. 2017, pp. 4243–4252, https://doi.org/10.1007/s00170-017-0061-3. Accessed 18 June 2023.

Fractory. "Types of Bearings | Uses & Working Mechanisms Explained." *Fractory*, 25 Aug. 2020, fractory.com/types-of-bearings/.

Hashimoto, Hiromu, and Masayuki Ochiai. "Optimization of Groove Geometry for Thrust Air Bearing to Maximize Bearing Stiffness." *Journal of Tribology*, vol. 130, no. 3, 23 June 2008, https://doi.org/10.1115/1.2913546. Accessed 6 Oct. 2022.

Loughborough University. "Powder Bed Fusion | Additive Manufacturing Research Group | Loughborough University." *Lboro.ac.uk*, 2010, www.lboro.ac.uk/research/amrg/about/the7categoriesofadditivemanufacturing/powderbedfusion/.

Mohd, et al. "Synergistic Effect of Loads and Speeds on the Dry Sliding Behaviour of Fused Filament Fabrication 3D-Printed Acrylonitrile Butadiene Styrene Pins with Different Internal Geometries." *Synergistic Effect of Loads and Speeds on the Dry Sliding Behaviour of Fused Filament Fabrication 3D-Printed Acrylonitrile Butadiene Styrene Pins with Different Internal Geometries*, vol. 108, no. 7-8, 1 June 2020, pp. 2525–2539, https://doi.org/10.1007/s00170-020-05573-7. Accessed 18 June 2023.

UNIVERSITI TEKNIKAL MALAYSIA MELAKA

Moore, Jacob. “6.1: Dry Friction.” *Engineering LibreTexts*, 30 Apr. 2021, eng.libretexts.org/Bookshelves/Mechanical_Engineering/Mechanics_Map_(Moore_et_al.)/06%3A_Friction_and_Friction_Applications/6.01%3A_Dry_Friction.

SimSolid FAST START TRAINING Fast Start Training Guide. (2015).

n.d. “Global Bearings Market Size, Share Analysis Report, 2023-2032.” *Polaris*, 2022, www.polarismarketresearch.com/industry-analysis/bearings-market. Accessed 18 June 2023.

n.d. “The History of the Bearing.” *Www.acorn-Ind.co.uk*, 28 Mar. 2022, www.acorn-ind.co.uk/insight/the-history-of-the-bearing/.

n.d. “Types.” *Nskamericas.com*, 2019, www.nskamericas.com/en/services/what-s-a-bearing/types.html.

n.d. “Types of Bearings.” *Engineering Learn*, 6 Nov. 2020, engineeringlearn.com/types-of-bearings/.

Nordin Mohamad Norani, M., Ilman Hakimi Chua Abdullah, M., Fadzli Bin Abdollah, M., Amiruddin, H., Redza Ramli, F., Tamaldin, N., Kejuruteraan Mekanikal, F., Teknikal Malaysia Melaka, U., Tuah Jaya, H., Tunggal, D., & Teknologi Kejuruteraan Mekanikal, F. (2020). Tribological analysis of a 3D-printed internal triangular flip ABS pin during running-in stage. In *Jurnal Tribologi* (Vol. 27).

Fesanghary, M., & Khonsari, M. M. (2012). Topological and shape optimization of thrust bearings for enhanced load-carrying capacity. *Tribology International*, *53*, 12–21. https://doi.org/10.1016/j.triboint.2012.03.018

Ma, S., He, G., Yan, K., Li, W., Zhu, Y., & Hong, J. (2022). Structural optimization of ball bearings with three-point contact at high-speed. *International Journal of Mechanical Sciences*, *229*. https://doi.org/10.1016/j.ijmecsci.2022.107494

Friedrich, K. (2018). Polymer composites for tribological applications. In *Advanced Industrial and Engineering Polymer Research* (Vol. 1, Issue 1, pp. 3–39). KeAi Communications Co. https://doi.org/10.1016/j.aiepr.2018.05.001

Payne, Dean. “The Complete History of Bearings You Need to Know.” *Www.bdsbearing.com*, 1 Nov. 2022, www.bdsbearing.com/blog/bearing-history.

SLS. “The Different Types of Bearing Materials.” *Blog.slsbearings.com*, blog.slsbearings.com/the-different-types-of-bearing-materials.

The Editors of Encyclopaedia Britannica. “Coefficient of Friction | Physics.” *Encyclopædia Britannica*, 24 June 2020, www.britannica.com/science/coefficient-of-friction.

The Editors of Encyclopedia Britannica. “Friction | Definition, Types, & Formula.” *Encyclopædia Britannica*, 25 Jan. 2019, www.britannica.com/science/friction.

WAZP. "Nylon 12 (PA-12) Material Characteristics - WAZP." *Www.wazp.io*, 25 May 2021, www.wazp.io/blogs/post/nylon-12-pa12-material-characteristics. Accessed 18 June 2023.
Hsu, Y.-L., Hsu, M.-S., & Chen, C.-T. (n.d.). *Interpreting results from topology optimization using density contours*. www.elsevier.com/locate/compstruc

Tadina, Matej, and Miha Boltežar. "Improved Model of a Ball Bearing for the Simulation of Vibration Signals due to Faults during Run-Up." *Journal of Sound and Vibration*, vol. 330, no. 17, Aug. 2011, pp. 4287–4301, https://doi.org/10.1016/j.jsv.2011.03.031. Accessed 20 Apr. 2022.

Jacobs, W., Boonen, R., Sas, P., & Moens, D. (2014). The influence of the lubricant film on the stiffness and damping characteristics of a deep groove ball bearing. *Mechanical Systems and Signal Processing*, *42*(1–2), 335–350. https://doi.org/10.1016/j.ymssp.2013.07.018

Zhang, W., Deng, S., Chen, G., & Cui, Y. (2017). Impact of lubricant traction coefficient on cage's dynamic characteristics in high-speed angular contact ball bearing. *Chinese Journal of Aeronautics*, *30*(2), 827–835. https://doi.org/10.1016/j.cja.2016.08.019

Olaru, D. N., Bălan, M. R. D., Tufescu, A., Cârlescu, V., & Prisacaru, G. (2017). Influence of the cage on the friction torque in low loaded thrust ball bearings operating in lubricated conditions. *Tribology International*, *107*, 294–305. https://doi.org/10.1016/j.triboint.2016.11.042

Liu, Y., Wang, W., Qing, T., Zhang, Y., Liang, H., & Zhang, S. (2020). The effect of lubricant temperature on dynamic behavior in angular contact ball bearings. *Mechanism and Machine Theory*, *149*. https://doi.org/10.1016/j.mechmachtheory.2020.103832

Wang, Q., Zhang, G., Zheng, X., Ni, Y., Liu, F., Liu, Y., & Xu, L. R. (2023). Efficient characterization on the interlayer shear strengths of 3D printing polymers. *Journal of Materials Research and Technology*, *22*, 2768–2780. https://doi.org/10.1016/j.jmrt.2022.12.147

Chang, Z., Hou, L., & Chen, Y. (2023). Nonlinear dynamics and thermal bidirectional coupling characteristics of a rotor-ball bearing system. *Applied Mathematical Modelling*, *119*, 513–533. https://doi.org/10.1016/j.apm.2023.03.009

Deng, K., Wu, H., Li, Y., Jiang, J., Yang, Z., Zhang, R., Liu, S., Chao, B., Fu, W., & Wang, M. (2023). Porous NFG/SiCnw composites fabricated by SLS for structural load-bearing and functionally integrated electromagnetic absorption. *Ceramics International*. https://doi.org/10.1016/j.ceramint.2023.06.122

Lu-Minh, C., Njiwa, P., Leclerc, K., Chen, Y. M., Delgado, J., & Cardey, P. F. (2022). Effectiveness of greases to prevent fretting wear of thrust ball bearings according to ASTM D4170 standard. *Results in Engineering*, *14*. https://doi.org/10.1016/j.rineng.2022.100468

Toumi, M. Y., Murer, S., Bogard, F., & Bolaers, F. (2018). Numerical simulation and experimental comparison of flaw evolution on a bearing raceway: Case of thrust ball bearing.

Journal of Computational Design and Engineering, *5*(4), 427–434. https://doi.org/10.1016/j.jcde.2018.01.004

Gao, S., Wang, L., & Zhang, Y. (2023). Modeling and dynamic characteristic analysis of high speed angular contact ball bearing with variable clearance. *Tribology International*, *182*. https://doi.org/10.1016/j.triboint.2023.108330

Wang, M., Yan, K., Tang, Q., Guo, J., Zhu, Y., & Hong, J. (2023). Dynamic modeling and properties analysis for ball bearing driven by structure flexible deformations. *Tribology International*, *179*. https://doi.org/10.1016/j.triboint.2022.108163

Yang, Y., Liu, H., Ma, H., Wang, P., Han, Q., & Wen, B. (2023). Experimental study on vibration characteristics due to cage damage of deep groove ball bearing. *Tribology International*, *185*. https://doi.org/10.1016/j.triboint.2023.108555

Wang, M., Yan, K., Zhang, X., Zhu, Y., & Hong, J. (2023). A comprehensive study on dynamic performance of ball bearing considering bearing deformations and ball-inner raceway separation. *Mechanical Systems and Signal Processing*, *185*. https://doi.org/10.1016/j.ymssp.2022.109826

Lee, Y. J., Lee, K. H., & Lee, C. H. (2018). Friction performance of 3D printed ball bearing: Feasibility study. *Results in Physics*, *10*, 721–726. https://doi.org/10.1016/j.rinp.2018.07.011

Patel, V. N., Tandon, N., & Pandey, R. K. (2012). Defect detection in deep groove ball bearing in presence of external vibration using envelope analysis and Duffing oscillator. *Measurement: Journal of the International Measurement Confederation*, *45*(5), 960–970. https://doi.org/10.1016/j.measurement.2012.01.047

Kwak, W., Lee, J., & Lee, Y. B. (2019). Theoretical and experimental approach to ball bearing frictional characteristics compared with cryogenic friction model and dry friction model. *Mechanical Systems and Signal Processing*, *124*, 424–438. https://doi.org/10.1016/j.ymssp.2019.01.056

Kecik, K., Smagala, A., & Ciecieląg, K. (2023). Diagnosis of angular contact ball bearing defects based on recurrence diagrams and quantification analysis of vibration signals. *Measurement: Journal of the International Measurement Confederation*, *216*. https://doi.org/10.1016/j.measurement.2023.112963

About FFT Spectrum Analyzers. (n.d.). www.thinkSRS.com

Shi, X., Lu, X., Feng, Y., & Qiu, Z. (2022). Tribo-dynamic analysis for aero ball bearing with 3D measured surface roughness. *Engineering Failure Analysis*, *131*. https://doi.org/10.1016/j.engfailanal.2021.105848

Zhang, X., Wu, D., Xia, Z., Li, Y., Wang, J., & Han, E. H. (2022). Characteristics and mechanism of surface damage of hybrid ceramic ball bearings for high-precision machine tool. *Engineering Failure Analysis*, *142*. https://doi.org/10.1016/j.engfailanal.2022.106784

UNIVERSITI TEKNIKAL MALAYSIA MELAKA

Russell, T., & Sadeghi, F. (2022). The effects of lubricant starvation on ball bearing cage pocket friction. *Tribology International*, *173*. https://doi.org/10.1016/j.triboint.2022.107630

Wu, D., Zhang, X. C., Li, Y. F., Wang, J., & Han, E. H. (2021). Characterization of machined surface quality and near-surface microstructure of a high speed thrust angular contact ball bearing. *Journal of Materials Science and Technology*, *86*, 219–226. https://doi.org/10.1016/j.jmst.2020.12.074

Han, C. F., Wu, C. C., Chu, H. Y., Tsai, P. H., Horng, J. H., Wei, C. C., Hwang, Y. C., & Lin, J. F. (2020). Uses of empirical mode decomposition and multi-entropy techniques to establish the correlations among vibrations, friction coefficients and component wear of ball-bearing-like specimens. *Measurement: Journal of the International Measurement Confederation*, *150*. https://doi.org/10.1016/j.measurement.2019.107021

Xie, Z., Yang, K., He, T., & Jiao, J. (2023). Experimental and theoretical analysis on the nonlinear rotor-dynamic performances and vibration characteristics of a novel bearing-rotor system. *Mechanical Systems and Signal Processing*, *199*. https://doi.org/10.1016/j.ymssp.2023.110416

Ji, Zhaoxia. "Use of Compositional and Combinatorial Nanomaterial Libraries for Biological Studies." *Science Bulletin*, vol. 61, no. 10, 1 May 2016, pp. 755–771, www.sciencedirect.com/science/article/abs/pii/S2095927316301190, https://doi.org/10.1007/s11434-016-1069-z. Accessed 5 Aug. 2022.

SLS. "The Different Types of Bearing Materials." *Blog.slsbearings.com*, 15 Apr. 2021, blog.slsbearings.com/the-different-types-of-bearing-materials.

Liang, X. M., Xing, Y. Z., Li, L. T., Yuan, W. K., & Wang, G. F. (2021). An experimental study on the relation between friction force and real contact area. Scientific Reports, 11(1). https://doi.org/10.1038/s41598-021-99909-2

Burdzik, R., & Burdzik, R. (2013). Research on the influence of engine rotational speed to the vibration penetration into the driver via feet-multidimensional analysis. In Article in Journal of Vibroengineering. https://www.researchgate.net/publication/286963461

Hendriks, C. P., & Franklin, S. E. (2010). Influence of surface roughness, material and climate conditions on the friction of human skin. Tribology Letters, 37(2), 361–373. https://doi.org/10.1007/s11249-009-9530-7

APPENDICES

APPENDIX A - Damage and Speed Frequencies

Equations:

Error Frequency of Inner Ring: BPFI= $\frac{f^{N}}{2} n\ (1 + (\frac{d}{D}) \cos\theta\ )$

Error Frequency of Outer Ring: BPFO= $\frac{f^{N}}{2} n\ (1 - (\frac{d}{D}) \cos\theta\ )$

Error Frequency of Balls: BSF= $\frac{f^{N}}{2} (\frac{D}{d})\ (1 -((\frac{d}{D} \cos\theta\ ))^2)$

Error Frequency of Cage: BPFI= $\frac{f^{N}}{2} (1 - (\frac{d}{D}) \cos\theta\ )$

Speed of Inner Ring: $f^{N} = \frac{N}{60}$

N = Motor speed (Rpm)

n = Number of rolling elements

D = Pitch circle diameter

d = Diameter of roller elements

ɵ = Contact angle

Schaeffler's Bearing Analysis for Standard Size

Basic Frequencies Factors

Error Frequency factor of inner ring: BPFI =7.3235

Error Frequency factor of outer ring: BPFO = 4.6765

Error Frequency factor of balls: BSF= 2.1564

Error Frequency factor of Cage: FTF= 0.3897; 0.6103

UNIVERSITI TEKNIKAL MALAYSIA MELAKA

APPENDIX B - Customized Material Properties for Nylon PA 12 in SIMSOLID

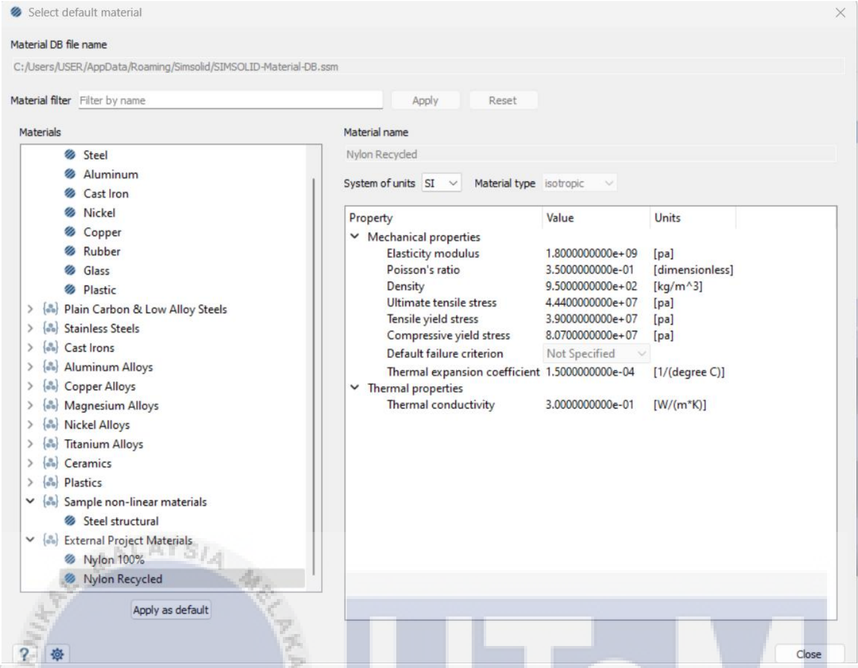

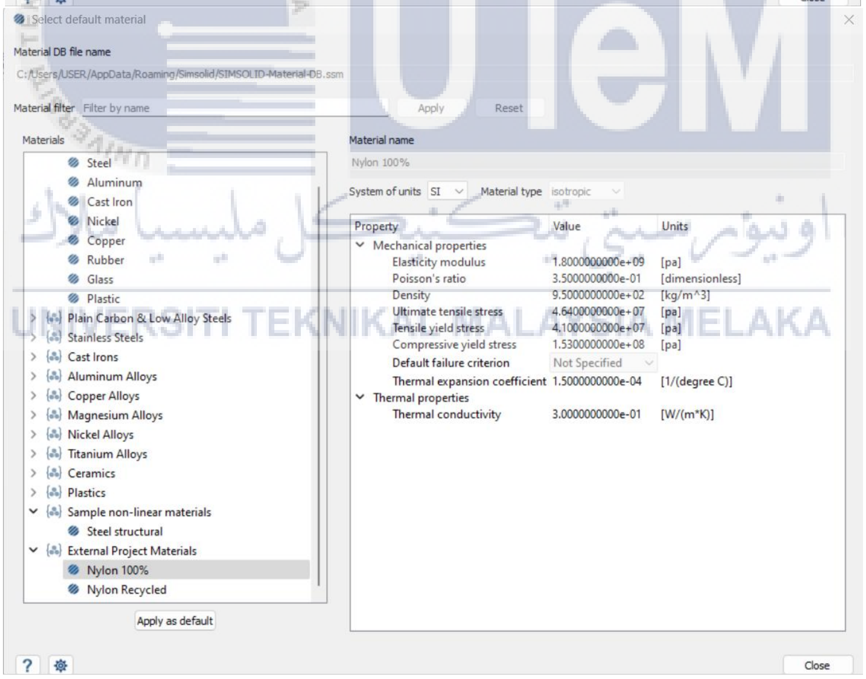

APPENDIX C - SIMSOLID Simulation Results

<u>Circle geometry</u>

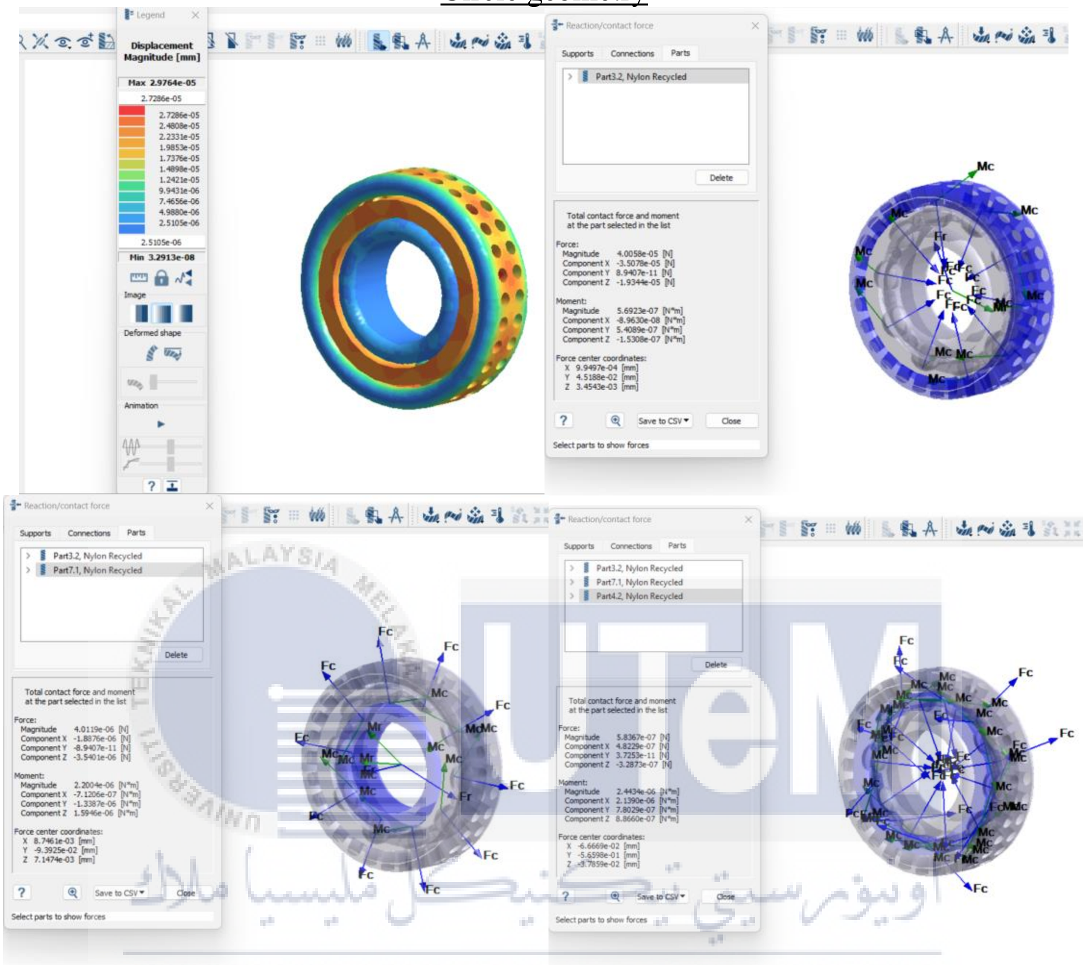

UNIVERSITI TEKNIKAL MALAYSIA MELAKA

<u>Rectangular geometry</u>

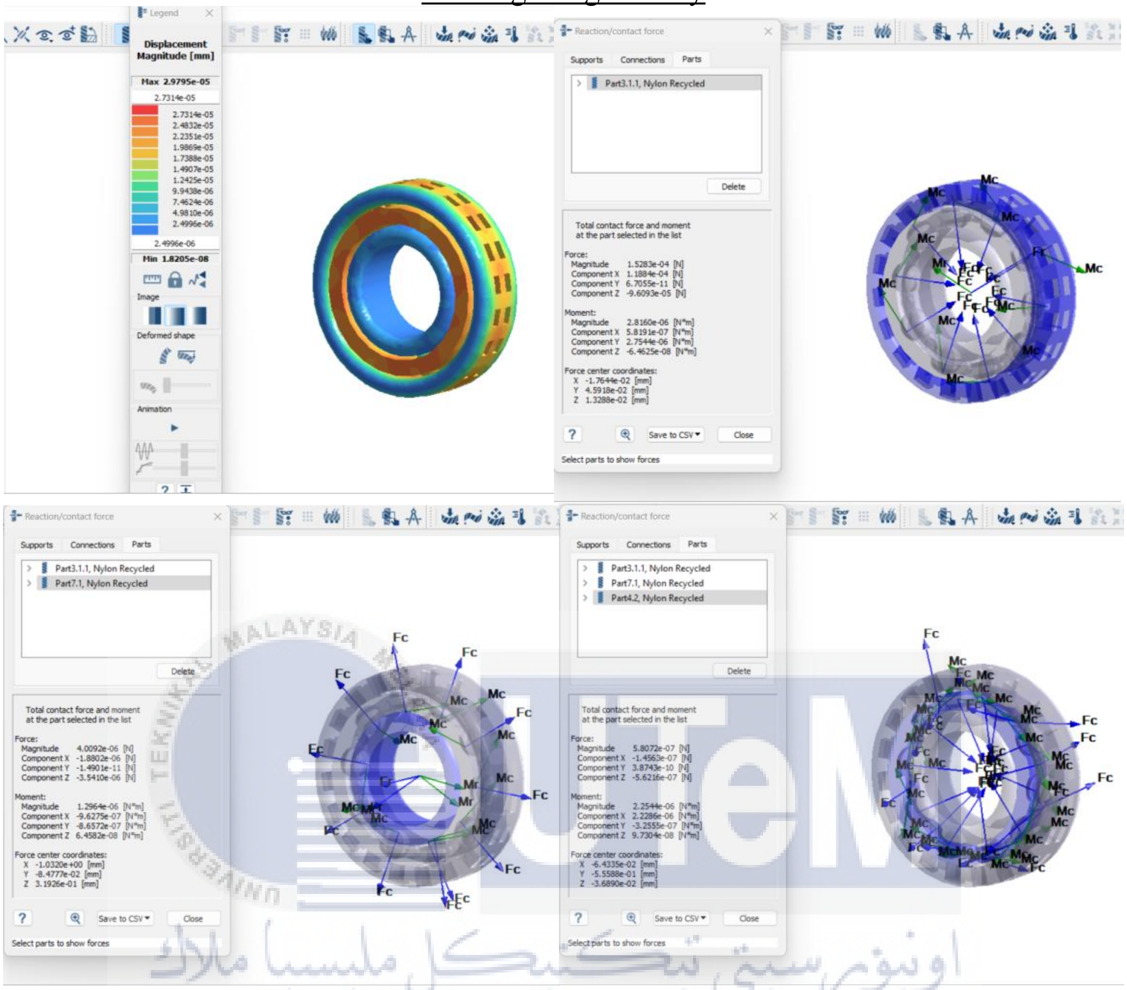

UNIVERSITI TEKNIKAL MALAYSIA MELAKA

<u>Solid geometry</u>

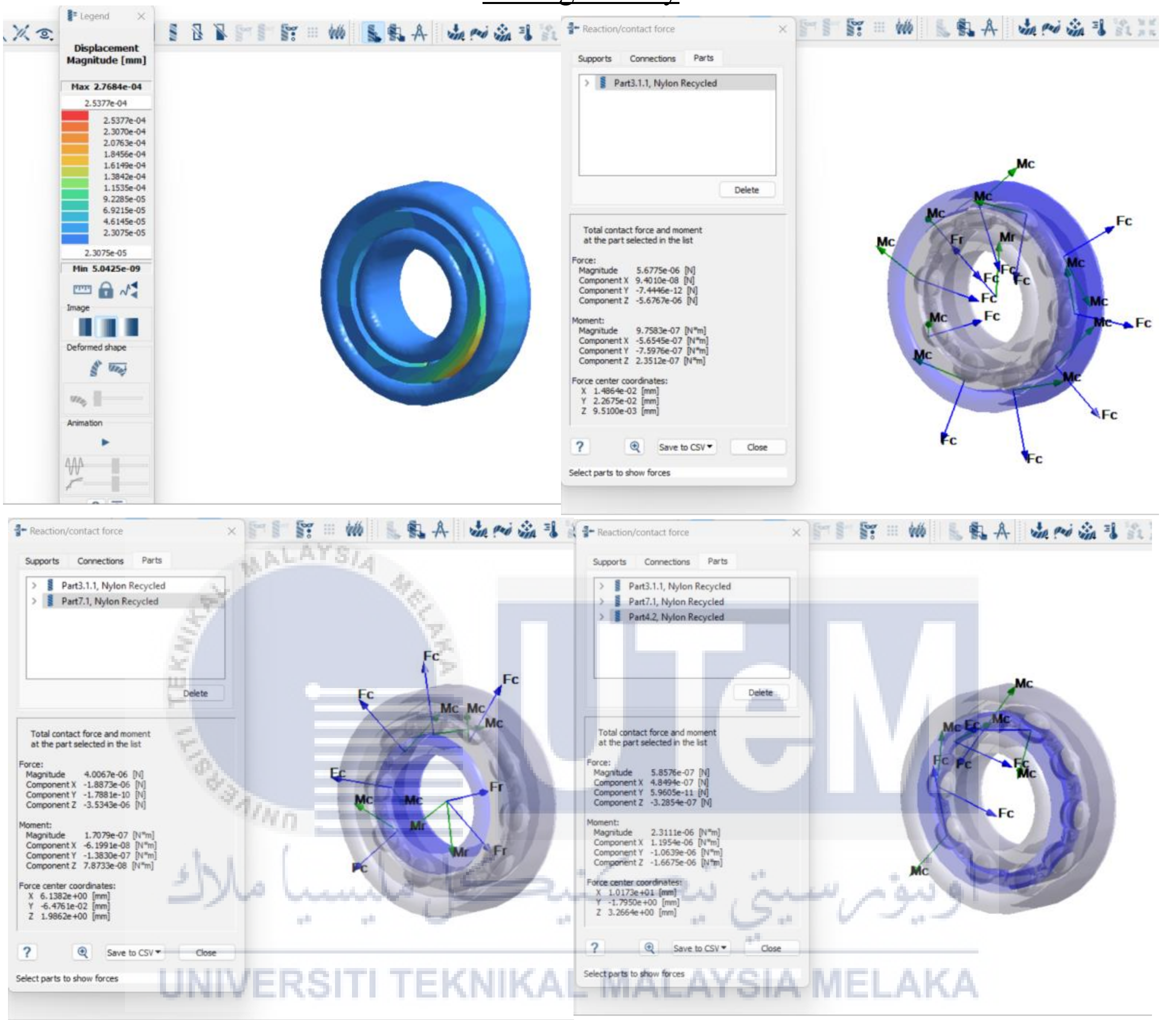

UNIVERSITI TEKNIKAL MALAYSIA MELAKA

Square geometry

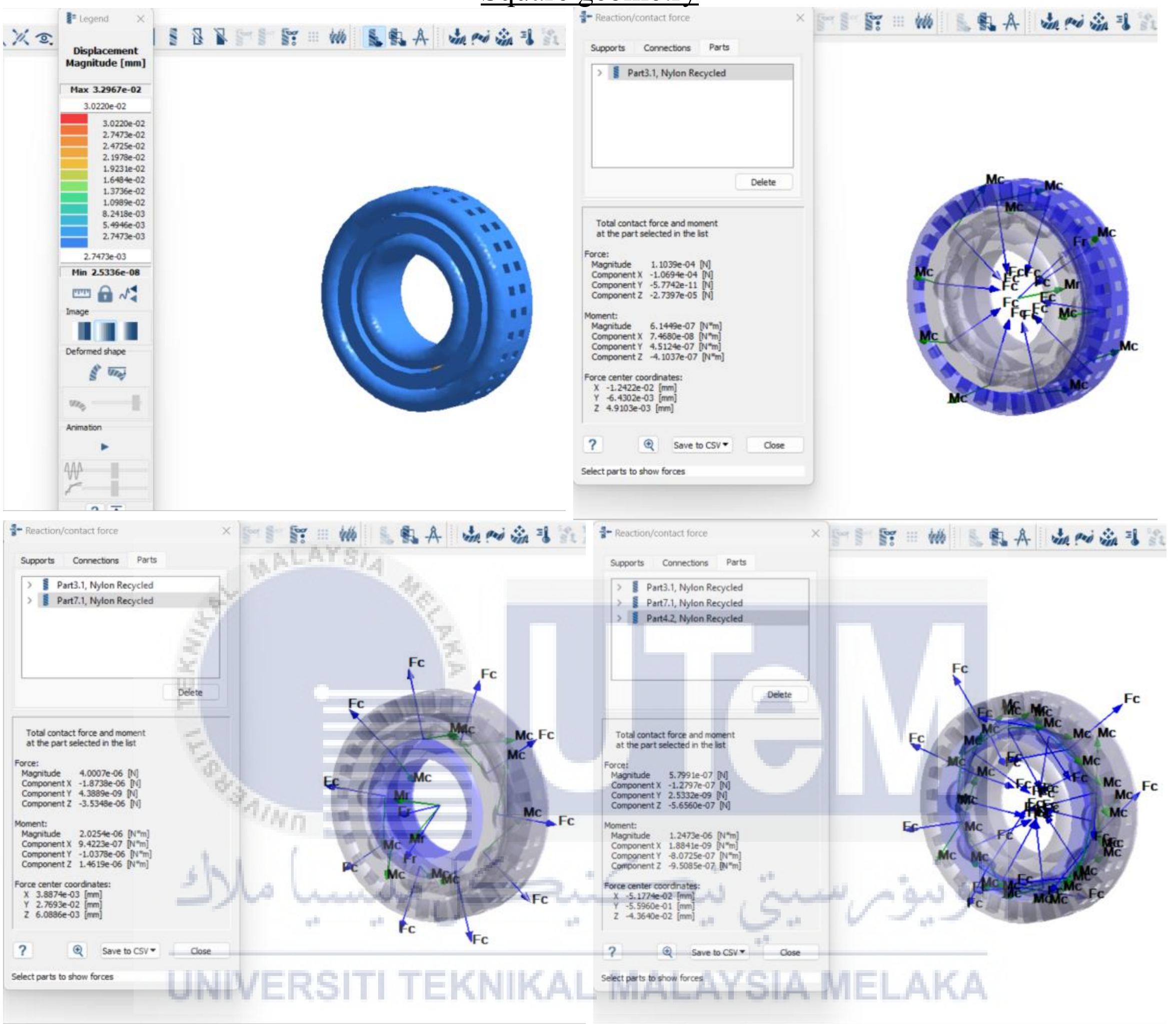

UNIVERSITI TEKNIKAL MALAYSIA MELAKA

<u>Triangle geometry</u>

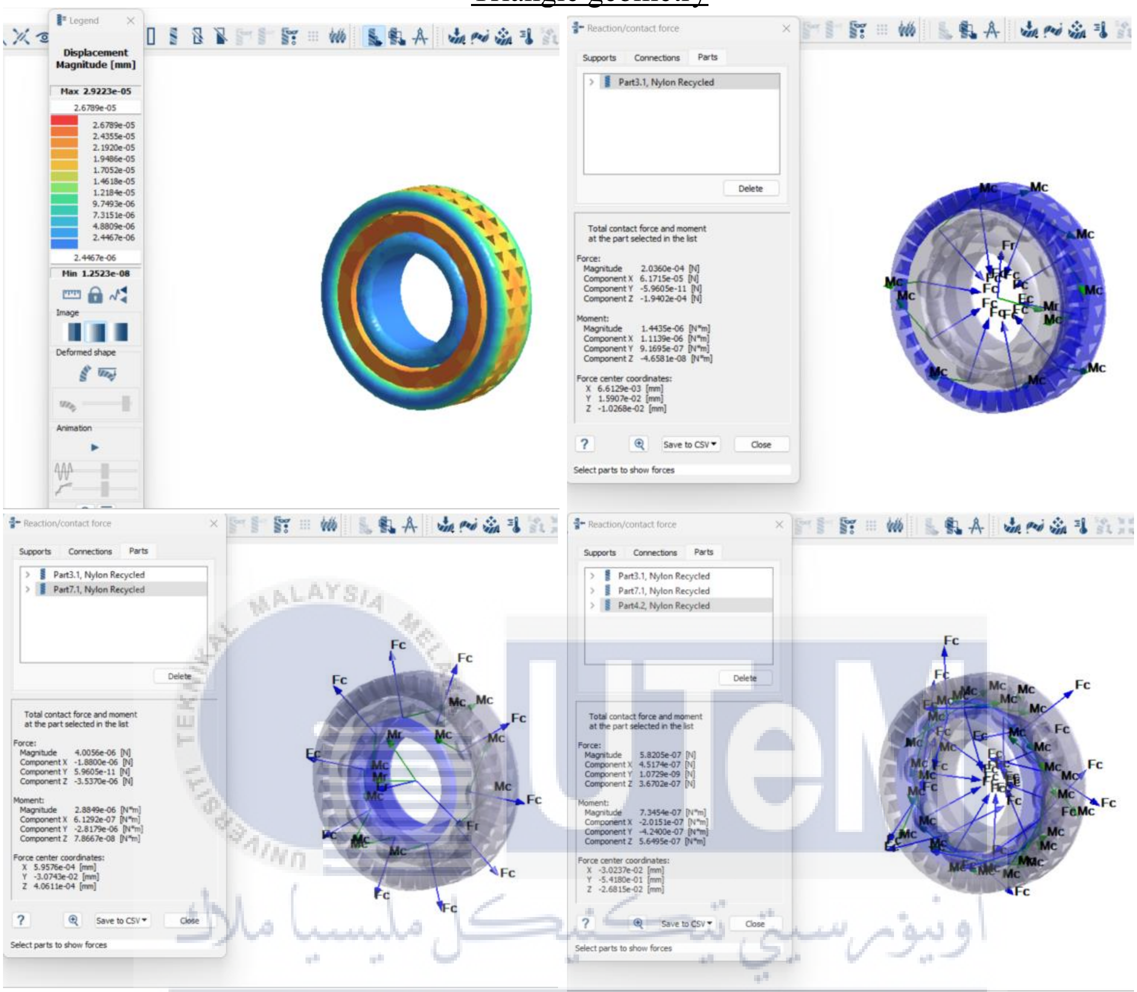

UNIVERSITI TEKNIKAL MALAYSIA MELAKA

APPENDIX D - Damage Frequency Detected in Envelope Analysis

Speed	Damaged frequency detected				
	Circle	Rectangle	Solid	Square	Triangle
600	2x BSF 2x BPFO	2x BSF 2x BPFO	2x BSF 2x BPFO	2x BSF 2x BPFO	1x BSF & 2x BSF 2x BPFO 1x BPFI
900	2x BSF 2x BPFO	2x BSF 2x BPFO 1x BPFI	2x BSF 2x BPFO	2x BSF 2x BPFO 1x BPFI	2x BSF 2x BPFO 1x BPFI
1200	2x BSF	2x BSF	2x BSF	2x BSF	2x BSF
1500	2x BSF	2x BSF	2x BSF	2x BSF	2x BSF
1800	1x BSF & 2x BSF	1x BSF & 2x BSF 1x BPFO	2x BSF	1x BSF & 2x BSF 1x BPFO 1x BPFI	1x BSF & 2x BSF 1x BPFO 1x BPFI

UTeM
اونيۏرسيتي تيكنيكل مليسيا ملاك
UNIVERSITI TEKNIKAL MALAYSIA MELAKA

APPENDIX E - Damage Index Detected in Envelope Analysis

Rpm	Geometry	Dmage Index (RMS)		
		Channel 1	Channel 2	Average
600	Circle	0.058	0.06	0.059
	Rectangular	0.027	0.03	0.0285
	Solid	0.017	0.02	0.0185
	Square	0.049	0.51	0.2795
	Triangle	0.085	0.087	0.086
900	Circle	0.162	0.165	0.1635
	Rectangular	0.083	0.085	0.084
	Solid	0.0475	0.0477	0.0476
	Square	0.086	0.088	0.087
	Triangle	0.198	0.2	0.199
1200	Circle	0.168	0.17	0.169
	Rectangular	0.255	0.257	0.256
	Solid	0.35	0.37	0.36
	Square	0.101	0.103	0.102
	Triangle	0.22	0.24	0.23
1500	Circle	0.28	0.3	0.29
	Rectangular	0.4	0.42	0.41
	Solid	0.255	0.257	0.256
	Square	0.17	0.19	0.18
	Triangle	0.39	0.41	0.4
1800	Circle	0.4	0.42	0.41
	Rectangular	0.63	0.65	0.64
	Solid	0.375	0.377	0.376
	Square	0.265	0.267	0.266
	Triangle	0.495	0.497	0.496

UNIVERSITI TEKNIKAL MALAYSIA MELAKA

APPENDIX F - Envelope Analysis & FFT Spectrum

<u>Circle geometry</u>

<u>600 rpm</u>

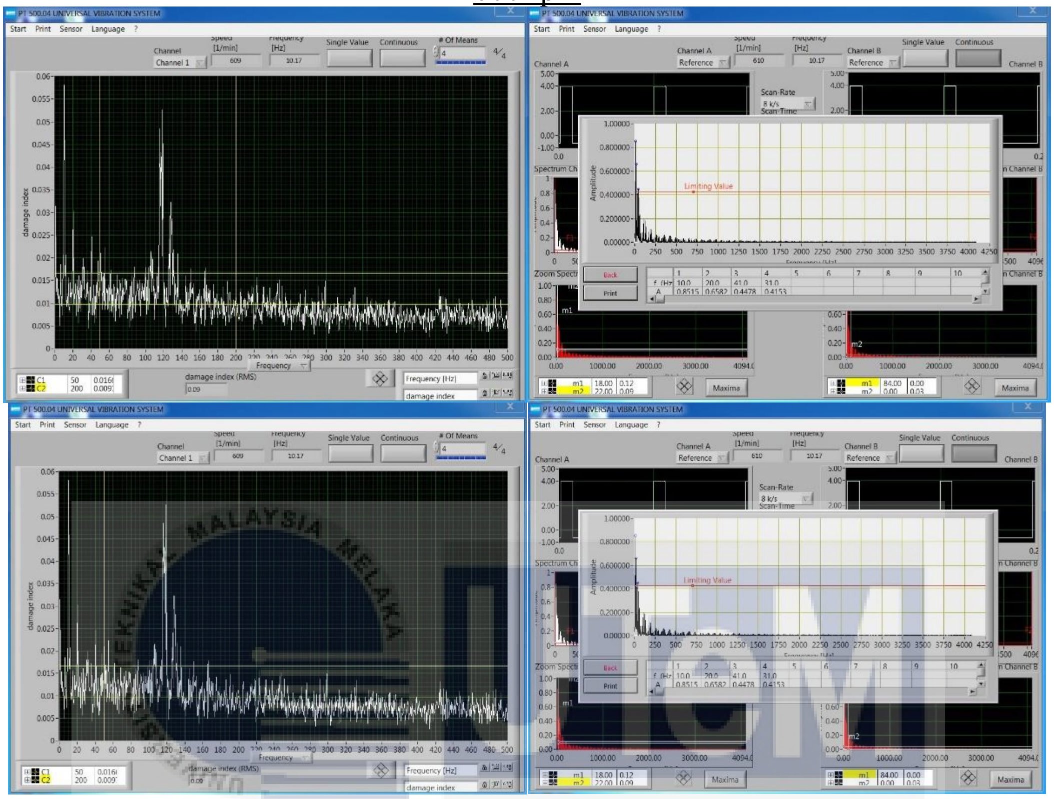

<u>900 rpm</u>

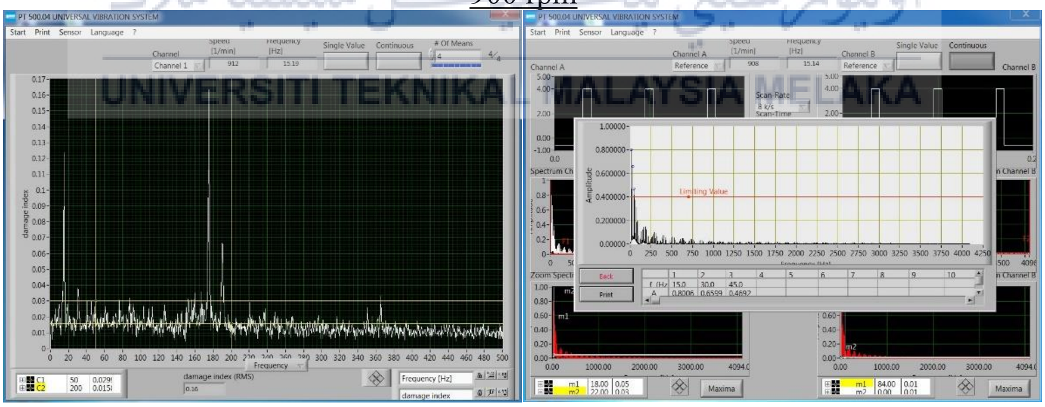

UNIVERSITI TEKNIKAL MALAYSIA MELAKA

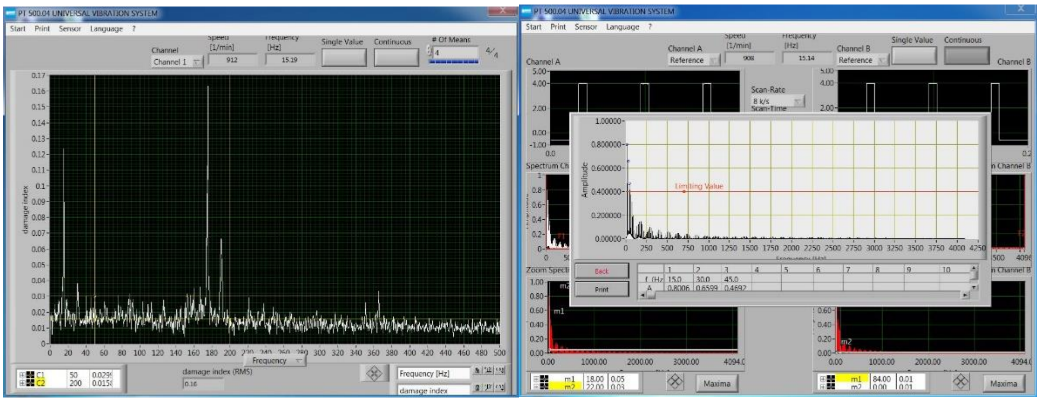

1200 rpm

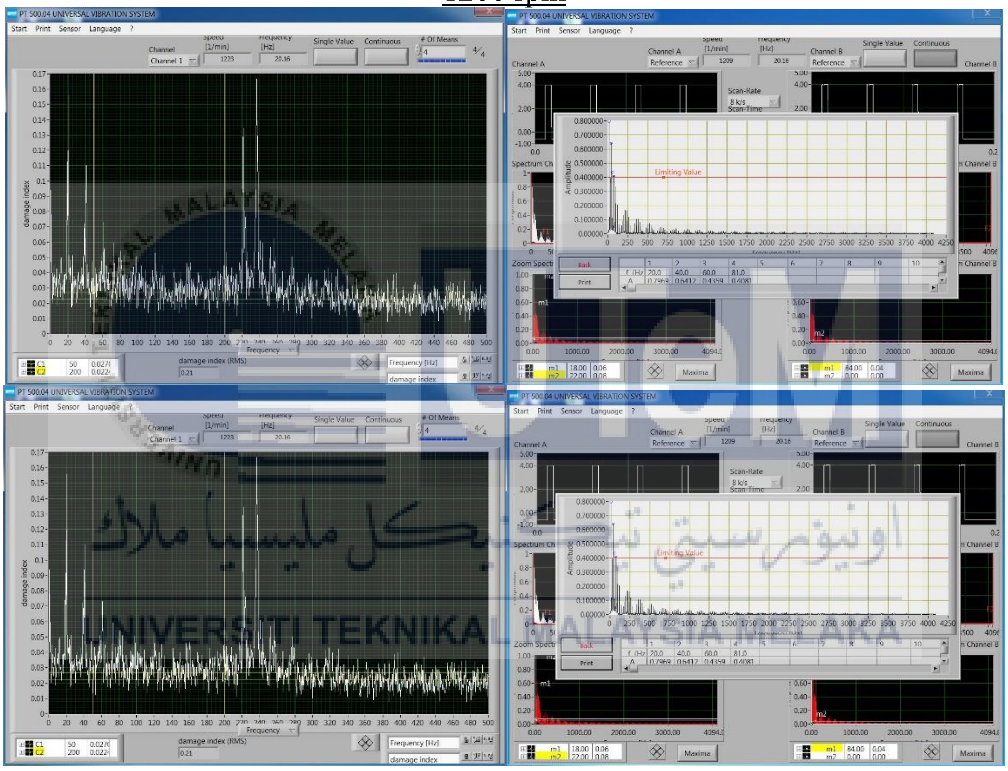

UNIVERSITI TEKNIKAL MALAYSIA MELAKA

1500 rpm

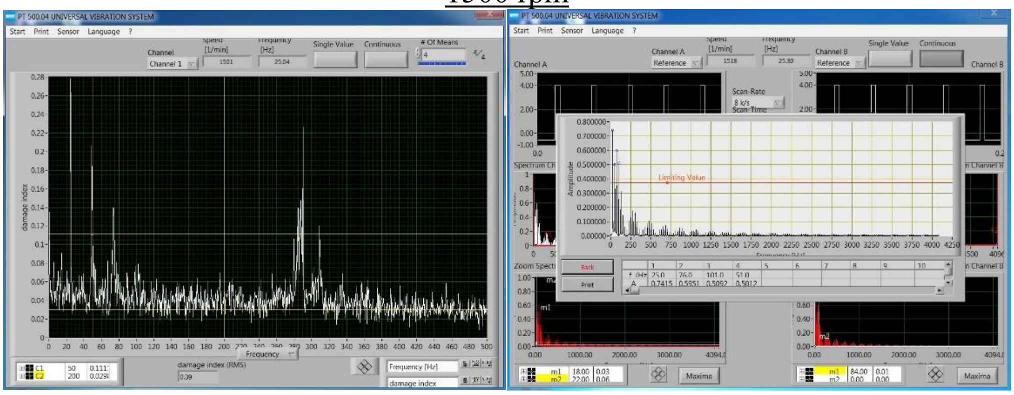

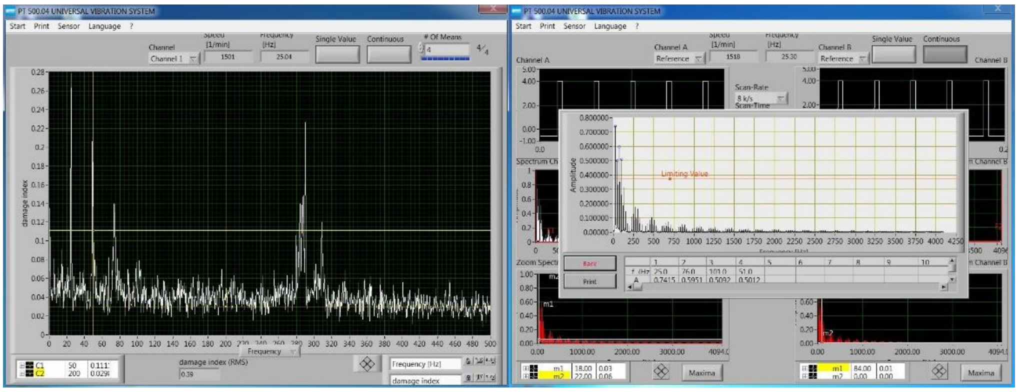

1800 rpm

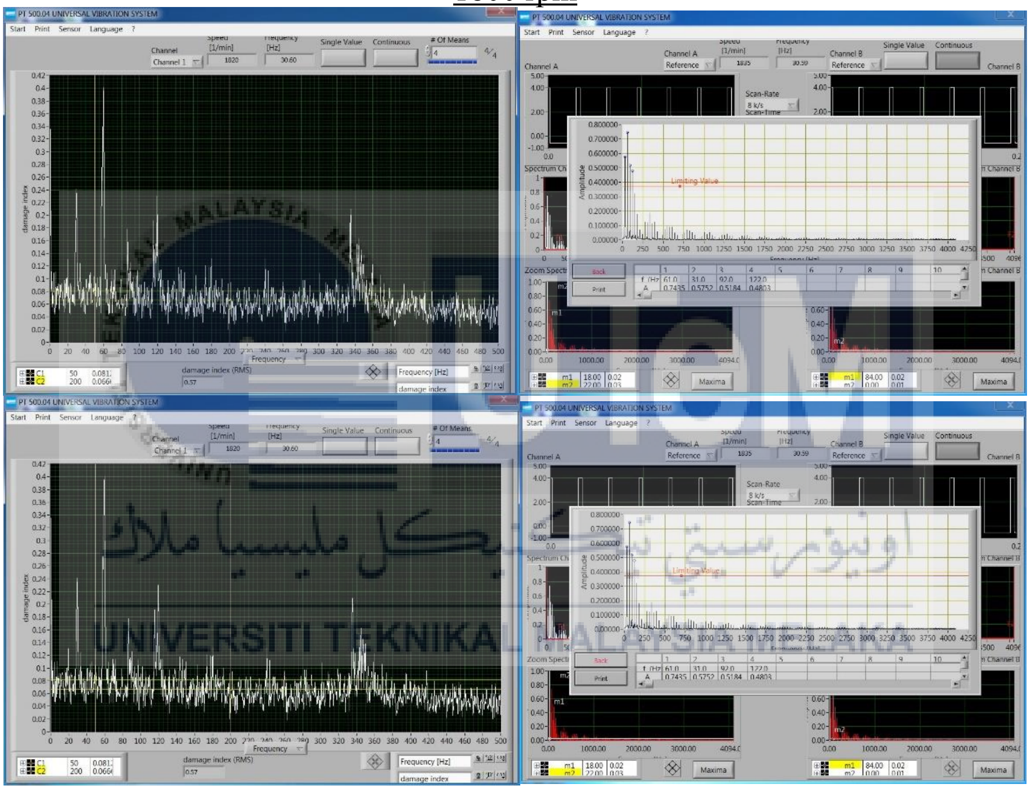

Rectangular geometry
600 rpm

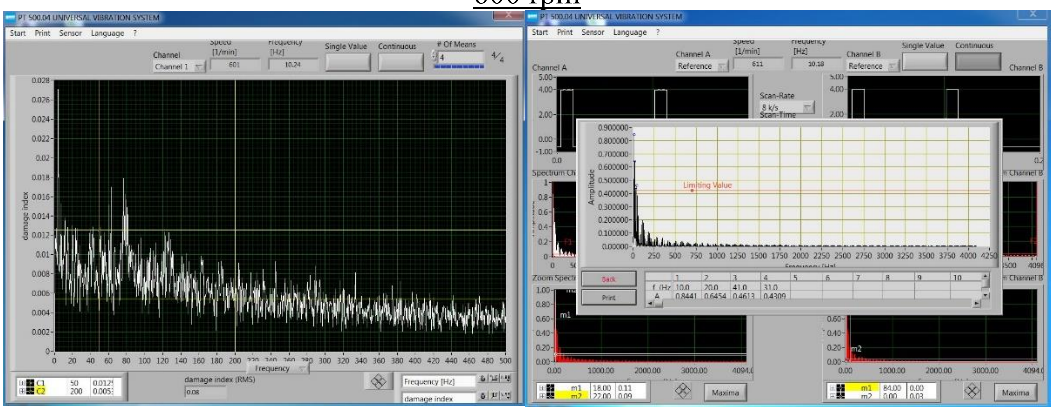

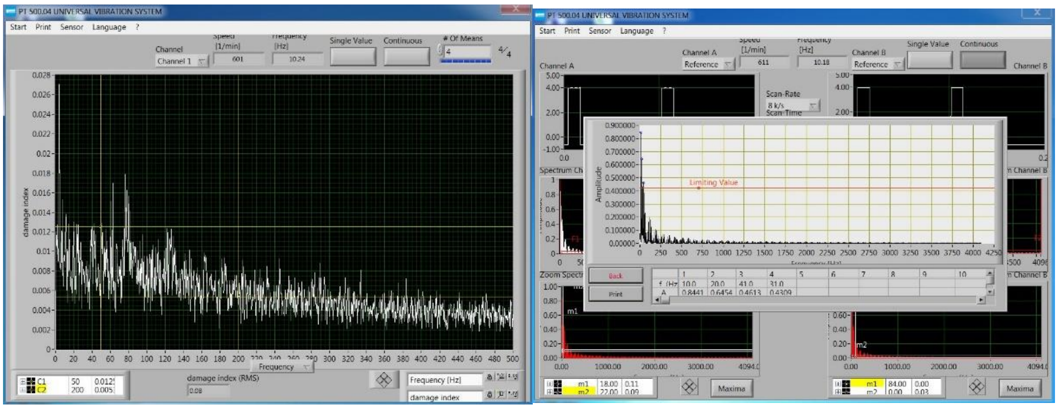

900 rpm

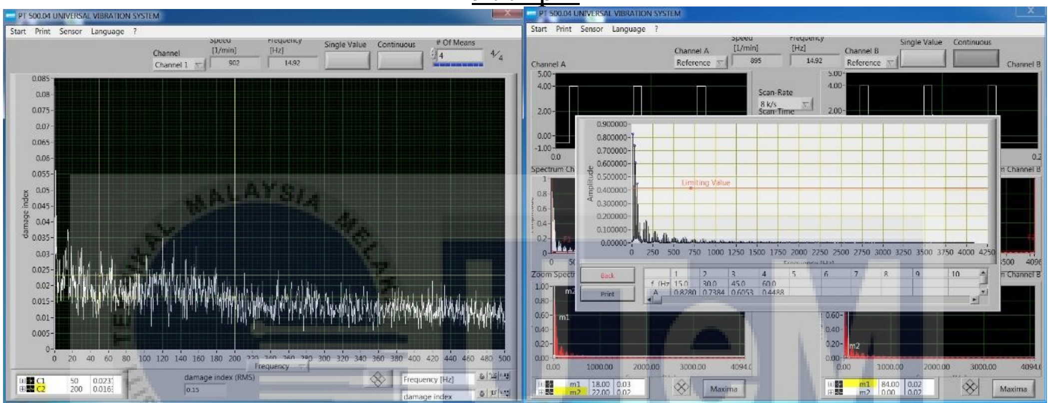

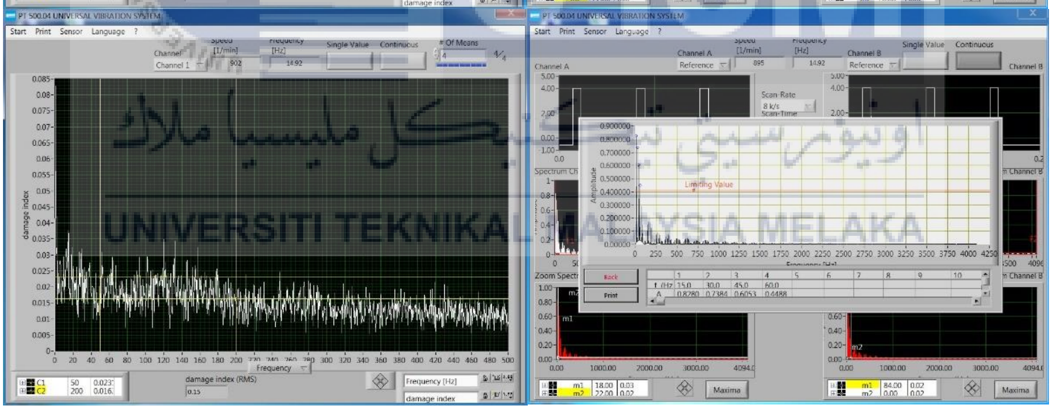

UNIVERSITI TEKNIKAL MALAYSIA MELAKA

1200 rpm

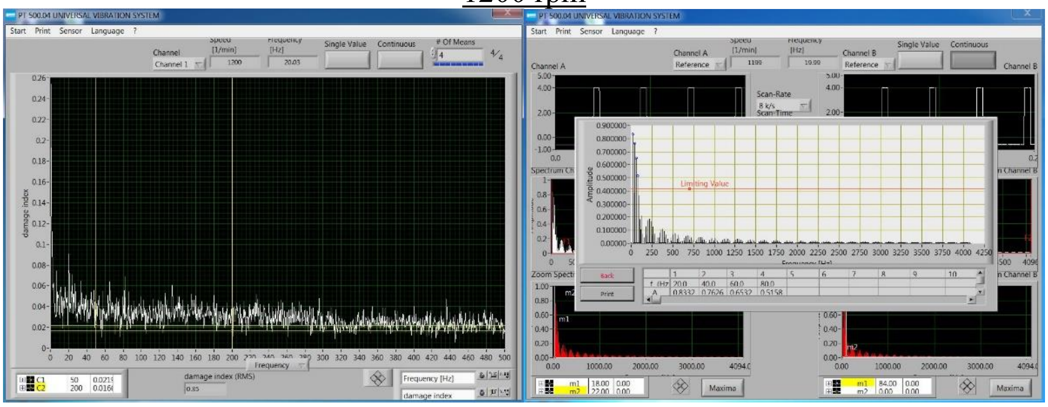

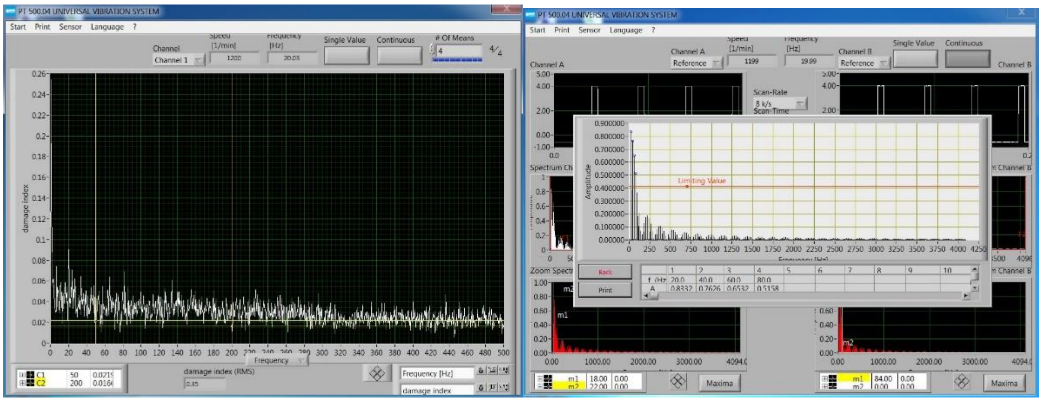

1500 rpm

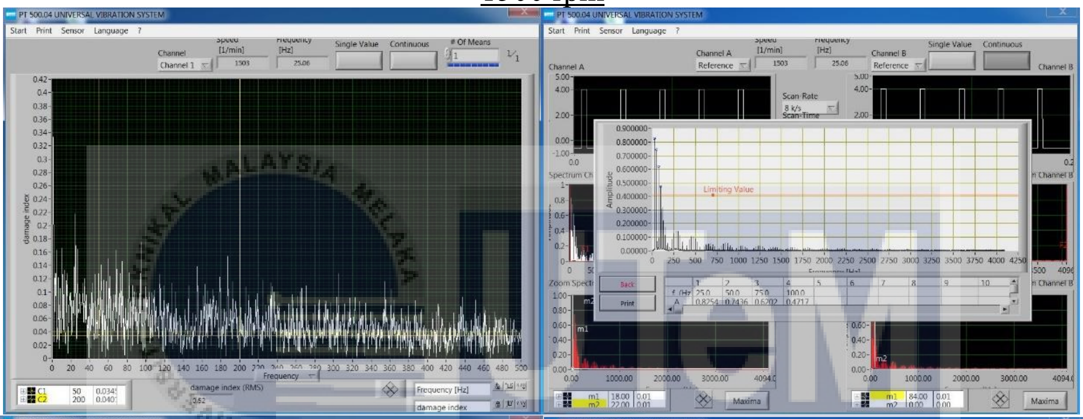

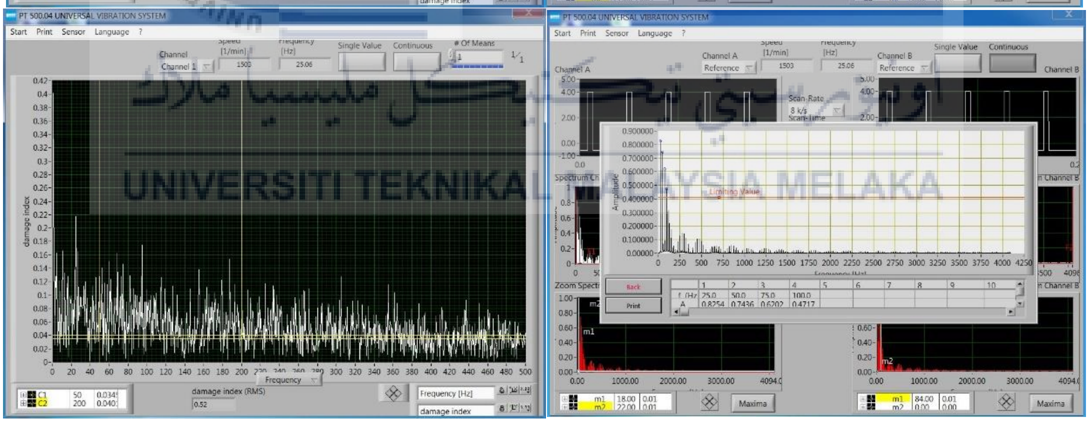

1800 rpm

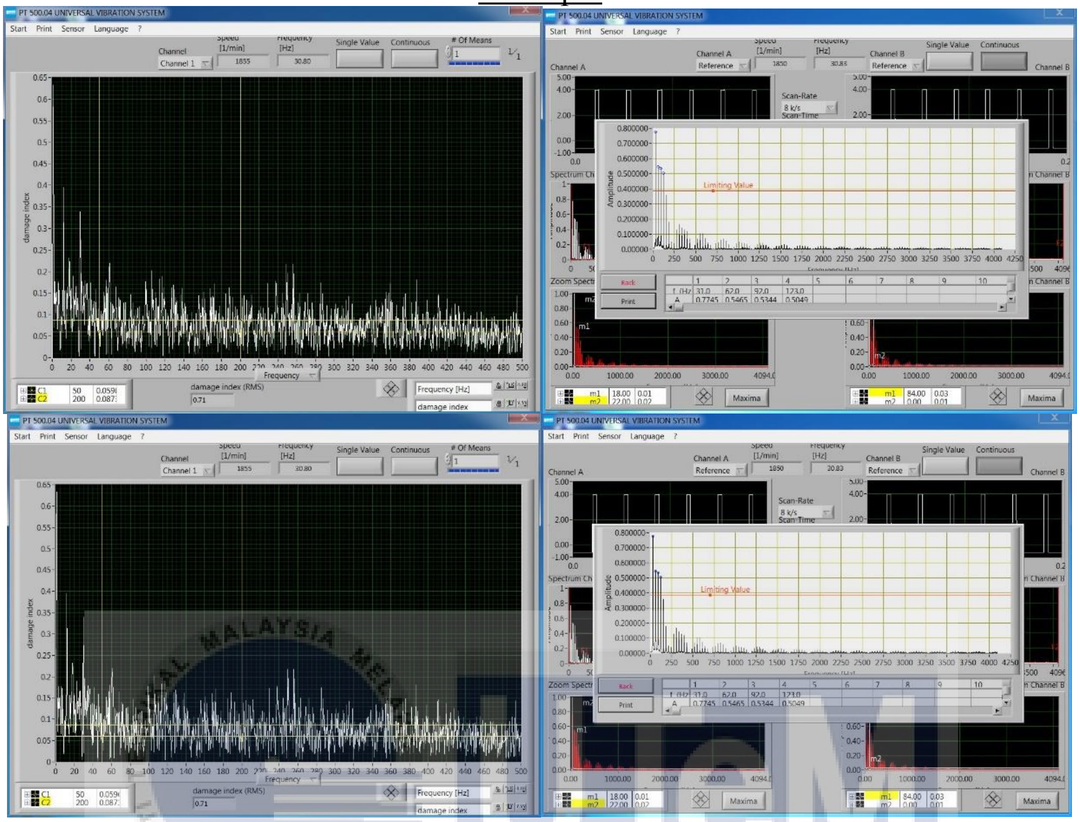

Solid geometry

600 rpm

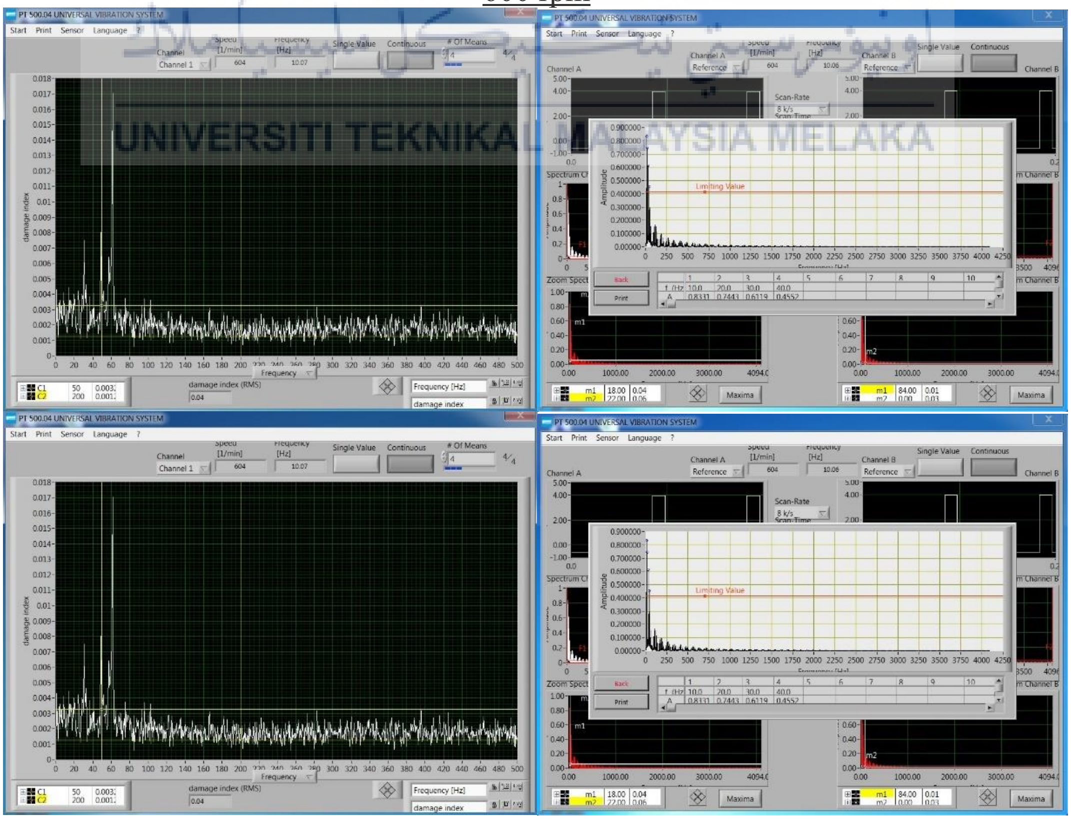

UNIVERSITI TEKNIKAL MALAYSIA MELAKA

900 rpm

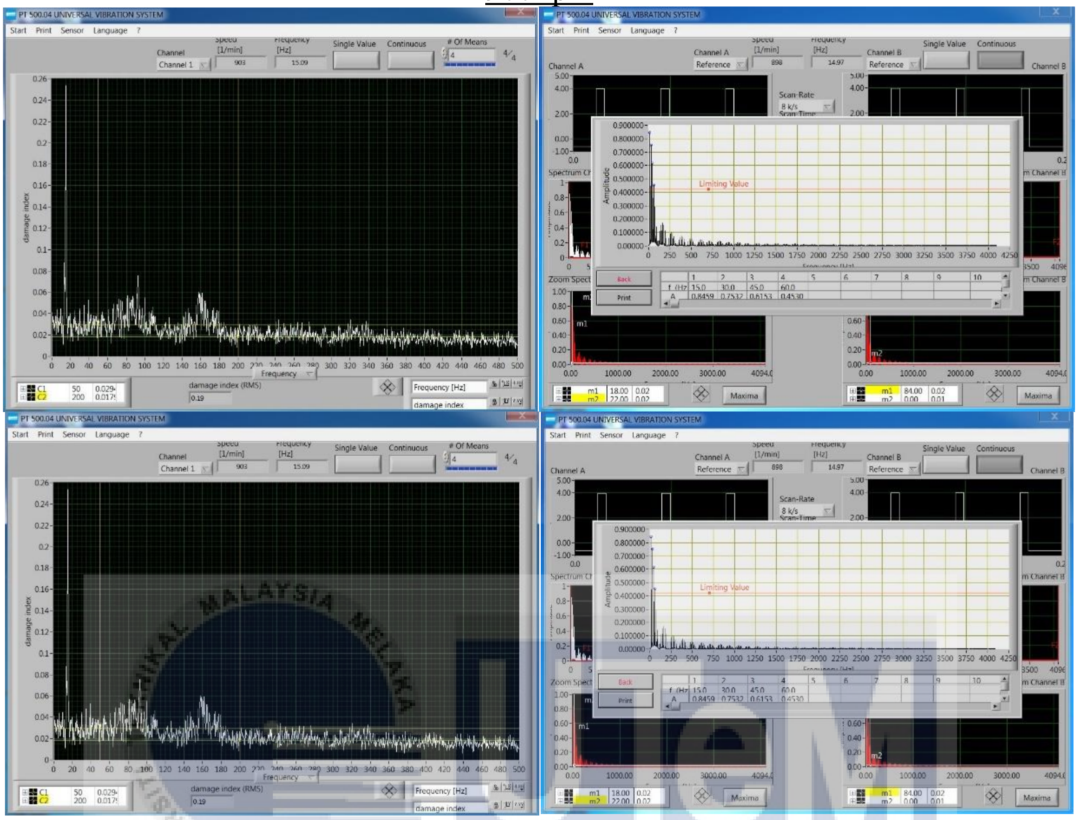

1200 rpm

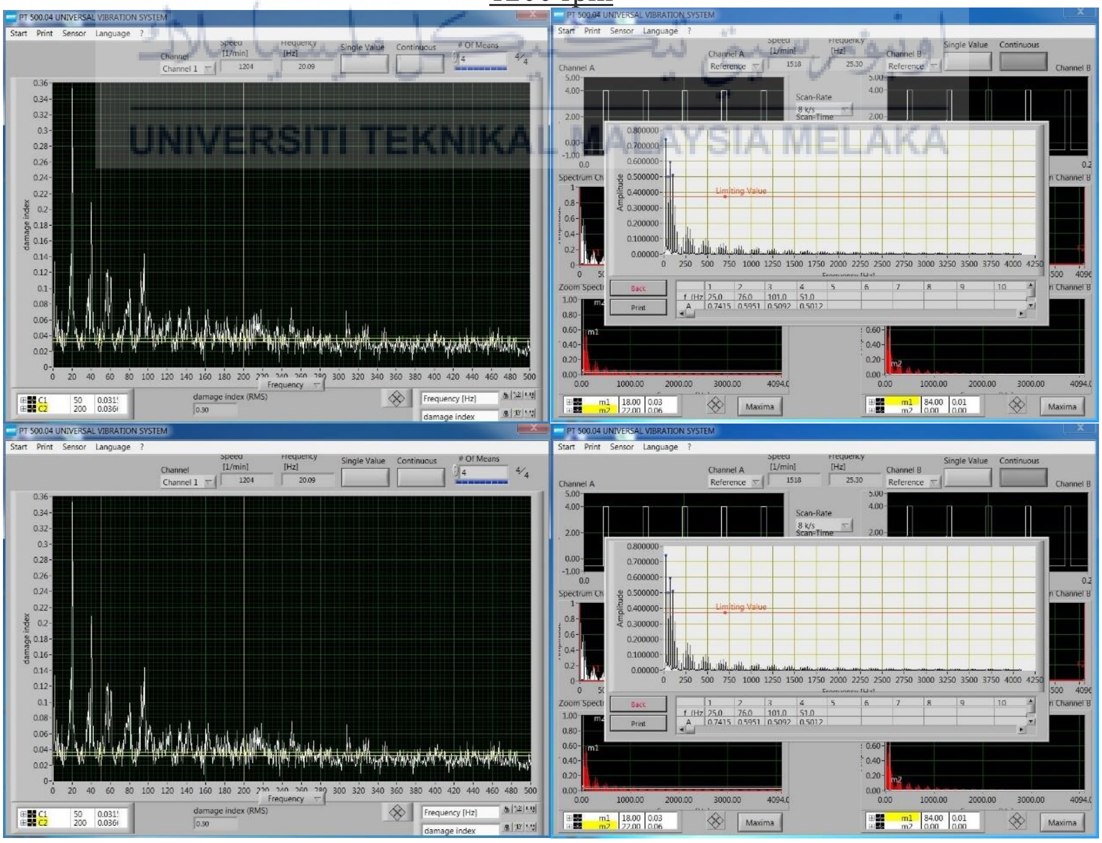

UNIVERSITI TEKNIKAL MALAYSIA MELAKA

1500 rpm

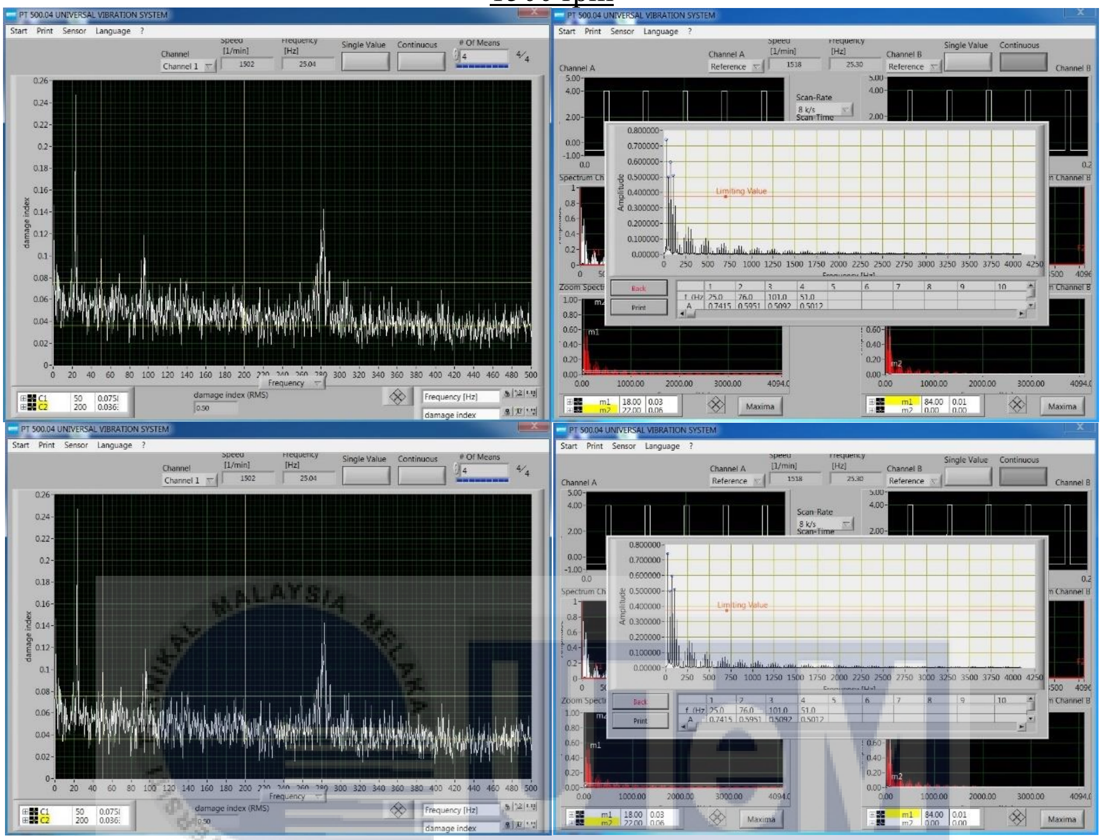

1800 rpm

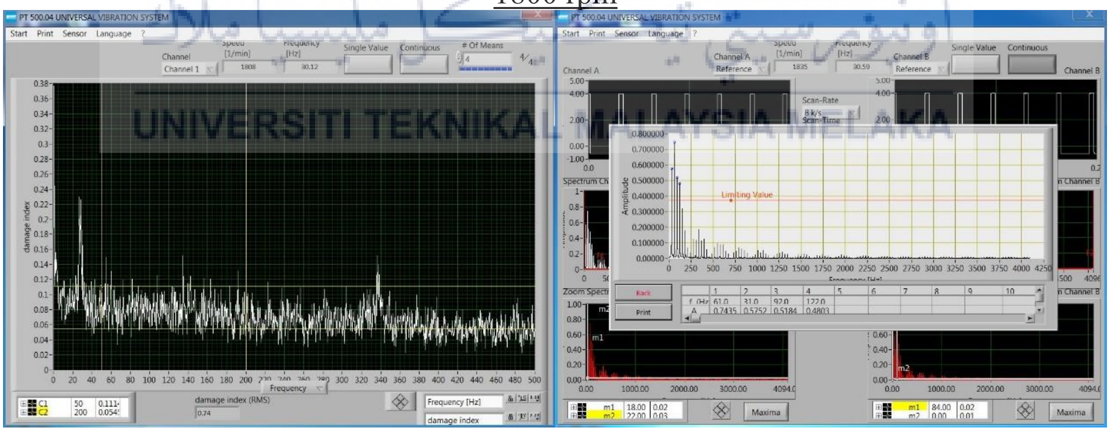

UNIVERSITI TEKNIKAL MALAYSIA MELAKA

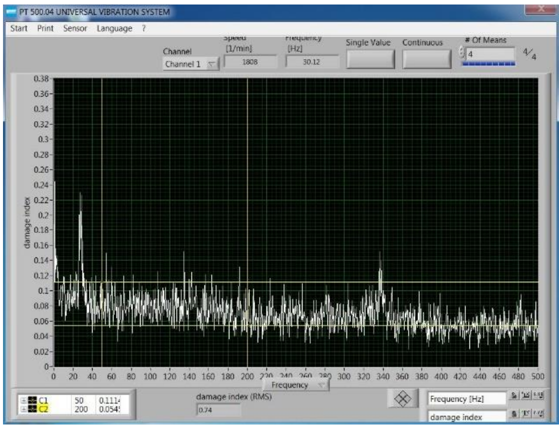

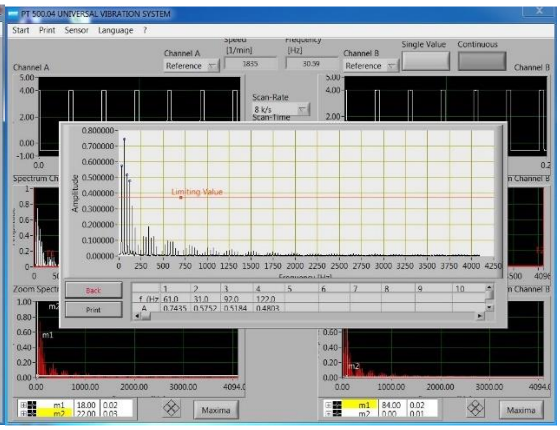

Square geometry
600 rpm

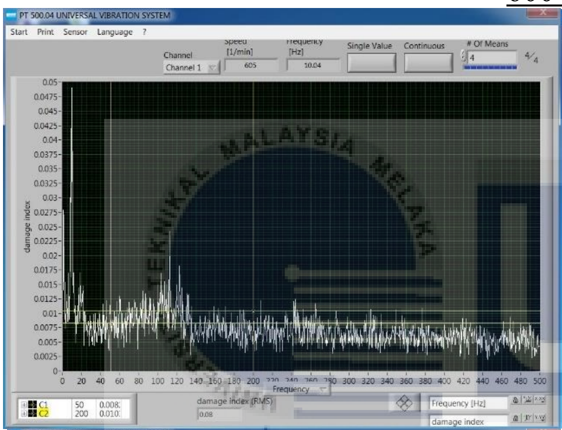

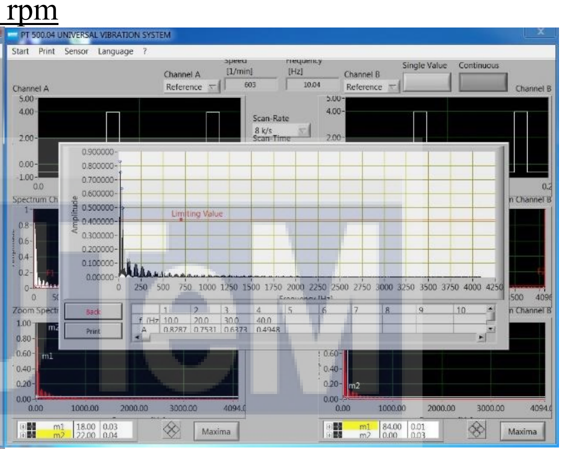

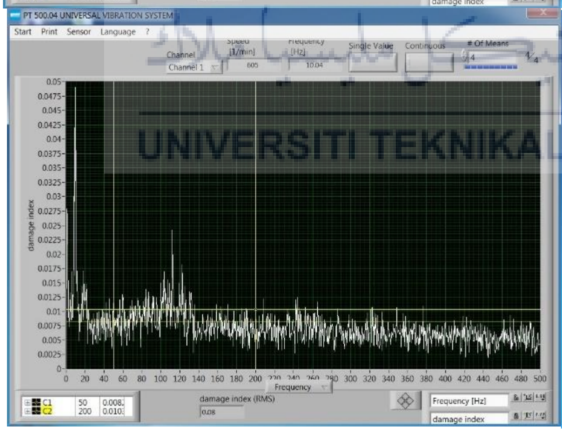

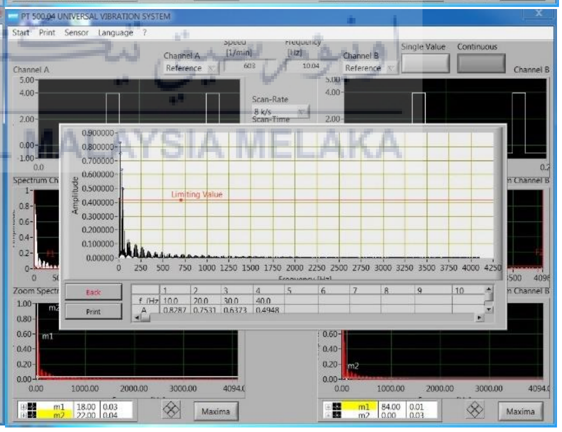

UNIVERSITI TEKNIKAL MALAYSIA MELAKA

900 rpm

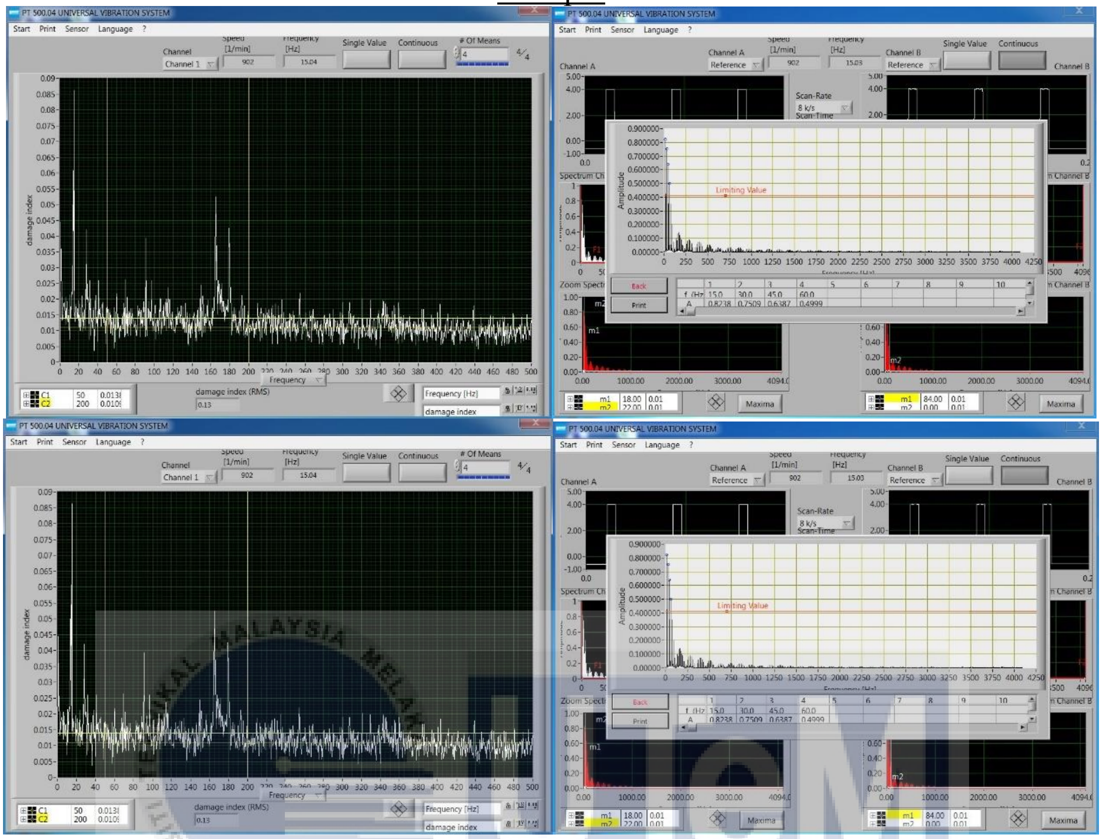

1200 rpm

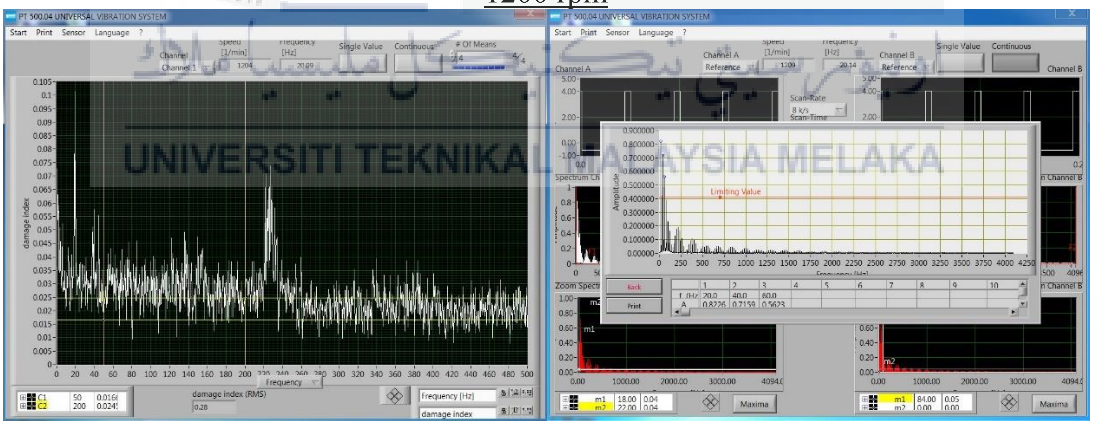

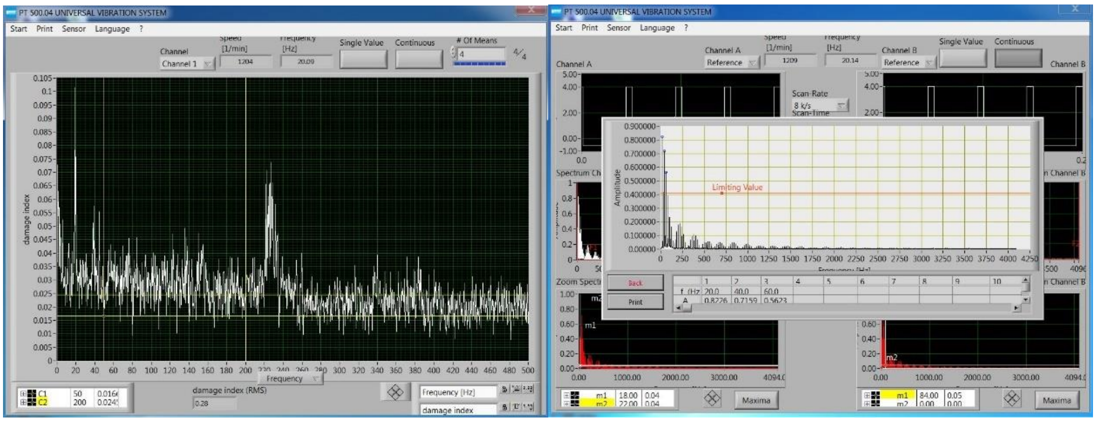

1500 rpm

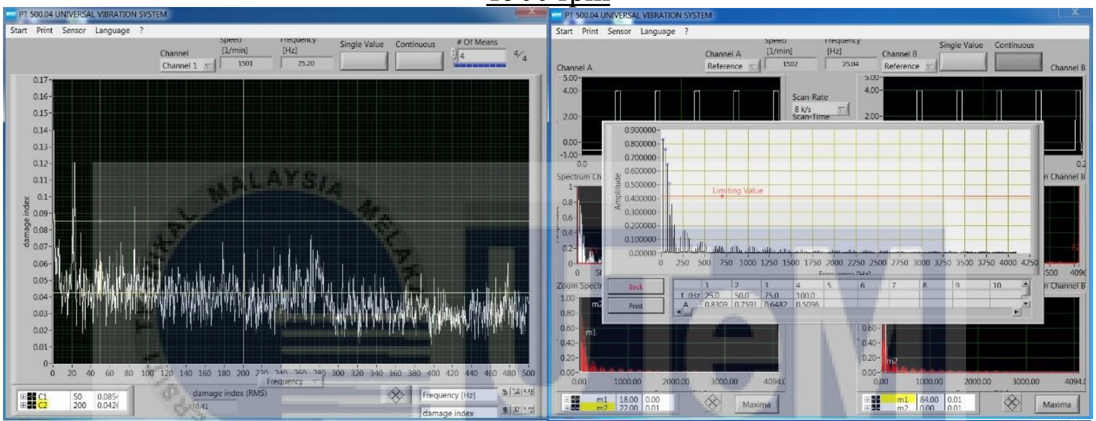

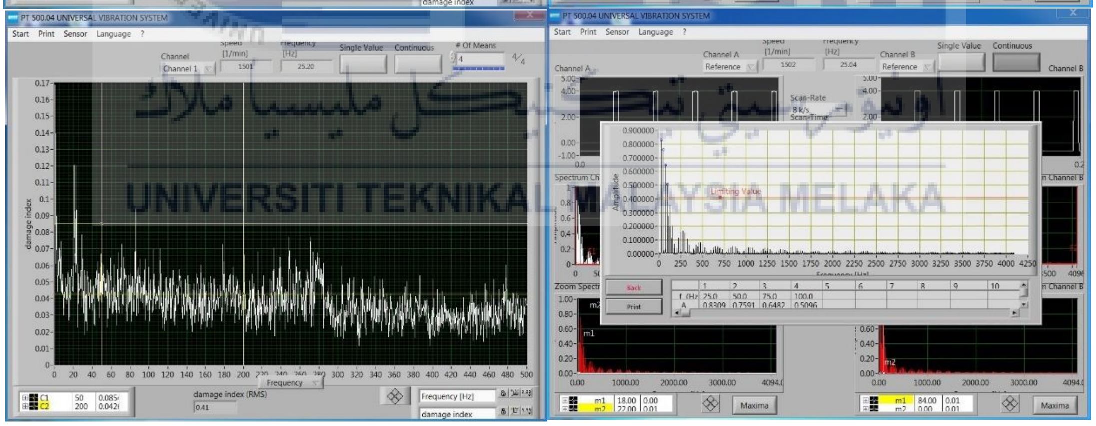

UNIVERSITI TEKNIKAL MALAYSIA MELAKA

1800 rpm

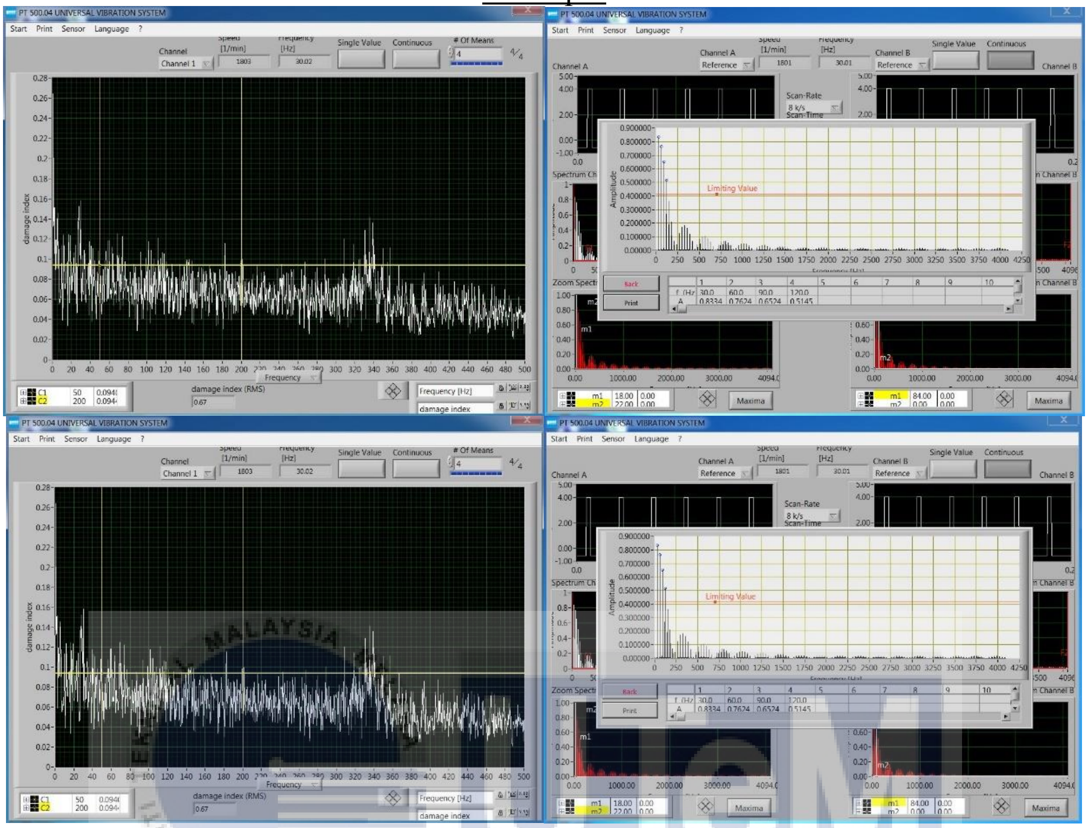

Triangle geometry

600 rpm

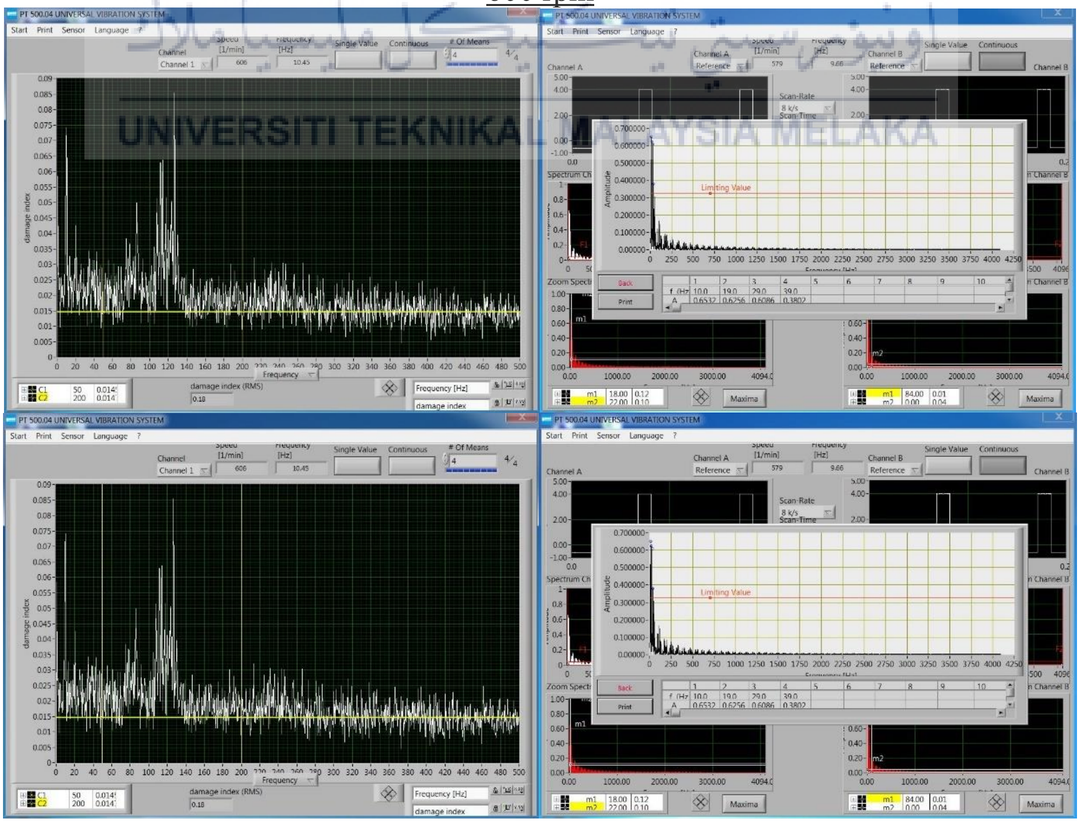

UNIVERSITI TEKNIKAL MALAYSIA MELAKA

900 rpm

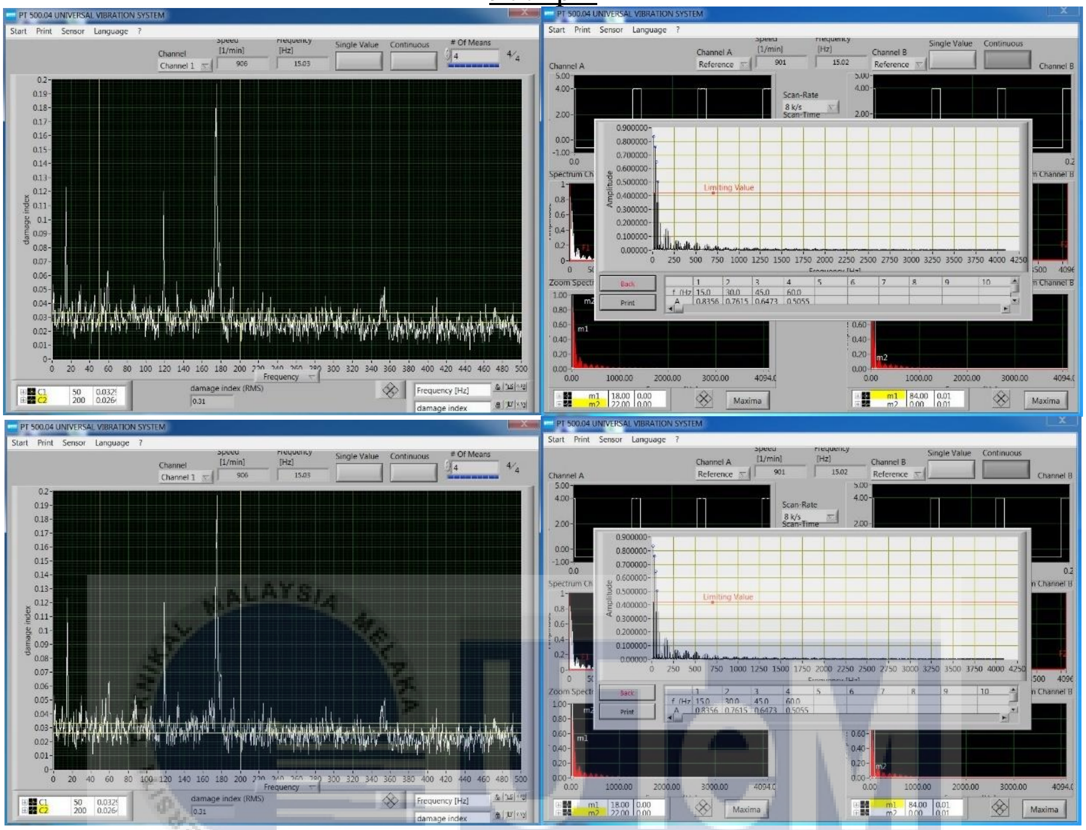

UNIVERSITI TEKNIKAL MALAYSIA MELAKA

1200 rpm

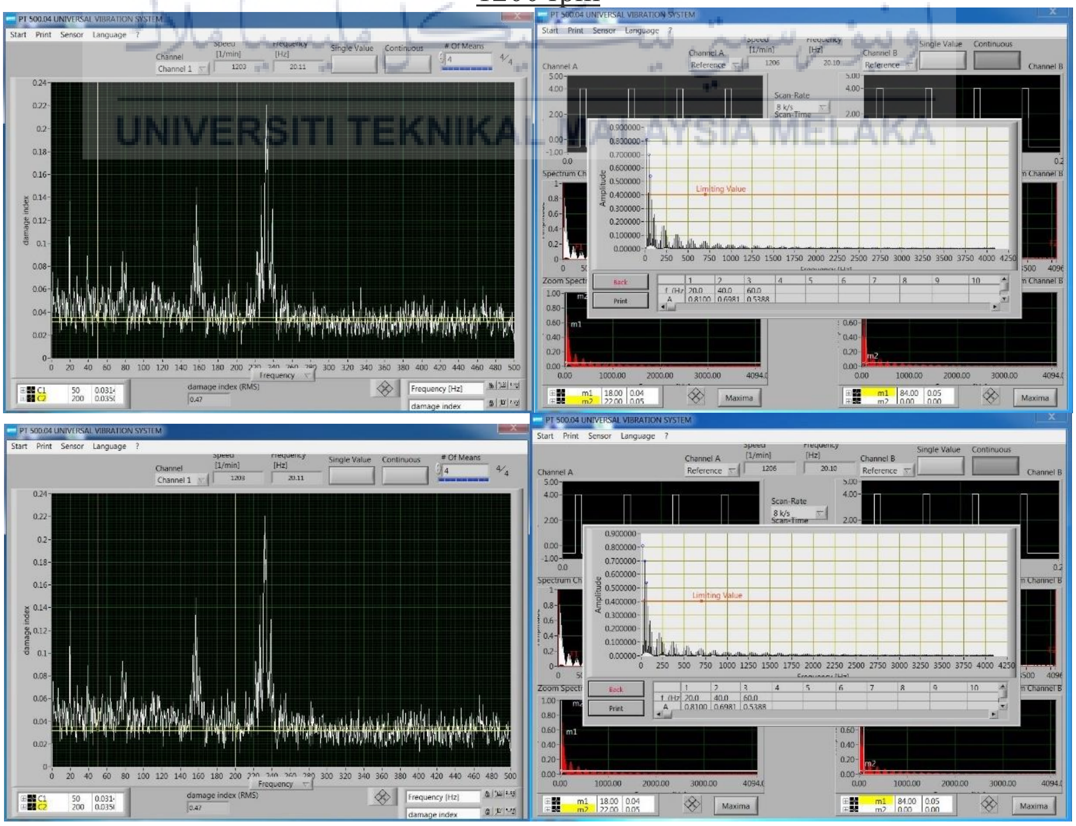

1500 rpm

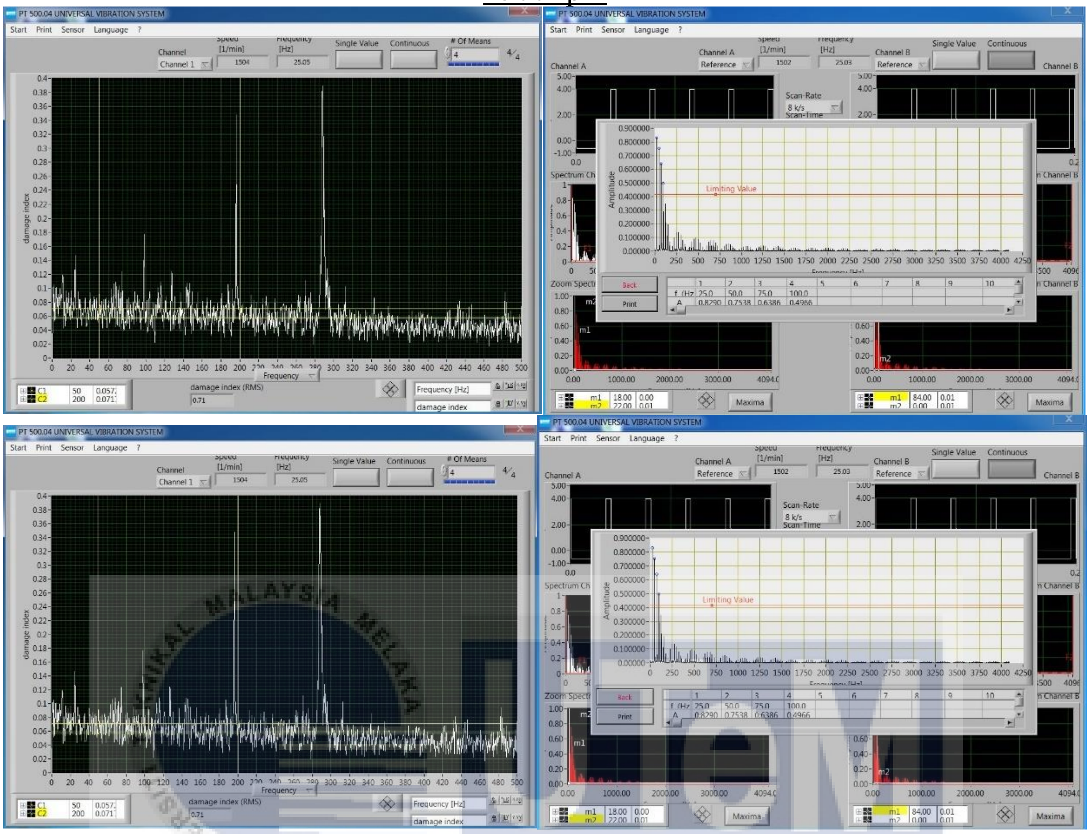

1800 rpm

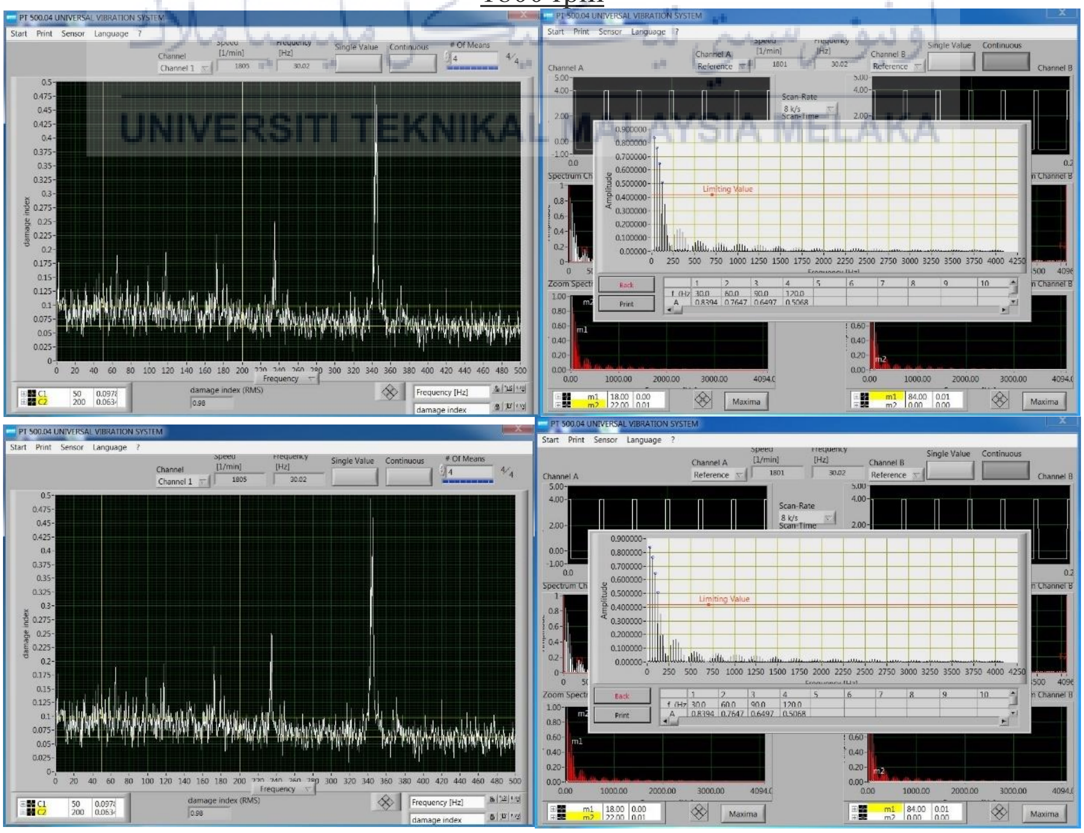

UNIVERSITI TEKNIKAL MALAYSIA MELAKA